

# Dynamics of Chemotactic Gliding-Aggregation in Myxobacteria on Bounded Domains: Stochastic Modeling, Analysis, and Deep Neural Network Simulations

Fugui Ma<sup>†,\*</sup> and Zhimeng Ouyang<sup>‡</sup>

*School of Mathematical Sciences, Peking University, 5 Yiheyuan Road,  
Haidian District, Beijing 100871, China*

<sup>†</sup>*mafugui@math.pku.edu.cn*

<sup>‡</sup>*ouyangzm@math.pku.edu.cn*

Wenyi Tian

*Center for Applied Mathematics and KL-AAGDM, Tianjin University, 92 Weijin Road,  
Nankai District, Tianjin 300072, China*  
*twymath@gmail.com*

Lei Wu

*Department of Mathematics, Lehigh University, Bethlehem, 17 Memorial Drive East,  
Bethlehem, PA 18015, USA*  
*lew218@lehigh.edu*

Received (Day Month Year)

Revised (Day Month Year)

Communicated by (xxxxxxxxxx)

Bacterial chemotactic movement and collective aggregation have long attracted substantial interest in mathematical biology and applied modeling. Classical Keller–Segel-type systems, however, are typically formulated under idealized laboratory assumptions, such as smooth agar substrates, and thus cannot adequately capture the gliding dynamics of myxobacteria in naturally rough environments like soil. In this paper, we propose a unified framework that integrates stochastic modeling, rigorous analysis, and deep neural network-based simulation of chemotactic gliding–diffusion and aggregation processes on bounded domains. Starting from a lattice-based discrete agent description and a subordinated Langevin equation driven by an inverse stable subordinator at the microscopic level, we characterize anomalous gliding dynamics on rough surfaces and derive a macroscopic time-nonlocal Keller–Segel-type chemotaxis model with logarithmic sensitivity. We then establish a comprehensive solution theory for the resulting model, covering mass conservation, novel regularity results, local well-posedness in any spatial dimension, and global well-posedness in two and three. The analysis relies on several newly developed ingredients, including a fractional Lyapunov functional, a variational inequality adapted to the time-nonlocal structure, logarithmic Sobolev-type estimates, Bregman distance techniques, and a weighted bootstrap mechanism adapted to the singular sensitivity and time-nonlocal memory. Finally, we design a mesh-free, positivity-preserving, multi-objective, time-marching physics-informed neural network method with separate architectures and tailored variable transformations. Numerical experiments on complex geometries, including a butterfly-shaped domain, demonstrate the robustness, accuracy, and flexibility of the proposed computational framework across a range of Keller–Segel-type systems.

*Keywords:* Chemotaxis-diffusion; time-nonlocal Keller-Segel system; Langevin equation; mild solution; deep neural network (DNN); time-marching PINNs.

AMS Subject Classification: 35A01, 35B65, 35K55, 35Q92, 60K50, 68T07, 92C17

\*The first author is the corresponding author.

## 1. Introduction

Unraveling the mechanisms of bacterial motility is essential for advancing our understanding of infection pathogenesis, microbial ecology, and collective cellular behavior<sup>28,70,122</sup>. Driven by these biological imperatives, the mathematical modeling of bacterial movement has evolved into a rigorous quantitative discipline, built upon fundamental studies (see, e.g., Refs. 3, 14, 21, 59, 100, 113). At the heart of this endeavor lies bacteria chemotaxis, the directed movement of cells along gradients of chemoattractants. A cornerstone model for this phenomenon, the Keller-Segel (KS) system (first introduced in Refs. 71 and 72), which has been extensively refined and applied across disciplines to describe diverse biological phenomena (see, e.g., Refs. 10, 13, 23, 29, 37, 52, 72, 81). Despite these advancements, a critical limitation remains, most existing models are based on simplified experimental conditions, typically assuming movement on smooth surfaces like agar or within uniform solutions.

In natural ecosystems, bacterial chemotaxis rarely occurs within the pristine, uniform conditions of the laboratory; rather, it unfolds on host surfaces marked by geometric roughness and structural complexity. This physical complexity directly affects how bacteria navigate and search. A prototypical example is soil-dwelling myxobacteria. Unlike the smooth, continuous expansion observed in standard laboratory assays (e.g., *E. coli* swimming in liquid or on soft agar<sup>28,69</sup>), myxobacterial navigation in soil is profoundly constrained by surface roughness and microscale granular obstacles (see, e.g., Refs. 93, 94, 135), which impose significant physical limits on their ‘gliding’ motility<sup>31</sup>. As cells glide across these rough terrains, they must continually circumvent obstacles and dynamically chart new paths for migration. These constraints drive cells into a discontinuous ‘stop-and-go’ pattern with frequent re-orientations<sup>58,101</sup>, an adaptive search strategy that breaks the Markovian assumption of classical diffusion. The accumulated effect of these interactions manifests as anomalous, memory-driven transport, wherein the population’s current state remains intrinsically coupled to its historical trajectory<sup>53</sup>. Consequently, existing chemotaxis models lack the capacity to reliably capture such historically dependent motility. To describe these history-guided dynamics, we introduce a new chemotaxis-diffusion model, a time-nonlocal KS system (1.1), that incorporates a time non-local operator.

### 1.1. The Model

Let  $\Omega \subset \mathbb{R}^d$  ( $d \geq 2$ ) be an open bounded domain with smooth boundary  $\partial\Omega$ . We model the chemotaxis gliding–diffusion–aggregation behavior of myxobacteria on rough surfaces using the following time-nonlocal KS system with singular sensitivity

$${}_0^C \mathcal{D}_t^\alpha n(\mathbf{x}, t) = \mathcal{D}\Delta n(\mathbf{x}, t) - \mathcal{D}\chi \nabla \cdot \left( \frac{n(\mathbf{x}, t)}{c(\mathbf{x}, t)} \nabla c(\mathbf{x}, t) \right), \quad (\mathbf{x}, t) \in \Omega \times (0, T], \quad (1.1a)$$

$${}_0^C \mathcal{D}_t^\alpha c(\mathbf{x}, t) = \mathcal{D}\Delta c(\mathbf{x}, t) - \gamma c(\mathbf{x}, t) + n(\mathbf{x}, t), \quad (\mathbf{x}, t) \in \Omega \times (0, T], \quad (1.1b)$$

$$n(\mathbf{x}, 0) = n_0(\mathbf{x}), \quad c(\mathbf{x}, 0) = c_0(\mathbf{x}), \quad \mathbf{x} \in \Omega, \quad (1.1c)$$

$$\frac{\partial n(\mathbf{x}, t)}{\partial \nu} = 0, \quad \frac{\partial c(\mathbf{x}, t)}{\partial \nu} = 0, \quad (\mathbf{x}, t) \in \partial\Omega \times (0, T], \quad (1.1d)$$

where  $n(\mathbf{x}, t)$  and  $c(\mathbf{x}, t)$  denote the density of myxobacteria and the concentration of slime trail, respectively. With  $\mathcal{D} > 0$  denoting the diffusion coefficient,  $\chi > 0$  the chemotactic sensitivity, and  $\gamma > 0$  the decay rate of the slime, the final time is set as  $T > 0$ . Initial conditions are given by positive functions  $n_0(\mathbf{x})$  and  $c_0(\mathbf{x})$ , and  $\nu$  denotes the unit outward normal vector on  $\partial\Omega$ . Time evolution is described by the Caputo fractional derivative  ${}_0^C \mathcal{D}_t^\alpha$  of order  $\alpha \in (0, 1)$ , which

is defined as

$${}_0^C \mathcal{D}_t^\alpha u(\mathbf{x}, t) \triangleq \frac{1}{\Gamma(1-\alpha)} \int_0^t (t-s)^{-\alpha} \frac{\partial u(\mathbf{x}, s)}{\partial s} ds. \quad (1.2)$$

This operator mathematically captures the anomalous diffusion and memory effects observed during myxobacterial gliding across rough surfaces. Importantly, when  $\alpha \rightarrow 1$ , System (1.1) simplifies to the classical KS model with singular (logarithmic) sensitivity, which characterizes chemotaxis under Markovian diffusion conditions.

The analysis of System (1.1) is rendered particularly challenging by two core mathematical features: (i) the non-local nature of the Caputo fractional derivative operator  ${}_0^C \mathcal{D}_t^\alpha$ ; and (ii) the singular chemotactic sensitivity  $\frac{1}{c(\mathbf{x}, t)} \nabla c(\mathbf{x}, t) = \nabla \log(c(\mathbf{x}, t))$ , which becomes unbounded as  $c(\mathbf{x}, t) \rightarrow 0$ . For  $\alpha \in (0, 1)$ , the system no longer possesses a standard local time-derivative structure; instead, the time non-local derivative operator introduces memory effects that break the Markovian property, while the singular sensitivity couples to this nonlocality, collectively yielding analytical difficulties well beyond those encountered in classical Keller–Segel models.

Despite these challenges, non-local models of this type possess substantial theoretical value, as they inherently capture the memory effects and anomalous transport characteristic of complex biological systems. We will show that the proposed model offers a more faithful description of the adaptive searching behavior of myxobacteria in natural, heterogeneous habitats, thereby providing greater ecological relevance and predictive capacity than conventional models formulated under homogeneous assumptions.

To this end, we systematically investigate the modeling validity of System (1.1) and establish its theoretical foundation via rigorous PDE analysis. Moreover, capitalizing on the mesh-free advantage of deep learning algorithms, we conduct numerical simulations to visualize the solution dynamics and verify the global existence of solutions in two spatial dimensions.

## 1.2. Connections with previous work and further motivations

Although bacterial chemotaxis is ubiquitous in nature, our understanding of it remains largely derived from laboratory studies of model organisms, most notably *E. coli*<sup>69,70</sup>. Research on *E. coli* has been instrumental in bridging microscopic molecular signaling and macroscopic population behavior<sup>3,28,113</sup>. On smooth agar surfaces, *E. coli* detects temporal chemical gradients via methyl-accepting proteins and modulates its motility through a phosphotransferase signaling cascade. This mechanism results in the characteristic ‘run-and-tumble’ motion directed toward attractants (see, e.g., Refs. 28, 70, 84, 113). This behavior is fundamentally Markovian at the microscopic scale.

To mathematically describe such population-level chemotactic behaviors, the Keller–Segel framework is a standard paradigm. In its general form, the system reads<sup>13</sup>

$$\partial_t n(\mathbf{x}, t) = -\nabla \cdot \mathcal{J}(n(\mathbf{x}, t), c(\mathbf{x}, t)) + f(n(\mathbf{x}, t), c(\mathbf{x}, t)), \quad \text{in } \Omega \times (0, T], \quad (1.3a)$$

$$\epsilon \partial_t c(\mathbf{x}, t) = \mathcal{D} \nabla^2 c(\mathbf{x}, t) + g(c(\mathbf{x}, t), n(\mathbf{x}, t)), \quad \text{in } \Omega \times (0, T]. \quad (1.3b)$$

Here, equation (1.3a) governs the evolution of the bacterial density  $n(\mathbf{x}, t)$ . The total flux  $\mathcal{J}(n, c)$  comprises two main contributions: (i) Fickian diffusion driven by the bacterial concentration gradient; and (ii) chemotactic drift, i.e., directed movement along chemical gradients (e.g., toward lower attractant or higher repellent concentrations). Equation (1.3b) describes the dynamics of the chemical signal  $c(\mathbf{x}, t)$  (e.g., protons or nutrients), which diffuses with coefficient  $\mathcal{D}$ . The

functions  $f(n, c)$  and  $g(n, c)$  represent source/sink terms associated with biological processes.  $f(n, c)$  typically models cellular proliferation or death, while  $g(n, c)$  accounts chemical production or consumption. By choosing specific constitutive forms for  $\mathcal{J}$  in (1.3), one recovers a variety of classical and phenomenological KS models (see Table 1 for the case  $f(n, c) = 0$ ). For a broader survey of KS-type models, we refer the reader to review articles such as Refs. 10, 51.

Table 1: Several phenomenological KS models satisfying (1.3) with  $f(n, c) = 0$  and  $\chi > 0$ .

Model Name <sup>Refs.</sup>	Determined Flux $\mathcal{J}(\cdot, \cdot)$	Source/Sink $g(\cdot, \cdot)$
Patlak-Keller-Segel model <sup>23,68,71</sup>	$-\mathcal{D}(\nabla n + \chi n \nabla c)$	$-c + n, \epsilon = 1$
Logistic model <sup>54,72,81,133,134</sup>	$-\mathcal{D}(\nabla n + \chi \frac{n}{c} \nabla c)$	$-cn, \epsilon = 1$
Modified KS <sup>84,85</sup>	$-\mathcal{D}(\nabla n + \chi \frac{n}{c+\beta} \nabla(c+\beta))$ †	$-\gamma nc$ or $-\gamma c^{3/2}n$
Volume-filling model I <sup>51</sup>	$-\mathcal{D}(\nabla n + \chi n(1 - \frac{n}{\Upsilon}) \nabla c)$ ‡	$-\gamma c + n, \epsilon = 1$
Volume-filling model II <sup>123,124</sup>	$-\mathcal{D}(\nabla n + \chi \frac{n}{1+\bar{\epsilon}n} \nabla c), \bar{\epsilon} > 0$	$n, \epsilon = 0$
Receptor model <sup>18,99,129</sup>	$-\mathcal{D}(\nabla n + \chi \frac{n}{(1+\bar{\epsilon}c)^2} \nabla c), \bar{\epsilon} > 0$	$n, \epsilon = 0$
Nonlinear-diffusion model <sup>10,51</sup>	$-\mathcal{D}(n^\kappa \nabla n + \chi n \nabla c), \kappa \in \mathbb{N}_+ \cup \{0\}$ ¶	$-\gamma c + n, \epsilon = 1$
Nonlocal-diffusion model <sup>37</sup>	$-\mathcal{D}(\nabla^{s-1} n + \chi n \nabla c), 1 < s < 2$	$-\gamma c + n, \epsilon = 1$

† The model reduces to the KS with logarithmic sensitivity as  $\beta \rightarrow 0$ ; ‡ For  $\Upsilon, \bar{\epsilon} > 0$ , the limit of  $\Upsilon \rightarrow \infty$  or  $\bar{\epsilon} \rightarrow 0$  leads to the KS; ¶ The limit of  $\kappa \rightarrow 0$  results in the KS.

The KS model with logarithmic (singular) sensitivity has been widely adopted due to its empirical success in capturing bacterial aggregation and pattern formation (see, e.g., Refs. 18, 84, 85, 99, 112, 122). Mathematically, this system often referred to as the logarithmic KS system, which exhibits rich behavior under Neumann boundary conditions, particularly concerning global solvability and long-time dynamics. Below we outline key theoretical milestones, focusing on the case where  $g(n, c) = -\gamma c + n$ ,  $f(n, c) \equiv 0$ ,  $\mathcal{D} > 0$ , and the initial data are sufficiently regular and positive. The global existence of solutions depends critically on the spatial dimension  $d$  and the chemotactic sensitivity coefficient  $\chi$ . In two dimensions ( $d = 2$ ), Ref. 4 establishes the global existence of classical solutions and characterizes their asymptotic behaviour. For general  $d \geq 2$ , Ref. 131 proves global classical solvability under the condition  $\chi < \sqrt{2/d}$ . Moreover, by means of a key inequality (Lemma 2.3 in Ref. 131), the same work also demonstrates the existence of global weak solutions for all  $d \geq 2$  whenever  $0 < \chi < \sqrt{(d+2)/(3d+4)}$ . A subsequent refinement in Ref. 134 clarifies that the condition  $\chi < \sqrt{2/d}$  essentially requires the ratio  $\chi^2/\mathcal{D} > 0$  to be sufficiently small; under this smallness assumption, classical solutions converge exponentially to the homogeneous steady state  $(\bar{n}_0, \bar{c}_0)$ , where  $\bar{u}_0 := \frac{1}{|\Omega|} \int_{\Omega} u(\mathbf{x}, 0) d\mathbf{x}$ .

The frontier was subsequently pushed to larger values of  $\chi$ . Through sophisticated analytical techniques, Ref. 117 establishes the existence of global weak solutions for arbitrary  $\chi > 0$ . Ref. 80 further demonstrates global solvability for  $d = 2$  with any finite  $\chi$ , for  $d = 3$  with  $\chi < \sqrt{8}$ , and for  $d \geq 4$  with  $\chi < \frac{d}{d-2}$ . These landmark results fundamentally rely on the classical parabolic PDE theory, including the comparison principle, Moser-type estimates, and energy functional methods<sup>4,80,117</sup>, all of which are intrinsically tied to the local-in-time derivative structure of the equations. This foundational framework, however, breaks down when the standard time derivative is replaced by a nonlocal operator. Consequently, the analytical tools developed for classical KS systems are no longer directly applicable, necessitating a fundamentally different approach, which is precisely the focus of the present work.

Recently, inspired by the success of non-ergodic anomalous diffusion models in capturing diffusion phenomena in non-equilibrium, heterogeneous, and porous media<sup>75</sup>, as well as by the efficacy of the KS model in describing chemotaxis-diffusion dynamics in homogeneous environments<sup>78,99</sup>, researchers are establishing the connection between non-ergodic anomalous diffusion and bacterial chemotaxis-diffusion<sup>50,53</sup>. By organically merging the two, the aim is to model and analyze more realistic and complex bacterial chemotaxis-diffusion dynamics that better reflect natural habitats.

Most current efforts in this direction focus on modifications of the Patlak–Keller–Segel (PKS) model. For instance, Ref. 37 incorporates super-diffusion into the bacterial chemotaxis-diffusion framework to characterize long-step bacterial movement in nutrient-scarce environments, achieved by replacing the spatial Laplace operator with a fractional Laplacian. Ref. 88 combines sub-diffusion with myxobacterial chemotaxis to describe the chemotactic aggregation dynamics in porous media, where the temporal local derivative is replaced by the non-local Caputo fractional derivative. The well-posedness and solution theory for these two classes of modified models, under various domains and generalized settings, have been systematically developed in Refs. 15, 27, 61, 83 and related woderivativerks.

It is worth emphasizing, however, that merging anomalous diffusion with bacterial chemotaxis–diffusion–aggregation dynamics requires more than mere operator substitutions; rigorous biophysical justification and careful model derivation are equally essential. Looking ahead, further refinements to generalized KS models, combined with experimental validation, are poised to accelerate progress in this emerging direction.

The transition to the time-nonlocal KS system represents far more than a technical generalization; it marks a fundamental conceptual shift. Specifically, the historical memory inherent in the time non-local derivative operator shatters the core analytical pillars, most notably the conventional Lyapunov functionals and comparison principles, upon which the established theory for logarithmic models has traditionally rested. This invalidation renders classical methods inapplicable, as the hereditary nature of the system prevents the direct translation of prior global existence results. Consequently, a profound theoretical void emerges. The central challenge of the present analysis, therefore, is to establish a novel analytical framework, designed to address the complex interdependencies and inherent nonlocal characteristics that fundamentally define the system.

Since analytical solutions to KS models are generally unavailable, numerical methods are indispensable for visualizing the system dynamics. For a broad class of simplified KS models, classical discretization techniques are widely employed, including finite element methods (see, e.g., Refs. 111, 118, 126), finite difference schemes (e.g., Refs. 36, 55, 128), finite volume approaches (e.g., Refs. 25, 39, 136), and Local Galerkin methods (e.g., Refs. 35, 46, 105). These methods rest on a solid theoretical foundation, providing well-established convergence and stability analyses, rigorous error estimates, and predictable computational costs. However, when applied to strongly nonlinear and coupled systems such as (1.1), these classical methods exhibit pronounced limitations. Prominent among them are high implementation complexity, the need for carefully tailored iterative solvers, cumbersome mesh generation on irregular domains, and the curse of dimensionality. To our knowledge, no existing numerical scheme addresses the logarithmic KS model, highlighting the urgent demand for methods tailored to this nonlocal, singular system. This motivates our adoption of a mesh-free deep learning strategy, which bypasses many of these difficulties and is naturally suited to the nonlocal structure of the system.

Physics-Informed Neural Networks (PINNs) offer a promising mesh-free approach, demonstrating strong adaptability to complex geometries and high-dimensional problems<sup>107</sup>. Their implementation leverages automatic differentiation for computing complex derivatives within a unified framework<sup>66</sup>, and they exhibit an inherent capacity for refinement during training<sup>96</sup>. Motivated by recent advances in hybrid methodologies that combine classical numerical methods with PINNs<sup>38,47</sup>, we propose a hybrid strategy to solve the strongly nonlinear, coupled time-nonlocal system (1.1), aiming to bridge the gap between biophysical realism and computational tractability.

### 1.3. *Main contributions and novelties of the paper*

The collective aggregation of myxobacteria serves as a paradigmatic example of self-organization across scales, from individual stochastic motion to population-level pattern formation. To capture this multiscale phenomenology, we develop an integrated framework that ties together biophysically grounded modeling, a rigorous existence theory for the resulting time-nonlocal system, and a robust hybrid numerical strategy. In particular, our model is designed to more faithfully describe the chemotactic gliding, diffusion, and aggregation of myxobacteria on rough surfaces, where surface roughness and physical obstacles profoundly modulate population dynamics. In doing so, we seek to forge a coherent narrative that bridges biological realism and analytical tractability. The main contributions of this work are summarized below.

- **Multiscale mathematical modeling (micro-to-macro):** We establish a novel mathematical framework that more faithfully characterizes the chemotactic gliding, diffusion and aggregation of myxobacteria on rough surfaces, where geometric irregularities and granular obstacles fundamentally modulate population behavior. By formulating a subordinated Langevin equation driven by an inverse  $\alpha$ -stable subordinator, we provide a rigorous bridge between microscopic stochastic trajectories and the macroscopic system. This derivation substantiates both the physical rationality and mathematical integrity of the proposed model.
- **Advanced solution theory and analytical innovation:** We establish a comprehensive well-posedness theory for the proposed time-nonlocal KS system (1.1) with logarithmic sensitivity. Our results include local well-posedness of mild solution in arbitrary spatial dimensions, mass conservation, positivity preservation, and regularity in generalized Sobolev spaces, as well as global well-posedness in dimensions two and three. The analysis rests on a suite of novel tools: a fractional Lyapunov functional, Caputo-type variational inequalities, fractional convexity estimates, logarithmic Sobolev-type inequalities, Bregman distance techniques, and a weighted bootstrap mechanism specifically adapted to the singular sensitivity and time-nonlocal memory.
- **Robust positivity-preserving time-marching PINNs:** We propose a multi-objective, positivity/non-negativity-preserving time-marching PINN algorithm. A distinctive feature of this approach is the use of independent neural networks for coupled variables, integrated with the  $L_1$  temporal semidiscrete scheme. To strictly enforce physical constraints, we introduce the transformations  $n = \rho^2 \geq 0$  and  $c = \exp(v) > 0$  directly into the continuous system, ensuring the algorithm's generalizability across a wide class of KS-type models.
- **Numerical validation in complex geometries:** We design original numerical examples to verify the robustness of our theoretical and algorithmic frameworks. By con-

structuring exact solutions with temporal Hölder continuity and performing simulations on a complex ‘butterfly-shaped’ domain, we validate the global existence of solutions and demonstrate the algorithm’s superior ability to handle irregular geometries and capture long-term evolutionary dynamics.

Overall, the proposed framework constitutes a promising and versatile approach for modeling biophysical dynamics in complex, irregular environments. Not only does it provide a powerful computational tool for capturing chemotactic dynamics within irregular geometries, but its intrinsic connection to non-equilibrium statistical physics also unlocks broad prospects for future theoretical and numerical explorations.

#### 1.4. *Organization of the paper*

The remainder of this paper is organized as follows. Section 2 presents the modeling framework. We begin by discussing the motility mechanisms of myxobacteria and constructing a discrete agent-based model to describe their trajectories on rough surfaces. Building on this microscopic description, we derive the macroscopic System (1.1) via a subordinated Langevin equation. Section 3 states the main theoretical results for the resulting system, including mass conservation, positivity preservation, local mild well-posedness in arbitrary spatial dimensions, and global well-posedness in dimensions two and three. Detailed technical proofs, along with further regularity estimates, are provided in Sections 4, 5, and 6. Section 7 then introduces a mesh-free, multi-objective, time-marching PINNs algorithm designed to preserve the non-negativity and positivity structures of the model. Numerical experiments on complex geometries are presented to demonstrate the accuracy, robustness, and flexibility of the proposed computational framework. Finally, Section 8 summarizes the main findings and outlines possible directions for future research.

## 2. Stochastic Modeling: From Micro to Macro

### 2.1. *The biology mechanism*

Myxobacteria are Gram-negative, rod-shaped bacteria that lack flagella and are thus incapable of swimming. Instead, they exhibit gliding motility to move across surfaces, including over the surfaces of sibling cells<sup>135</sup>. These bacteria exhibit social behaviors, such as cooperative feeding, coordinated movement, and social development<sup>125</sup>. Gliding occurs on solid surfaces as well as at the water-air interface, and is characterized by cell bending and slime secretion. Their gliding speed ranges between 10 and 60  $\mu\text{m}/\text{min}$ , depending on temperature, nutrient availability, and initial cell density<sup>31</sup>. Myxobacteria cells are typically rod-shaped, with dimensions that varies by species; they generally measure between 0.6–0.9  $\mu\text{m}$  in wide and 3–8  $\mu\text{m}$  in length<sup>31</sup>. Vegetative cells commonly exhibit one of two morphological types: either slender, flexible rods with tapered ends, or cylindrical, rigid rods with rounded ends<sup>110</sup>.

Soil constitutes a primary natural habitat for myxobacteria<sup>31</sup>. These facultatively multicellular microorganisms are commonly found in topsoil environments and exhibit gliding motility, characterized by a smooth, non-rotational movement along the long axis of the cell<sup>95</sup>. During gliding, cells frequently pause and reverse direction, manifesting as ‘*stop-and-go*’ patterns under electron microscopy (see, e.g., Refs. 76, 77, 108). As they move, myxobacteria deposit a slime trail behind them on the substrate. Each cell produces a distinct slime trail, visible as a phase-bright

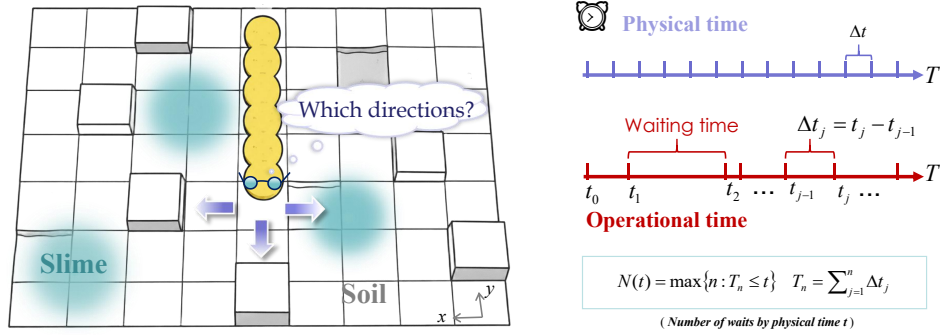


Fig. 1: Schematic illustration of myxobacterial gliding on a rough surface and the corresponding random-walk timelines. (a) Myxobacteria gliding on a rough surface: In the discrete agent model, each bacterium occupies connected grid cells. During each update, the bacterium moves forward by extending its head to one of the four nearest-neighbor sites that is not occupied by its own body. Blue shaded areas indicate regions of bacterial aggregation and high slime concentration. (b) Continuous time random walk timelines: The upper (blue) timeline represents physical time, sampled at regular intervals  $\Delta t$ , which corresponds to the waiting-time distribution  $\psi(t) = \delta(t - \Delta t)$ . The lower (red) timeline represents the internal (operational) time of the random-walk process, where each segment corresponds to a waiting time drawn from the distribution (2.1) for an individual movement event.

line, with clusters forming wider trails and single cells leaving narrower ones. When a cell encounters an existing trail, it tends to turn (probably through the acute angle of intersection), to follow the pre-deposited trail. This turning behavior is thought to arise from the alignment maximizing cohesive interactions between newly secreted slime filaments and those already present in the trail. For further biological details, see, e.g., Refs. 74, 94, 114.

Under starvation conditions, myxobacteria aggregate into large colonies and form fruiting bodies, ranging from 10 to 100  $\mu\text{m}$  in size<sup>135</sup>, through directed cell movement. It has been experimentally demonstrated that *Myxococcus* can detect and glide directly toward nearby colonies of potential prey to feed on them<sup>65</sup>. Fruiting body formation is induced by nutritional deficiency and is regulated by factors such as nutrient concentration, pH, cation availability, and temperature, see Ref. 31 for further details.

Building on this biological background, the following sections analyze the characteristic motility patterns of microorganisms, with particular emphasis on the gliding behavior of myxobacteria and the associated diffusion and dissipation dynamics of slime trails.

## 2.2. The discrete agent model for micro patterns

Building on the biological mechanisms detailed in Section 2.1, this section explores the chemotactic diffusion patterns of myxobacteria and the spatial evolution of slime on a  $100 \times 100$  square-grid domain subject to Neumann boundary conditions. These analyses lay the theoretical groundwork for the stochastic modeling presented hereafter.

Following established agent-based frameworks (see, e.g., Refs. 102, 116), we treat each cell as an autonomous agent governed by the simple rules introduced in Sec. 2.1, together with the

following specific assumptions (see Fig. 1 for an illustration):

- A.1.** Each myxobacteria is represented as an  $8 \times 1$  filament, occupying eight contiguous grid cells.
- A.2.** At each step, a myxobacterium glides to one of the four cells adjacent to its marked pole, which we refer to as the ‘head’ for descriptive purposes, though it carries no biological meaning.
- A.3.** The complex structure of soil acts as a formidable obstacle to myxobacteria, resulting in frequent and prolonged trapping events. This behavior is captured by a heavy-tailed power-law waiting-time distribution (cf. e.g., Ref. 75):

$$\psi(t) \sim \frac{\tau^\alpha}{t^{1+\alpha}}, \quad 0 < \alpha < 1, \quad (2.1)$$

where  $\tau$  is the characteristic time scale of the distribution.

Based on these assumptions, we construct a discrete lattice-based agent model as follows.

Let  $\mathcal{P} = \{1, 2, \dots, 100\}$  and define the set of lattice points as  $\mathcal{P}^2$ . We establish the discrete lattice model on  $\mathcal{P}^2$ . For each site  $x \in \mathcal{P}^2$ , let  $N_x$  be the set of its four nearest neighbors (up, down, left, right), as specified in Assumption **A.2.** and illustrated in Fig. 1 (a). Consistent with Assumption **A.1.**, the sites occupied by myxobacteria  $k$  at time  $t_j$  are given by  $\mathcal{B}_k(t_j) = \{(x_1, \dots, x_8) : x_i \in \mathcal{P}^2, i = 1, 2, \dots, 8\}$ , with head orientation  $h_k(t_j) \in \{(1, 0), (0, 1), (-1, 0), (0, -1)\}$ . Let  $\mathcal{I}_x(t_j) = \#\{y \in \mathcal{B}_k(t_j), k = 1, 2, \dots, m : x = y\}$  denote the number of myxobacteria segments covering lattice point  $x$  at time  $t_j$ . The bacterial density  $\mathcal{N}(x, t_j) : \mathcal{P}^2 \times \mathbb{N} \rightarrow \mathbb{R}_+$  and slime concentration  $\mathcal{C}(x, t_j) : \mathcal{P}^2 \times \mathbb{N} \rightarrow \mathbb{R}_+$  evolve according to production rates  $\kappa_n, \kappa_c \geq 0$  and decay rates  $\lambda_n, \lambda_s \geq 0$ , along with a slime diffusion coefficient  $D_c$ .

The dynamics of slime production are specified as follows. The myxobacterial density evolves according to the update rule in Ref. 116, given by

$$\mathcal{N}(x, t_{j+1}) = (1 - \lambda_n)\mathcal{N}(x, t_j) + \kappa_n \mathcal{I}_x(t_j), \quad \mathcal{N}(x, 0) = \kappa_n \mathcal{I}_x(0). \quad (2.2)$$

Slime dynamics are governed by a threshold-dependent production mechanism. Production commences at  $t_0(x)$ , defined as the first instant when  $\mathcal{I}_x(t_j) \geq M_1$  for some  $M_1 \in \mathbb{N}_+$ , with initial slime concentration set to  $\mathcal{C}(x, t_0) = \kappa_c \mathcal{I}_x(t_0)$ . Subsequently, slime is produced if either the occupancy exceeds  $M_1$  or the local slime concentration surpasses the sensing threshold  $M_2$ . The complete evolution, integrating diffusion, decay, and production (adapted from Ref. 116), is

$$\mathcal{C}(x, t_{j+1}) = \underbrace{(1 - \lambda_c)}_{\text{Decay}} \left( \underbrace{(1 - D_c)\mathcal{C}(x, t_j)}_{\text{Retention}} + \underbrace{\sum_{y \in N_x} \frac{D_c}{4} \mathcal{C}(y, t_j)}_{\text{Diffusion Inflow}} \right) + \underbrace{\kappa_c \mathcal{I}_x(t_j)}_{\text{Secretion}}. \quad (2.3)$$

If neither production condition is satisfied, the same update rule applies with the production term set to zero (i.e.,  $\kappa_c \mathcal{I}_x(t_j) = 0$ ). During the update process of slime concentration  $\mathcal{C}(\cdot, t_j)$  and myxobacteria density  $\mathcal{N}(\cdot, t_j)$ , the transition from the current time step  $t_j$  to the next  $t_{j+1}$  must follow the waiting-time distribution  $\psi(t)$  specified in (2.1), as prescribed by Assumption **A.3.** (see also Fig. 1 (b)).

In model (2.3), the term  $\kappa_c \mathcal{I}_x(t_j)$  acts as a ‘source term’, representing localized slime secretion by myxobacteria at a rate proportional to the local occupancy count  $\mathcal{I}_x$ . Spatial spreading of the chemical is governed by an isotropic diffusion scheme with coefficient  $D_c$ ; the term  $(1 - D_c)\mathcal{C}(x, t_j)$  accounts for mass retention at the current site, while the summation  $\sum_{y \in N_x} \frac{D_c}{4} \mathcal{C}(y, t_j)$  captures the diffusive flux from the four nearest neighbors ( $N_x$ ), each contributing one quarter of its

diffusing mass. The prefactor  $(1 - \lambda_c)$  models linear degradation or environmental evaporation of slime over each discrete time step.

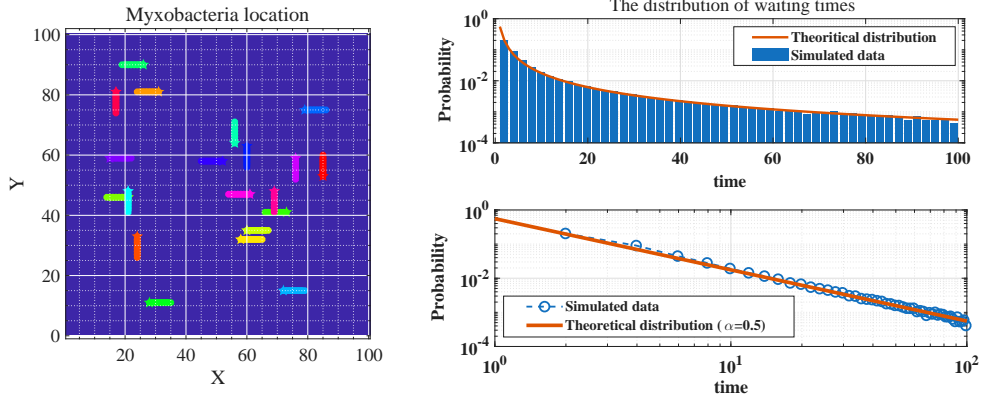


Fig. 2: (Color online) Microscopic simulation setup and statistical validation of the heavy-tailed waiting time distribution. (*Left*) Initial configuration: 20 myxobacteria are randomly distributed across a  $100 \times 100$  lattice. Each agent occupies 8 contiguous cells. Movement is restricted to four cardinal directions: up, down, left, and right, but are not allowed to reverse their direction abruptly. For instance, if an individual is currently moving upward, its next move may only proceed to the left, right, or continuing upward by one grid cell. Overlapping between different myxobacteria is permitted to simulate high-density aggregation. (*Right*) Comparative analysis of theoretical predictions and simulated waiting time distributions. The data are obtained from Fig. 3, based on statistics collected from 1000 agents over 1000 discrete steps ( $t_{min} = 1, t_{max} = 100$ ). The top-right inset presents a frequency histogram with a fitted curve, visually highlighting the heavy-tailed characteristic of the waiting time distribution. The bottom-right plot demonstrates the robust agreement between the theoretical model and simulated data under the exponent  $\alpha = 0.50$ , substantiating the use of time-nonlocal operators to capture anomalous delay effects.

To incorporate the observed directional persistence in myxobacterial motion, we introduce a directional weight factor  $d(\cdot, \cdot, \cdot)$  that biases the bacterium's 'head' toward grid points aligned with its current orientation in the next time step. Following Ref. 116, we define

$$d(x_0, y, h_k(t_j)) = \begin{cases} 10, & \text{if } y \text{ aligns with } h_k(t_j); \\ 1, & \text{otherwise.} \end{cases}$$

This weight ensures that, in the absence of chemotactic cues (i.e.,  $\mathcal{N} = 0$  and  $\mathcal{C} = 0$ ), the bacterium maintains its trajectory over a distance roughly comparable to its body length, thereby preventing non-physical, erratic reorientations.

Let  $w_n, w_c \geq 0$  denote the weight factors for myxobacteria density and slime concentration, respectively. The probability  $P_{k,x_0}(x, t+1)$  for the head of the  $k_{th}$  myxobacterium, initially located at  $x_0$  at time  $t_j$ , moves to a neighboring site  $x \in N_{x_0}$  with  $x \notin \mathcal{B}_k(t_j)$  at time  $t_{j+1}$  is define as<sup>116</sup>

$$P_{k,x_0}(x, t_{j+1}) = \frac{w_c \mathcal{C}(x, t_j) + (w_n \mathcal{N}(x, t_j) + \kappa_n) d(x_0, y, h_k(t_j))}{\sum_{y \in N_{x_0}, y \notin \mathcal{B}_k(t_j)} (w_c \mathcal{C}(y, t_j) + (w_n \mathcal{N}(y, t_j) + \kappa_n) d(x_0, y, h_k(t_j)))}, \quad (2.4)$$

with  $P_{k,x_0}(x, t_{j+1}) = 0$  for  $x \in \mathcal{B}_k(t_j)$ . This transition probability is shaped by three principal biological mechanisms:

- **Chemotaxis** ( $w_c \mathcal{C}$ ): biases the agent toward higher chemoattractant (slime) concentration; the weight  $w_c$  modulates the sensitivity to chemical gradients.
- **Contact Guidance** ( $w_n \mathcal{N} + \kappa_n$ ): encodes “trail-following” behavior, where  $w_n \mathcal{N}$  favors movement toward areas of higher historical bacterial density (i.e., existing slime trails), while the baseline constant  $\kappa_n$  ensures mobility in previously unexplored terrain.
- **Directional persistence**  $d(\cdot, \cdot, \cdot)$ : the multiplication of the contact guidance term by  $d(x_0, y, h_k(t_j))$  prioritizes alignment with the current heading, reflecting the mechanical difficulty that a rod-shaped bacterium faces when attempting sharp turns along a slime trail.
- **Normalization**: The denominator sums these weights over all neighboring sites not occupied by the bacterium’s own body ( $\mathcal{B}_k$ ), ensuring that  $\sum_x P_{k,x_0}(x, t_{j+1}) = 1$ .

Equation (2.3) governs the spatio-temporal evolution of slime concentration by integrating local secretion, isotropic grid-based diffusion, and linear decay. The stochastic motion of myxobacteria is then captured by the transition probability in (2.4). Together, these rules define a biased random walk whose movement direction is determined by a linearly weighted combination of three biological drivers: chemoattractant toward slime gradients, contact guidance along existing trails, and directional persistence along the current heading.

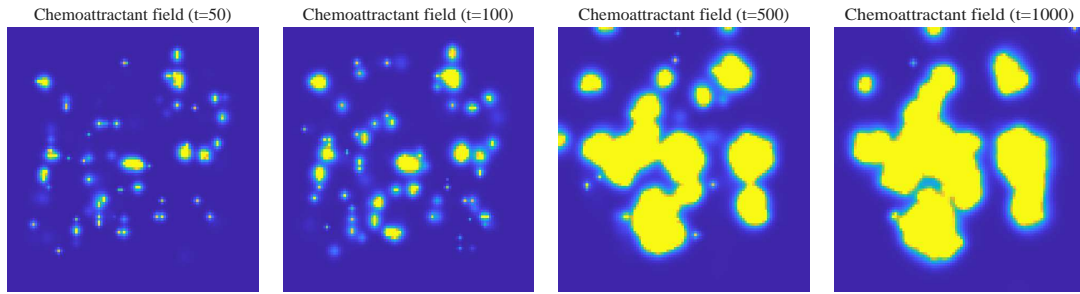


Fig. 3: (Color online) Spatiotemporal evolution of slime concentration  $c$  and the emergence of fruiting body patterns. This simulation tracks 1000 myxobacteria on a  $100 \times 100$  lattice, capturing the transition from stochastic gliding to collective aggregation. The numerical results demonstrate that the gliding motility of the bacteria, along with the diffusion and degradation of slime, largely reproduces the dynamical behaviors observed under laboratory microscopy. Specifically, the myxobacteria exhibit directed gliding toward regions of higher slime concentration and aggregate there. Upon reaching a critical density threshold ( $M_1 = 5$ ), these clusters secrete additional slime to facilitate social growth and structural reinforcement. The model effectively resolves the coarsening dynamics of the population, where adjacent spores merge into large-scale fruiting bodies while transient, smaller structures undergo apoptosis-like dissolution. Simulation parameters are set as:  $\Lambda_n = 0.10$ ,  $\Lambda_c = 0.02$ ,  $\kappa_n = 0.20$ ,  $\kappa_c = 0.30$ ,  $D_c = 1.00$ ,  $w_n = 11.00$ ,  $w_c = 111.00$ , with a fractional exponent  $\alpha = 0.50$  over 1000 time steps.

All the above simulations performed under the parameter regime  $d < w_n \ll w_c$  are illustrated in Figs. 2 and 3. These results demonstrate a robust qualitative agreement with biological obser-

vations documented in foundational cinematographic studies (e.g., 76, 77, 108). Such alignment with both classical experimental recordings and recent scholarly reviews 58, 94 corroborates our modeling framework and validates the hypotheses **A.1–A.3**.

### 2.3. Macroscopic dynamics via stochastic subordination

The microscopic stochastic simulations in the preceding section confirm the validity of our model assumptions (**A.1–A.3**) and corroborate the underlying biophysical mechanisms. Building on these physically plausible microscopic assumptions and the associated biological rationale, we now derive the macroscopic system (1.1) rigorously through a multiscale stochastic modeling approach. This derivation not only endows the model with a sound biophysical interpretation from the micro-scale up, but also highlights its accuracy and indispensability in capturing realistic chemotactic dynamics.

Following the standard theory of stochastic differential equations (see, e.g., Ref. 109), the classical Fokker-Planck equation is statistically equivalent to the Langevin dynamics  $\dot{x}(t) = A + \sqrt{2D}\dot{W}(t)$ , where  $W(t)$  is a standard Wiener process. Combining the biological mechanisms of myxobacteria described in Sec. 2.1 with the lattice-based agent model introduced in Sec. 2.2, we model the directed gliding motion toward aggregates via the subordinated Langevin equation

$$\dot{x}(t) = A(x(\mathcal{S}(t)), \mathcal{S}(t)) \dot{\mathcal{S}}(t) + \sqrt{2D} \dot{W}_{\mathcal{S}(t)}, \quad (2.5)$$

where  $\mathcal{S}(t) := \inf \{\bar{\tau} \geq 0 : T(\bar{\tau}) > t\}$  is the inverse  $\alpha$ -stable subordinator (see e.g., Ref. 9). The drift term  $A(x, t)$ , which characterizes the directional bias of gliding, is defined by

$$A(x, t) := \underbrace{\chi \delta_x^2 / (2\tau^\alpha)}_{(\text{coefficient})} \times \underbrace{v(x, t)^{-1} \cdot \partial_x v(x, t)}_{(\text{effective force field})}. \quad (2.6)$$

The quantity  $\delta_x^2 / (2\tau^\alpha)$  represents an effective mobility associated with the migration rate, with  $\delta_x$  the fixed gliding step and  $\tau$  the characteristic timescale in the waiting-time distribution (2.1). The logarithmic gradient  $\partial_x \ln v(x, t) = v(x, t)^{-1} \partial_x v(x, t)$  acts as an effective driving force generated by spatial variations in the concentration potential; this form follows from the asymptotic expansion of transition probabilities (see (A.3) in Sec. A.1 for details) and implies that bacteria preferentially move toward regions with higher potential. In the spatially homogeneous case  $\partial_x v = 0$ , the drift vanishes and the dynamics reduce to symmetric subdiffusion.

The process  $\dot{\mathcal{S}}(t)$  denotes increments in operational time<sup>92</sup>, which maps discrete gliding events onto physical time  $t$ . Biologically, this captures the “stop-and-go” motility of myxobacteria: each myxobacteria glides and then enters a trapped state for a random duration governed by a power-law distribution. During trapping intervals,  $\dot{\mathcal{S}}(t) = 0$ , so both deterministic forcing and stochastic fluctuations are effectively suspended; dynamical updates occur only upon escape, when  $\dot{\mathcal{S}}(t) > 0$ . Consequently, the particle experiences fluctuations solely during active displacement phases, leading to transport that is slower than classical Brownian diffusion.

The stochastic equation (2.5) is formally equivalent to the following system of coupled stochastic differential equations in the overdamped limit

$$\begin{cases} \dot{x}(t) = y(\mathcal{S}(t)), \\ \dot{y}(\bar{\tau}) = A(y(\bar{\tau}), \bar{\tau}) + \sqrt{2D} \dot{W}(\bar{\tau}). \end{cases} \quad (2.7)$$

The process  $T(\bar{\tau})$  acts as a “random clock” capturing the heavy-tailed waiting times and is characterized by the Laplace exponent  $\mathbb{E}[e^{-zT(\bar{\tau})}] = e^{-\bar{\tau}z^\alpha}$ ,  $z > 0$ , see Refs. 86, 89, 92. Here,  $\bar{\tau}$

denotes the operational time. Unlike the physical time variable  $t$ , the operational time evolves continuously during active motion, while the random clock  $\mathcal{S}(t)$  introduces intermittent trapping events and thereby produces anomalous temporal scaling. The noise term  $\mathcal{W}(\bar{\tau})$  is assumed to be Gaussian white noise, independent of the subordinator, with  $\langle \mathcal{W}(\bar{\tau}) \rangle = 0$  and  $\langle \mathcal{W}(\bar{\tau}_1) \mathcal{W}(\bar{\tau}_2) \rangle = \delta(\bar{\tau}_1 - \bar{\tau}_2)$ . In (2.7), inertial effects have been neglected. This overdamped approximation is justified because, in strongly dissipative media, the momentum relaxation time is much shorter than the characteristic waiting time associated with the power-law distribution (2.1). Hence, over the timescales relevant to aggregation dynamics, the motion is effectively governed by force balance rather than inertia.

Model (2.7) is thus constructed directly from the underlying biological mechanisms. On the operational timescale  $T(\bar{\tau})$ , the bacterium undergoes overdamped stochastic motion driven by the external concentration field governed by (2.3), while the mapping from operational time to physical time is determined by the heavy-tailed waiting-time distribution (2.1). As a result, the model consistently captures both chemotactic gliding and anomalous diffusive transport in a unified framework.

Starting from either the drift structure (2.6) or the stochastic system (2.7), we can derive the macroscopic equation (1.1a). Let  $\mathcal{G}(x, \bar{\tau})$  denote the probability density function (PDF) of the process  $y(\bar{\tau})$ . Then  $\mathcal{G}$  satisfies the classical Fokker-Planck equation (see, e.g., Refs. 33, 50, 91, 92),

$$\frac{\partial}{\partial \bar{\tau}} \mathcal{G}(x, \bar{\tau}) = -\frac{\partial}{\partial x} (A(x, \bar{\tau}) \mathcal{G}(x, \bar{\tau})) + \mathcal{D} \frac{\partial^2}{\partial x^2} \mathcal{G}(x, \bar{\tau}), \quad \mathcal{G}(x, 0) = n(x, 0). \quad (2.8)$$

Define the operator  $\mathcal{L}_x := -\frac{\partial}{\partial x} (A(x, \bar{\tau}) \cdot) + \mathcal{D} \frac{\partial^2}{\partial x^2}$ . Taking the Laplace transform with respect to the operation time  $\bar{\tau}$  gives

$$s \widehat{\mathcal{G}}(x, s) - \mathcal{G}(x, 0) = \mathcal{L}_x \widehat{\mathcal{G}}(x, s), \quad \forall s \in \mathbb{C}, \quad (2.9)$$

and hence  $\widehat{\mathcal{G}}(x, s) = (s - \mathcal{L}_x)^{-1} \mathcal{G}(x, 0)$ . Next, let  $\mathcal{H}(\bar{\tau}, t)$  denote the PDF of the inverse  $\alpha$ -stable subordinator  $S(t)$ . Its Laplace transform with respect to  $t$  satisfies (see (6)-(7) in Ref. 92)

$$\mathfrak{L}_{t \rightarrow z} \{ \mathcal{H}(\bar{\tau}, t) \} = -\partial_{\bar{\tau}} (e^{-\bar{\tau} z^\alpha}) z^{-1} = z^{\alpha-1} e^{-\bar{\tau} z^\alpha}, \quad \forall z \in \mathbb{C}. \quad (2.10)$$

Now let  $n(x, t)$  denote the PDF of the process  $y(\mathcal{S}(t))$  (equivalently,  $x(t)$ ). By the total probability formula and the independence of  $y(\bar{\tau})$  and  $\mathcal{S}(t)$ , we get that the PDF  $n(x, t) = \int_0^\infty \mathcal{G}(x, \bar{\tau}) \mathcal{H}(\bar{\tau}, t) d\bar{\tau}$  (see Ref. 97). Taking the Laplace transform with respect to  $t$  yields  $\widehat{n}(x, z) = z^{\alpha-1} \widehat{\mathcal{G}}(x, z^\alpha)$  (cf. (9) in Ref. 92). Substituting  $s = z^\alpha$  into the resolvent representation above gives A.1

$$\widehat{\mathcal{G}}(x, z^\alpha) = (z^\alpha - \mathcal{L}_x)^{-1} \mathcal{G}(x, 0), \quad (2.11)$$

which implies

$$z \widehat{n}(x, z) - n(x, 0) = z^{1-\alpha} \mathcal{L}_x \widehat{n}(x, z). \quad (2.12)$$

For  $\alpha \in (0, 1)$ , applying the inverse Laplace transform together with the standard identities for Riemann-Liouville fractional operators, namely  $\mathfrak{L}_{t \rightarrow z} \{ {}_0 D_t^{1-\alpha} f(t) \} = z^{1-\alpha} \widehat{f}(z)$  and  ${}_0 I_t^{1-\alpha} (\frac{d}{dt} n(x, t)) = {}_0^C \mathfrak{D}_t^\alpha n(x, t)$ , yields the fractional Fokker-Planck equation

$${}_0^C \mathfrak{D}_t^\alpha n(x, t) = -\chi \mathcal{D} \frac{\partial}{\partial x} \left( \frac{n(x, t)}{v(x, t)} \frac{\partial}{\partial x} v(x, t) \right) + \mathcal{D} \frac{\partial^2 n(x, t)}{\partial x^2}, \quad \forall t > 0. \quad (2.13)$$

Here,

$${}_0I_t^{1-\alpha}u(t) := \frac{1}{\Gamma(\alpha)} \int_0^t (t-s)^{\alpha-1}u(s)ds$$

and

$${}_0D_t^{1-\alpha}f(t)u(t) := \frac{1}{\Gamma(1-\alpha)} \frac{d}{dt} \int_0^t (t-s)^{-\alpha}u(s)ds$$

denote the Riemann-Liouville fractional integral and derivative, respectively (see, e.g., Ref. 104).

Finally, extending the single-particle dynamics (2.5) to a system of interacting particles leads to the macroscopic equation (1.1a); see, for instance, Ref. 115). Specifically, the trajectory of the  $i_{th}$  particle is governed by

$$\dot{x}_i(t) = A(x_i(\mathcal{S}_i(t)), \mathcal{S}_i(t)) \dot{\mathcal{S}}_i(t) + \sqrt{2\mathcal{D}} \dot{\mathcal{W}}_{\mathcal{S}_i(t)}^{(i)}, \quad (2.14)$$

where  $\mathcal{W}^{(i)}$  are mutually independent Wiener processes and  $\{\mathcal{S}_i(t)\}_{i \geq 1}$  are independent inverse  $\alpha$ -stable subordinators. Thus, each particle possesses its own random waiting clock, corresponding to an independent continuous-time random walk. Since independent superposition preserves the one-particle statistical law, the collective particle density still satisfies the fractional Fokker-Planck equation (2.13). Setting  $v(x, t) = c(x, t)$ , where  $c(x, t)$  denotes the slime concentration (as described later), (2.13) directly reduces to (1.1a), which is the target macroscopic equation.

**Remark 2.1.** The quantity  $\delta_x^2/(2\tau^\alpha)$ , which has physical dimension [length<sup>2</sup>/time <sup>$\alpha$</sup> ], serves as a generalized diffusion coefficient and characterizes the effective transport rate of particles in the medium. Here,  $\delta_x^2$  denotes the characteristic jump intensity, while  $\tau^\alpha$  captures the temporal memory effect induced by the heavy-tailed waiting-time distribution. The ratio  $\delta_x^2/(2\tau^\alpha)$  thus quantifies the balance between particle mobility and trapping effects. In the classical diffusive regime  $\alpha = 1$ , this expression reduces to the standard diffusion coefficient  $\mathcal{D} = \delta_x^2/(2\tau)$ , which has physical dimension [length<sup>2</sup>/time]. Hence,  $\delta_x^2/(2\tau^\alpha)$  can be regarded as a natural generalization of the classical diffusion coefficient to anomalous diffusion, linking the microscopic stochastic parameters ( $\delta_x, \tau$ ) to the macroscopic transport behavior characterized by  $\mathcal{D}$ .

**Remark 2.2.** The field  $v(x, t)$  primarily characterizes the influence of the chemoattractant concentration on bacterial chemotaxis, governing the directional bias of cell movement. Varying  $v(x, t)$  provides considerable modeling flexibility and naturally leads to different macroscopic formulations. For instance, setting  $v(x, t) = c(x, t)$  recovers the macroscopic equation derived in this work. Alternatively, choosing the exponential form  $v(x, t) = \exp(-\beta c(x, t))$  (see, e.g., Ref. 78) regularizes the chemotactic sensitivity and yields a non-singular drift term of the form  $-\mathcal{D}\chi \nabla \cdot (n(x, t)\nabla c(x, t))$ .

Similarly, to describe slime diffusion in a multi-particle setting, we consider the subordinated Langevin equation

$$\dot{x}_i(t) = \sqrt{2\mathcal{D}} \dot{\mathcal{W}}_{\mathcal{S}_i(t)}^{(i)}, \quad (2.15)$$

which corresponds to purely diffusive motion without directional bias. Here,  $\mathcal{W}^{(i)}_{i \geq 1}$  are mutually independent Wiener processes, and  $\mathcal{S}_i(t)_{i \geq 1}$  are independent inverse  $\alpha$ -stable subordinators

that account for trapping effects and anomalous waiting times. Applying the same subordination argument as above yields the time-fractional Fokker–Planck equation

$${}_0^C \mathfrak{D}_t^\alpha c(x, t) = \frac{\delta_x^2}{2\tau^\alpha} \frac{\partial^2 c(x, t)}{\partial x^2}, \quad (2.16)$$

which describes the anomalous diffusion of the slime concentration field  $c(x, t)$ .

The remaining reaction terms in (1.1b) cannot be derived directly from the stochastic dynamics (2.15), as they originate from biological processes rather than random motion. Specifically, following Refs. 86, 116, the term  $-\gamma c(x, t)$  models the natural degradation of slime at rate  $\gamma$ , while  $+n(x, t)$  represents slime production induced by myxobacterial aggregation and activity. Incorporating these biologically motivated mechanisms into the fractional diffusion equation yields the macroscopic model (1.1b).

### 3. Solution Theory

#### 3.1. Preliminaries

Let  $\Omega \subset \mathbb{R}^d$  (with  $d \geq 2$ ) denote an open bounded domain with smooth boundary  $\partial\Omega$ . We begin by briefly recalling several function spaces used throughout this work.

For any  $\kappa \in \mathbb{N}_+$  and  $1 \leq p \leq \infty$ , let  $L^p(\Omega)$  and  $W^{\kappa,p}(\Omega)$  denote the usual Lebesgue and Sobolev spaces, respectively, as outlined in Refs. 2, 44, 62. When  $0 < \kappa < 1$  and  $1 \leq p < \infty$ , the Sobolev space  $W^{\kappa,p}(\Omega)$  is referred to as fractional Sobolev space, which is defined as

$$W^{\kappa,p}(\Omega) = \left\{ \omega \in L^p(\Omega) : |\omega|_{W^{\kappa,p}} := \left( \int_{\Omega} \int_{\Omega} \frac{|\omega(\mathbf{x}) - \omega(\mathbf{y})|^p}{|\mathbf{x} - \mathbf{y}|^{d+p\kappa}} d\mathbf{x} d\mathbf{y} \right)^{1/p} < \infty \right\},$$

equipped with the norm of  $\|\omega(\mathbf{x}, t)\|_{W^{\kappa,p}} := (\|\omega(\mathbf{x}, t)\|_{L^p}^p + |\omega(\mathbf{x}, t)|_{W^{\kappa,p}}^p)^{1/p}$ . Under the smoothness assumption on  $\partial\Omega$ , fractional Sobolev spaces may also be characterized via the  $K$ -method of interpolation. In particular, for  $0 < \kappa < 1$  and  $p = 2$ , the Hilbertian Sobolev spaces are denoted by  $H^\kappa(\Omega) := [L^2(\Omega), H^1(\Omega)]_\kappa$  (see, e.g., Ref. 62), with equivalent norms.

Let  $\mathcal{A} = -\Delta$  be the Neumann Laplacian on  $L^p(\Omega)$  with domain (e.g., Ref. 120)

$$D(\mathcal{A}) := \left\{ \omega(\mathbf{x}) \in W^{2,p}(\Omega) : \frac{\partial \omega(\mathbf{x})}{\partial \nu} = 0 \text{ on } \partial\Omega \right\}.$$

where  $\nu$  denotes the outward unit normal vector on  $\partial\Omega$ . It is well-known that for a bounded domain  $\Omega$  with smooth boundary,  $\mathcal{A}$  is a closed sectorial operator on  $L^p(\Omega)$  and generates a bounded analytic semigroup  $\{e^{-t\mathcal{A}}\}_{t \geq 0}$  on  $L^p(\Omega)$ . The associated eigenvalue problem reads

$$\begin{cases} \mathcal{A}\varphi_j = \lambda_j \varphi_j, & \text{in } \Omega, \\ \frac{\partial \varphi_j}{\partial \nu} = 0, & \text{on } \partial\Omega, \end{cases} \quad j = 1, 2, \dots \quad (3.1)$$

The sequence of eigenvalues satisfies  $0 = \lambda_1 < \lambda_2 \leq \lambda_3 \leq \dots$ ,  $\lambda_j \rightarrow \infty$  ( $j \rightarrow \infty$ ), and the corresponding eigenfunctions  $\{\varphi_j\}_{j=1}^\infty$  form a complete orthonormal basis of  $L^2(\Omega)$ , i.e.,  $\|\varphi_j\|_{L^2} = 1$ ,  $(\varphi_i, \varphi_j)_\Omega = \delta_{ij}$  with  $(\cdot, \cdot)_\Omega$  denoting the  $L^2$  inner product defined on  $\Omega$ . Accordingly, for  $s \geq 0$ , the spectral Sobolev space associated with the Neumann Laplacian defined by

$$H_{\mathcal{A}}^s(\Omega) = \mathcal{D}((I + \mathcal{A})^{s/2}) := \left\{ \omega \in L^2(\Omega) : \sum_{j=1}^{\infty} (1 + \lambda_j)^s \left( \int_{\Omega} \omega \varphi_j d\mathbf{x} \right)^2 < \infty \right\}.$$

The norm is naturally given by  $\|\omega\|_{H_{\mathcal{A}}^s}^2 = \sum_{j=1}^{\infty} (1 + \lambda_j)^s |(\omega, \varphi_j)_{\Omega}|^2$ .

**Remark 3.1.** Since  $\Omega \subset \mathbb{R}^d$  ( $d \geq 2$ ) is a bounded domain with smooth boundary, the spectral spaces  $H_{\mathcal{A}}^s(\Omega)$  are equivalent to the classical Sobolev spaces  $H^s(\Omega)$  (see, e.g., Refs. 7, 22, 40). Consequently, the standard Sobolev and Morrey embeddings remain valid for  $H_{\mathcal{A}}^s(\Omega)$ . More precisely, the following continuous embeddings hold.

- (i) If  $0 \leq s < d/2$  and  $2 \leq p \leq \frac{2d}{d-2s}$ , then  $H_{\mathcal{A}}^s(\Omega) \hookrightarrow L^p(\Omega)$ . If  $s = d/2$ , then  $H_{\mathcal{A}}^s(\Omega) \hookrightarrow L^p(\Omega)$ ,  $2 \leq p < \infty$ .
- (ii) If  $s > d/2$ , then  $H_{\mathcal{A}}^s(\Omega) \hookrightarrow C^{0,\mu}(\overline{\Omega})$  with  $\mu \in (0, s - d/2)$ .
- (iii) If  $-d/2 < s \leq 0$  and  $p \geq \frac{2d}{d-2s}$ , then  $L^p(\Omega) \hookrightarrow H_{\mathcal{A}}^s(\Omega)$ .
- (iv) For all  $p > d$ , the embedding  $W^{1,p}(\Omega) \hookrightarrow C^{0,1-d/p}(\overline{\Omega}) \hookrightarrow L^{\infty}(\Omega)$  is valid.
- (v) For every  $1 < p < \infty$ , the shifted square-root norm of the Neumann Laplacian is equivalent to the  $W^{1,p}$ -norm; more precisely,  $D((I + \mathcal{A})^{1/2}) = W^{1,p}(\Omega)$  with equivalent norms, and  $\|u\|_{W^{1,p}} \simeq \|(I + \mathcal{A})^{1/2}u\|_{L^p}$ . In particular,  $\|u\|_{W^{1,p}} \leq C(\|u\|_{L^p} + \|\mathcal{A}^{1/2}u\|_{L^p})$ .

The embeddings in (i)–(iv) follow from the classical Sobolev embedding theorem together with the equivalence between the spectral and classical Sobolev scales on smooth bounded domains; see, for instance, Refs. 2, 22, 44, 120. Furthermore, the assertion in (v) is based on the  $L^p$  square-root estimate for the Neumann Laplacian (see, e.g., Ref. 11) and on the  $L^p$ -boundedness of the associated Neumann Riesz transform (see, e.g., Ref. 60, 98). More precisely, for every  $1 < p < \infty$ ,  $\|\mathcal{A}_p^{1/2}u\|_{L^p} \simeq \|\nabla u\|_{L^p}$ . Here the estimate  $\|\mathcal{A}_p^{1/2}u\|_{L^p} \leq C\|\nabla u\|_{L^p}$  is the  $L^p$  square-root estimate, while the converse estimate  $\|\nabla u\|_{L^p} \leq C\|\mathcal{A}_p^{1/2}u\|_{L^p}$  is the boundedness of the Neumann Riesz transform  $\nabla \mathcal{A}_p^{-1/2}$ , understood through the functional calculus of the Neumann Laplacian. Consequently,  $\|u\|_{W^{1,p}} \simeq \|u\|_{L^p} + \|\mathcal{A}_p^{1/2}u\|_{L^p} \simeq \|(I + \mathcal{A}_p)^{1/2}u\|_{L^p}$ .

Additionally, we present the following lemmas to support subsequent analysis and validation efforts.

**Lemma 3.1 (Comparison principle<sup>5</sup>).** *Let  $\Omega \subset \mathbb{R}^d$  ( $d \geq 2$ ) be a bounded domain with smooth boundary, and let  $\mathcal{A} = -\Delta$ . Suppose that  $\omega(\mathbf{x}, t) \in C([0, T]; H^2(\Omega))$  satisfies*

$$\begin{cases} {}_0^C \mathfrak{D}_t^\alpha \omega + \mathcal{A}\omega + \gamma\omega \geq 0, & \text{in } \Omega \times (0, T], \\ \partial_\nu \omega = 0, & \text{on } \partial\Omega \times (0, T], \\ \omega(\mathbf{x}, 0) \geq 0, & \text{in } \Omega, \end{cases} \quad (3.2)$$

where  $\gamma \geq 0$  is a constant. Then  $\omega \geq 0$  holds in  $\Omega \times [0, T]$ .

**Lemma 3.2 (Generalized Grönwall inequality<sup>6</sup>).** *Let  $y(t)$  be a non-negative, absolutely continuous function satisfying the fractional differential inequality*

$${}_0^C \mathfrak{D}_t^\alpha y(t) \leq C_1 y(t) + C_2(t), \quad 0 < \alpha \leq 1,$$

for almost all  $t$  in  $[0, T]$ , where  $C_1 > 0$  and  $C_2(t)$  is an integrable nonnegative function on  $[0, T]$ . Then

$$y(t) \leq y(0)E_\alpha(C_1 t^\alpha) + \Gamma(\alpha) E_{\alpha,\alpha}(C_1 t^\alpha) {}_0 I_t^\alpha (C_2(t)), \quad (3.3)$$

where  $E_\alpha(z)$  and  $E_{\alpha,\beta}(z)$  are the one- and two-parameter Mittag-Leffler functions defined by  $E_\alpha(z) := \sum_{n=0}^{\infty} z^n / \Gamma(\alpha n + 1)$  and  $E_{\alpha,\beta}(z) := \sum_{n=0}^{\infty} z^n / \Gamma(\alpha n + \beta)$ , respectively.  ${}_0 I_t^\alpha u(t) := \frac{1}{\Gamma(\alpha)} \int_0^t (t-s)^{1-\alpha} u(s) ds$  denotes the Riemann-Liouville fractional integral.

### 3.2. Main results

Building upon the functional spaces and notations established earlier, we now present the primary well-posedness results for problem (1.1). Detailed proofs of these theorems will be provided in the subsequent sections. To this end, we assume that the initial data  $n_0(\mathbf{x})$  and  $c_0(\mathbf{x})$  satisfy the following assumptions

$$\begin{cases} n_0(\mathbf{x}) \in C^0(\overline{\Omega}) \text{ with } n_0 \geq 0 \text{ in } \Omega \text{ and } n_0 \not\equiv 0; \\ c_0(\mathbf{x}) \in W^{1,\infty}(\Omega) \text{ such that } c_0 > 0 \text{ in } \overline{\Omega}. \end{cases} \quad (3.4)$$

These regularity and positivity assumptions are natural from a modeling perspective and essential for establishing the well-posedness of the system (1.1). The continuity of  $n_0(\mathbf{x})$  and  $W^{1,\infty}(\Omega)$  regularity of  $c_0(\mathbf{x})$  ensure that the initial configurations are physically meaningful, while the non-negativity and positivity conditions reflect the biological interpretations of myxobacteria density and slime concentration, respectively.

Let  $C(\overline{\Omega} \times [0, \infty))$  be the space of continuous functions on  $\overline{\Omega} \times [0, \infty)$ , and let  $C([0, \infty); W^{1,p}(\Omega))$  be the space of continuous functions from  $[0, \infty)$  into  $W^{1,p}(\Omega)$ , with  $p > d$ . Under the assumptions given in (3.4), the primary results on the solution theory for problem (1.1) are stated in the following theorems.

**Theorem 3.1.** *Let  $\Omega \subset \mathbb{R}^d$  ( $d \geq 2$ ) be a bounded domain with smooth boundary. Assume that the initial data  $n_0(\mathbf{x})$  and  $c_0(\mathbf{x})$  satisfy (3.4). Then, for all  $t > 0$ , the solution component  $n(\mathbf{x}, t)$  of problem (1.1) satisfies the mass conservation law,*

$$\int_{\Omega} n(\mathbf{x}, t) \, d\mathbf{x} = \int_{\Omega} n_0(\mathbf{x}) \, d\mathbf{x}, \quad (3.5)$$

while the component  $c(\mathbf{x}, t)$  satisfies the following estimate,

$$\int_{\Omega} c(\mathbf{x}, t) \, d\mathbf{x} \leq \max \left\{ \frac{t^\alpha}{\Gamma(1+\alpha)} \int_{\Omega} n_0(\mathbf{x}) \, d\mathbf{x}, \int_{\Omega} c_0(\mathbf{x}) \, d\mathbf{x} \right\}. \quad (3.6)$$

To facilitate further analysis of system (1.1), we introduce a novel fractional Lyapunov functional of the form (detailed in Sec. 6.1) as follows

$$\mathcal{E}[(n, c)](t) := \int_0^t (t-s)^{\alpha-1} \mathcal{F}(s) \, ds, \quad t > 0, \quad (3.7)$$

where the integrand  $\mathcal{F}$  is a jointly convex functional given by

$$\mathcal{F}(t) := \mathcal{F}[(n, c)](t) = \int_{\Omega} n \log \left( \frac{n}{\bar{n}} \right) \, d\mathbf{x} + \theta \int_{\Omega} \frac{|\nabla c|^2}{c} \, d\mathbf{x}. \quad (3.8)$$

Here,  $\bar{n} := \frac{1}{|\Omega|} \int_{\Omega} n \, d\mathbf{x}$  denotes the spatial average of  $n$ , and  $\theta$  is specified positive constant. We show that  $\mathcal{F}(t) \leq \mathcal{F}(0)$  and  $\mathcal{E}[(n, c)](t) < \infty$  for all  $t \in [0, \infty)$  (see Lemma 6.3). Crucially, this uniform upper bound provides a key priori estimate that prevents finite-time blow-up and underpins the global existence of solutions. The resulting regularity and stability properties are stated in Theorem 3.2.

**Theorem 3.2.** *Let  $\Omega \subset \mathbb{R}^d$  ( $d = 2, 3$ ) be a bounded domain with smooth boundary. Suppose  $0 < \chi < 1/2$ , and assume the initial data  $n_0(\mathbf{x})$  and  $c_0(\mathbf{x})$  satisfy (3.4). Then, for  $p > d$ , problem*

(1.1) admits a unique global mild solution  $(n(\mathbf{x}, t), c(\mathbf{x}, t))$  possessing the following regularity properties:

$$\begin{cases} n \in C([0, \infty); L^\infty(\Omega)) \cap C^{0, \alpha/2}((0, \infty); W^{1,p}(\Omega)) \cap C((0, \infty); D(\mathcal{A})), \\ c \in C([0, \infty); W^{1,p}(\Omega)) \cap C^{0, \alpha/2}((0, \infty); W^{2,p}(\Omega)) \cap C((0, \infty); D(\mathcal{A})). \end{cases} \quad (3.9)$$

Furthermore, the solution satisfies  $n(\mathbf{x}, t) \geq 0$  and  $c(\mathbf{x}, t) > 0$  in  $\Omega \times (0, \infty)$ , along with the uniform bound

$$\sup_{t>0} (\|n(\cdot, t)\|_{L^\infty} + \|c(\cdot, t)\|_{W^{1,p}}) \leq M. \quad (3.10)$$

The proofs of Theorems 3.1 and 3.2 are carried out in the subsequent sections via a series of lemmas. Our approach integrates novel energy estimates, refined regularity analysis, and several new PDE techniques to establish a robust framework capable of handling the intrinsic difficulties of System (1.1).

Before turning to the proofs, we fix the convention that, throughout the estimates below,  $C$  denotes a generic positive constant independent of  $t$  and  $T$ , whose value may vary from line to line.

#### 4. Fundamental Lemmas for the Solution Theory

Before we get into the main proofs, let's lay down some basic tools. In this section, we introduce a few auxiliary functions and some handy lemmas will support our construction of the solution theory.

Let's begin with a useful special function. For  $\kappa > -1$  and  $\lambda \in \mathbb{C}$ , the Wright function  $W(\kappa, \lambda; z)$  is defined by the series (see Ref. 73 )

$$W(\kappa, \lambda; z) := \sum_{j=0}^{\infty} \frac{z^j}{j! \Gamma(\kappa j + \lambda)}, \quad \forall z \in \mathbb{C}, \quad (4.1)$$

where  $\Gamma(\cdot)$  denotes the Euler–Gamma function. When  $\kappa > -1$ , this series converges for all  $z$ , so  $W(\kappa, \lambda; z)$  is an entire function. A particularly important special case is when  $\kappa = -\alpha$  and  $\lambda = 1 - \alpha$ . Then the Wright function becomes the Mainardi function  $M_\alpha(z)$ , which satisfies the neat integral identity<sup>27,62,87,88</sup>

$$\int_0^\infty t^\gamma M_\alpha(t) dt = \frac{\Gamma(1 + \gamma)}{\Gamma(1 + \alpha\gamma)}, \quad \gamma > -1. \quad (4.2)$$

Now we set up the operators needed for our analysis. Recall that  $\mathcal{A} := -\Delta$  be the Neumann Laplacian on  $L^p(\Omega)$ , and  $\mathcal{A}_\gamma := \mathcal{A} + \gamma I$  with  $\gamma > 0$ . Then,  $-\mathcal{A}$  generates the usual Neumann heat semigroup  $e^{-t\mathcal{A}} = e^{t\Delta}$ , while  $-\mathcal{A}_\gamma$  generates its exponentially damped version  $e^{-t\mathcal{A}_\gamma} = e^{t(\Delta - \gamma)} = e^{-\gamma t} e^{t\Delta}$  for  $t > 0$ . Both semigroups are bounded on  $L^p(\Omega)$  and enjoy the standard heat-kernel smoothing estimates from  $L^p(\Omega)$  to  $L^p(\Omega)$  for suitable exponents  $1 \leq q \leq p \leq \infty$  (see, e.g., Refs. 89, 130).

To represent mild solutions of System (1.1), we require the Mittag-Leffler operator families associated with  $\mathcal{A}$  and  $\mathcal{A}_\gamma$ . Using the scalar functions  $E_{\alpha, \beta}$  (with  $E_\alpha := E_{\alpha, 1}$ ) recalled from the previous section, we now define the families  $\{E_\alpha(-t^\alpha \mathcal{A})\}_{t \geq 0}$ ,  $\{E_{\alpha, \alpha}(-t^\alpha \mathcal{A})\}_{t \geq 0}$ , along with their  $\mathcal{A}_\gamma$ -analogues  $\mathcal{A}_\gamma$ -analogues  $\{E_\alpha(-t^\alpha \mathcal{A}_\gamma)\}_{t \geq 0}$ ,  $\{E_{\alpha, \alpha}(-t^\alpha \mathcal{A}_\gamma)\}_{t \geq 0}$ .

A useful bridge between these time-nonlocal operator families and the standard heat semigroup is provided by the Mainardi function  $M_\alpha$ , via the integral identities

$$\begin{cases} E_\alpha(-t^\alpha \mathcal{A}) := \int_0^\infty M_\alpha(s) e^{st^\alpha \Delta} ds, & E_\alpha(-t^\alpha \mathcal{A}_\gamma) := \int_0^\infty M_\alpha(s) e^{st^\alpha (\Delta - \gamma)} ds, \\ E_{\alpha, \alpha}(-t^\alpha \mathcal{A}) := \int_0^\infty \alpha s M_\alpha(s) e^{st^\alpha \Delta} ds, & E_{\alpha, \alpha}(-t^\alpha \mathcal{A}_\gamma) := \int_0^\infty \alpha s M_\alpha(s) e^{st^\alpha (\Delta - \gamma)} ds. \end{cases} \quad (4.3)$$

These representations will be instrumental in the subsequent derivation of smoothing estimates and time-regularity properties. We collect their main properties in the following lemmas.

**Lemma 4.1 (Continuity<sup>27,88</sup>).** *For each  $1 \leq q < \infty$ , the Mittag-Leffler operator families associated with  $\mathcal{A}$  and  $\mathcal{A}_\gamma$ , namely  $\{E_\alpha(-t^\alpha \mathcal{A})\}_{t \geq 0}$ ,  $\{E_\alpha(-t^\alpha \mathcal{A}_\gamma)\}_{t \geq 0}$ ,  $\{E_{\alpha, \alpha}(-t^\alpha \mathcal{A})\}_{t \geq 0}$ , and  $\{E_{\alpha, \alpha}(-t^\alpha \mathcal{A}_\gamma)\}_{t \geq 0}$  are strongly continuous in  $t > 0$  on  $L^q(\Omega)$ .*

Utilizing the  $L^p$ - $L^q$  estimates for the Neumann heat semigroup from Refs. 88, 130, we derive the following estimates for the Mittag-Leffler operators.

**Lemma 4.2 ( $L^p$ - $L^q$  estimates).** *Let  $\mathcal{A} = -\Delta$  be the Neumann Laplacian on  $L^p(\Omega)$  with homogeneous Neumann boundary conditions, and set  $\mathcal{A}_\gamma := \mathcal{A} + \gamma I$  with  $\gamma > 0$ . The operators  $E_\alpha(-t^\alpha \mathcal{A})$ ,  $E_{\alpha, \alpha}(-t^\alpha \mathcal{A})$ , and their  $\mathcal{A}_\gamma$  counterparts are defined as in (4.3). For every  $t > 0$  and  $1 \leq q \leq p \leq \infty$ , there exist positive constants  $\{c_j\}_{j \in \mathbb{N}_+}$ , dependent only on  $\Omega$ ,  $\alpha$ ,  $d$ ,  $q$  and  $p$ , such that the following estimates hold:*

$$\|E_\alpha(-t^\alpha \mathcal{A})\|_{L^q \rightarrow L^p} \leq c_1 \left(1 + t^{-\frac{\alpha d}{2}(\frac{1}{q} - \frac{1}{p})}\right), \quad \frac{d}{2} \left(\frac{1}{q} - \frac{1}{p}\right) < 1; \quad (4.4)$$

$$\|E_{\alpha, \alpha}(-t^\alpha \mathcal{A}) \nabla \cdot\|_{L^q \rightarrow L^p} \leq c_2 \left(1 + t^{-\frac{\alpha}{2} - \frac{\alpha d}{2}(\frac{1}{q} - \frac{1}{p})}\right), \quad \frac{d}{2} \left(\frac{1}{q} - \frac{1}{p}\right) < \frac{3}{2}; \quad (4.5)$$

$$\|\mathcal{A}^{1/2} E_{\alpha, \alpha}(-t^\alpha \mathcal{A})\|_{L^q \rightarrow L^p} \leq c_3 \left(1 + t^{-\frac{\alpha}{2} - \frac{\alpha d}{2}(\frac{1}{q} - \frac{1}{p})}\right), \quad \frac{d}{2} \left(\frac{1}{q} - \frac{1}{p}\right) < \frac{3}{2}; \quad (4.6)$$

$$\|E_{\alpha, \alpha}(-t^\alpha \mathcal{A}_\gamma)\|_{L^q \rightarrow L^p} \leq c_4 \left(1 + t^{-\frac{\alpha d}{2}(\frac{1}{q} - \frac{1}{p})}\right), \quad \frac{d}{2} \left(\frac{1}{q} - \frac{1}{p}\right) < 1; \quad (4.7)$$

$$\|E_{\alpha, \alpha}(-t^\alpha \mathcal{A}_\gamma) \nabla \cdot\|_{L^q \rightarrow L^p} \leq c_5 \left(1 + t^{-\frac{\alpha}{2} - \frac{\alpha d}{2}(\frac{1}{q} - \frac{1}{p})}\right), \quad \frac{d}{2} \left(\frac{1}{q} - \frac{1}{p}\right) < \frac{3}{2}; \quad (4.8)$$

$$\|\mathcal{A}^{1/2} E_{\alpha, \alpha}(-t^\alpha \mathcal{A}_\gamma)\|_{L^q \rightarrow L^p} \leq c_6 \left(1 + t^{-\frac{\alpha}{2} - \frac{\alpha d}{2}(\frac{1}{q} - \frac{1}{p})}\right), \quad \frac{d}{2} \left(\frac{1}{q} - \frac{1}{p}\right) < \frac{3}{2}. \quad (4.9)$$

**Proof.** Fix  $1 \leq q \leq \infty$  and  $\omega(\mathbf{x}, t) \in L^q(\Omega)$ . To prove (4.4), we use the identity (4.2) together with the heat semigroup estimate under homogenous Neumann boundary conditions (Lemma 3.1 (17) in Ref. 88). This gives

$$\begin{aligned} \|E_\alpha(-t^\alpha \mathcal{A}) \omega(\mathbf{x}, t)\|_{L^p} &\leq \int_0^\infty M_\alpha(s) \left\| e^{st^\alpha \Delta} \omega(\mathbf{x}, t) \right\|_{L^p} ds \\ &\leq C \int_0^\infty M_\alpha(s) \left(1 + (st^\alpha)^{-\frac{d}{2}(\frac{1}{q} - \frac{1}{p})}\right) \|\omega(\mathbf{x}, t)\|_{L^q} ds \\ &\leq C \left(1 + t^{-\frac{\alpha d}{2}(\frac{1}{q} - \frac{1}{p})} \frac{\Gamma(1 - \frac{d}{2}(\frac{1}{q} - \frac{1}{p}))}{\Gamma(1 + \alpha(-\frac{d}{2}(\frac{1}{q} - \frac{1}{p})))}\right) \|\omega(\mathbf{x}, t)\|_{L^q} \\ &\leq C \left(1 + t^{-\frac{\alpha d}{2}(\frac{1}{q} - \frac{1}{p})}\right) \|\omega(\mathbf{x}, t)\|_{L^q}, \quad t > 0. \end{aligned}$$

The condition  $\frac{d}{2}(\frac{1}{q} - \frac{1}{p}) < 1$  is required for the convergence of the singular integral and implies both  $1 - \frac{d}{2}(\frac{1}{q} - \frac{1}{p}) > 0$  and  $1 + \alpha(1 - \frac{d}{2}(\frac{1}{q} - \frac{1}{p})) > 0$  hold, thereby it ensures that the arguments of the Gamma functions are well defined. The estimate (4.7) follows by the same argument.

Next, we establish (4.5). Using identity (4.2) and estimate (19) from Lemma 3.1 in Ref. 88, we derive

$$\begin{aligned} & \|E_{\alpha,\alpha}(-t^\alpha \mathcal{A}) \nabla \cdot \omega(\mathbf{x}, t)\|_{L^p} \leq \int_0^\infty \alpha s M_\alpha(s) \left\| e^{st^\alpha \Delta} \nabla \cdot \omega(\mathbf{x}, t) \right\|_{L^p} ds \\ & \leq C \int_0^\infty \alpha s M_\alpha(s) \left(1 + (st^\alpha)^{-\frac{1}{2} - \frac{d}{2}(\frac{1}{q} - \frac{1}{p})}\right) \|\omega(\mathbf{x}, t)\|_{L^q} ds \\ & \leq C \left( \frac{\Gamma(2)}{\Gamma(1+\alpha)} + t^{-\frac{\alpha}{2} - \frac{\alpha d}{2}(\frac{1}{q} - \frac{1}{p})} \frac{\Gamma(\frac{3}{2} - \frac{d}{2}(\frac{1}{q} - \frac{1}{p}))}{\Gamma(1 + \alpha(\frac{1}{2} - \frac{d}{2}(\frac{1}{q} - \frac{1}{p})))} \right) \|\omega(\mathbf{x}, t)\|_{L^q} \\ & \leq C_2 \left(1 + t^{-\frac{\alpha}{2} - \frac{\alpha d}{2}(\frac{1}{q} - \frac{1}{p})}\right) \|\omega(\mathbf{x}, t)\|_{L^q}, \quad t > 0. \end{aligned}$$

Here, the condition  $\frac{d}{2}(\frac{1}{q} - \frac{1}{p}) < \frac{3}{2}$  ensures the convergence of the singular integral and well-definedness of the Gamma functions.

Finally, the remaining estimates (4.6), (4.8), and (4.9) follow by the same reasoning, using (4.2) together with the heat semigroup estimates (17)-(19) from Lemma 3.1 in Ref. 88. This completes the proof.  $\square$

To simplify notation without loss of generality, we set  $\mathcal{D} = 1$  in (1.1). Applying the Laplace transform to (1.1) and employing the identity  $\mathfrak{L}_{t \rightarrow z}\{t^{\beta-1} E_{\alpha,\beta}(-t^\alpha \mathcal{A})\} = z^{\alpha-\beta} (z^\alpha I + \mathcal{A})^{-1}$ , valid for  $\alpha > 0$ ,  $0 < t \leq T$ , and  $\beta \in \mathbb{R}$  (see, e.g., Refs. 27, 88), we obtain, after inverse Laplace transform, the following Duhamel integral system,

$$\begin{cases} n(\mathbf{x}, t) = E_\alpha(-t^\alpha \mathcal{A}) n_0(\mathbf{x}) - \chi \int_0^t (t-s)^{\alpha-1} E_{\alpha,\alpha}(-(t-s)^\alpha \mathcal{A}) \nabla \cdot \left(\frac{n}{c} \nabla c\right)(\mathbf{x}, s) ds; \\ c(\mathbf{x}, t) = E_\alpha(-t^\alpha \mathcal{A}_\gamma) c_0(\mathbf{x}) + \int_0^t (t-s)^{\alpha-1} E_{\alpha,\alpha}(-(t-s)^\alpha \mathcal{A}_\gamma) n(\mathbf{x}, s) ds. \end{cases} \quad (4.10)$$

Following Definition 4.1 in Ref. 88, we call a pair  $(n, c)$  satisfying (4.10) a mild solution of system (1.1). Additionally, the forms of  $n(\mathbf{x}, t)$  and  $c(\mathbf{x}, t)$  in (4.10) directly give rise to the properties stated in the lemmas below.

**Lemma 4.3 (Conservation of Mass).** *Let the initial data  $n_0(\mathbf{x})$  and  $c_0(\mathbf{x})$  satisfy (3.4). For every  $t > 0$  and  $\alpha \in (0, 1)$ , the total masses of  $n(\mathbf{x}, t)$  and  $c(\mathbf{x}, t)$  evolve according to the following identities,*

$$\int_\Omega n(\mathbf{x}, t) d\mathbf{x} = \int_\Omega n_0(\mathbf{x}) d\mathbf{x}, \quad (4.11)$$

and

$$\int_\Omega c(\mathbf{x}, t) d\mathbf{x} + \frac{\gamma}{\Gamma(\alpha)} \int_0^t (t-s)^{\alpha-1} \int_\Omega c(\mathbf{x}, s) d\mathbf{x} ds = \frac{t^\alpha}{\Gamma(1+\alpha)} \int_\Omega n_0(\mathbf{x}) d\mathbf{x} + \int_\Omega c_0(\mathbf{x}) d\mathbf{x}. \quad (4.12)$$

**Proof.** Applying the Riemann-Liouville fractional integral operator  ${}_0 I_t^{1-\alpha}$  to both sides of (1.1a) gives

$$n(\mathbf{x}, t) - n_0(\mathbf{x}) = \frac{1}{\Gamma(\alpha)} \int_0^t (t-s)^{\alpha-1} \left( \Delta n(\mathbf{x}, s) - \chi \nabla \cdot \left(\frac{n}{c} \nabla c\right)(\mathbf{x}, s) \right) ds.$$

Integrating over  $\Omega$  and using the divergence theorem, we obtain, for all  $t > 0$

$$\begin{aligned} \int_{\Omega} (n(\mathbf{x}, t) - n_0(\mathbf{x})) d\mathbf{x} &= \frac{1}{\Gamma(\alpha)} \int_0^t (t-s)^{\alpha-1} \int_{\Omega} \left( \Delta n - \chi \nabla \cdot \left( \frac{n}{c} \nabla c \right) \right) (\mathbf{x}, s) d\mathbf{x} ds \\ &= \frac{1}{\Gamma(\alpha)} \int_0^t (t-s)^{\alpha-1} \int_{\partial\Omega} \frac{\partial n(\mathbf{x}, s)}{\partial \nu} dS ds \\ &\quad - \frac{\chi}{\Gamma(\alpha)} \int_0^t (t-s)^{\alpha-1} \int_{\partial\Omega} \frac{n(\mathbf{x}, s)}{c(\mathbf{x}, s)} \frac{\partial c(\mathbf{x}, s)}{\partial \nu} dS ds, \end{aligned}$$

where  $dS$  denotes the boundary area element. The homogeneous Neumann boundary conditions in (1.1c) make both boundary integrals vanish, and (4.11) follows.

The same argument applied to the equation of  $c(x, t)$  gives (4.12), using the identity  $\frac{1}{\Gamma(\alpha)} \int_0^t (t-s)^{\alpha-1} ds = \frac{t^\alpha}{\Gamma(1+\alpha)}$ . This completes the proof.  $\square$

**Lemma 4.4.** *Let  $T > 0$  be appropriately small, and the initial data  $n_0(\mathbf{x})$  and  $c_0(\mathbf{x})$  satisfy (3.4). Then, for all  $(\mathbf{x}, t) \in \Omega \times [0, T]$  with  $\Omega \subset \mathbb{R}^d$  ( $d \geq 2$ ), the solution component  $n(\mathbf{x}, t)$  of the mild solution to the system (1.1) remains nonnegative (i.e.,  $n \geq 0$ ).*

**Proof.** We prove the non-negativity of  $n(\mathbf{x}, t)$  by considering its negative part  $u(\mathbf{x}, t) := \max\{0, -n(\mathbf{x}, t)\}$  (see Ref. 56). Clearly,  $u(\mathbf{x}, t) \geq 0$ , and by definition,

$$\begin{cases} n(\mathbf{x}, t) = -u(\mathbf{x}, t), & \nabla n(\mathbf{x}, t) = -\nabla u(\mathbf{x}, t), & \text{for } n(\mathbf{x}, t) < 0, \\ u(\mathbf{x}, t) = 0, & \nabla u(\mathbf{x}, t) = 0, & \text{for } n(\mathbf{x}, t) \geq 0. \end{cases} \quad (4.13)$$

Consequently, according to the definition of  $u$ ,  $n$  is non-negative if and only if  $u(\mathbf{x}, t) \equiv 0$  throughout  $\Omega \times [0, T]$ .

The standard local existence theory for fractional parabolic equations in  $L^q$  ensures that  $n(\mathbf{x}, t)$  is absolutely continuous in  $t$  for a.e.  $\mathbf{x} \in \Omega$ , justifying the use of the fractional convexity inequality. Multiply (1.1a) by  $\text{sgn}(n)$  with  $\text{sgn}(\cdot)$  being defined as the standard sign function, and applying the fractional convexity inequality (A.6) (Lemma Appendix A.1), and integrating over  $\Omega$ , we obtain

$${}_0^C \mathcal{D}_t^\alpha \int_{\Omega} |n| d\mathbf{x} \leq \int_{\Omega} \text{sgn}(n) \Delta n d\mathbf{x} - \chi \int_{\Omega} \text{sgn}(n) \nabla \cdot (n\mathbf{v}) d\mathbf{x},$$

where  $\mathbf{v} := \frac{\nabla c}{c}$ . Using  $\nabla \cdot (n\mathbf{v}) \text{sgn}(n) = \nabla \cdot (|n|\mathbf{v})$  and  $\Delta n \text{sgn}(n) \leq \Delta |n|$  (Kato's inequality; see Refs. 56, 67), we get

$${}_0^C \mathcal{D}_t^\alpha \int_{\Omega} |n| d\mathbf{x} \leq \int_{\Omega} \Delta |n| d\mathbf{x} - \chi \int_{\Omega} \nabla \cdot (|n|\mathbf{v}) d\mathbf{x}.$$

By the divergence theorem and the Neumann boundary conditions, we find  $\int_{\Omega} \Delta |n| d\mathbf{x} = \int_{\partial\Omega} \nabla |n| \cdot \vec{\nu} dS = 0$  and  $\int_{\Omega} \nabla \cdot (|n|\mathbf{v}) = \int_{\partial\Omega} \nabla |n| \cdot \mathbf{v} \cdot \vec{\nu} dS = 0$ . Hence

$${}_0^C \mathcal{D}_t^\alpha \int_{\Omega} |n| d\mathbf{x} \leq 0.$$

Meanwhile, Lemma 4.3 gives  ${}_0^C \mathcal{D}_t^\alpha \int_{\Omega} n d\mathbf{x} = 0$ . Subtracting yields

$${}_0^C \mathcal{D}_t^\alpha \int_{\Omega} (|n| - n) d\mathbf{x} \leq 0. \quad (4.14)$$

22 *F.G. Ma, Z.M. Ouyang, W.Y. Tian & L. Wu*

Since  $|n| - n = 2u$ , by (4.14), we have

$${}_0^C \mathcal{D}_t^\alpha \int_{\Omega} 2u(\mathbf{x}, t) \, d\mathbf{x} \leq 0. \quad (4.15)$$

The initial non-negativity  $n_0 \geq 0$  implies  $u(\mathbf{x}, 0) = 0$ , hence  $\int_{\Omega} u(\mathbf{x}, 0) \, d\mathbf{x} = 0$ . Applying the generalized Grönwall lemma (Lemma 3.2) to (4.15) gives  $\int_{\Omega} u(\mathbf{x}, t) \, d\mathbf{x} \leq 0 \cdot E_{\alpha,1}(Ct^\alpha) = 0$  for all  $t \in [0, T]$ , so

$$\int_{\Omega} u(\mathbf{x}, t) \, d\mathbf{x} \equiv 0, \quad \text{a.e. } (\mathbf{x}, t) \in \Omega \times [0, T].$$

By the definition of  $u$ , implies  $n \geq 0$  almost everywhere on  $(\mathbf{x}, t) \in \Omega \times [0, T]$ . This completes the proof.  $\square$

**Lemma 4.5.** *Assume  $c(\mathbf{x}, 0)$  satisfies the condition stated in (3.4). Then for  $\alpha \in (0, 1)$ , the following hold:*

(i) *For every  $t \in (0, T]$ , the solution  $c(\mathbf{x}, t)$  of (1.1) satisfies*

$$c(\mathbf{x}, t) \geq \frac{t^{-\alpha}}{t^{-\alpha} + \gamma \Gamma(1-\alpha)} \inf_{\mathbf{x} \in \Omega} c(\mathbf{x}, 0), \quad t > 0, \quad (4.16)$$

*ensuring that  $c(\mathbf{x}, t) > 0$  for all  $(\mathbf{x}, t) \in \Omega \times [0, T]$ .*

(ii) *There exists a constant  $C_* > 0$  such that  $\inf_{\mathbf{x} \in \Omega, t \geq 0} c(\mathbf{x}, t) \geq C_*$ .*

**Proof.** We first construct a spatially homogeneous comparison function  $c_h(t)$  satisfying the time fractional ordinary differential equation  ${}_0^C \mathcal{D}_t^\alpha c_h(t) = -\gamma c_h(t)$  for all  $t > 0$ , equipped with initial condition  $c_h(0) := m_0 = \inf_{\mathbf{x} \in \Omega} c(\mathbf{x}, 0) > 0$ . The explicit solution is  $c_h(t) = m_0 E_{\alpha,1}(-\gamma t^\alpha)$ . Define the auxiliary function  $w(\mathbf{x}, t) := c(\mathbf{x}, t) - c_h(t)$ . Applying the Caputo derivative operator to  $w$  and using the second equation of (1.1), we get, for  $t > 0$ ,

$$\begin{aligned} {}_0^C \mathcal{D}_t^\alpha w(\mathbf{x}, t) &= {}_0^C \mathcal{D}_t^\alpha c(\mathbf{x}, t) - {}_0^C \mathcal{D}_t^\alpha c_h(t) \\ &= \Delta c(\mathbf{x}, t) - \gamma c(\mathbf{x}, t) + n(\mathbf{x}, t) - (-\gamma c_h(t)) \\ &= \Delta w(\mathbf{x}, t) - \gamma w(\mathbf{x}, t) + n(\mathbf{x}, t). \end{aligned}$$

Treating the term  $n(\mathbf{x}, t)$  as a source term, and using its non-negativity guaranteed by Lemma 4.4, the solution  $w(\mathbf{x}, t)$  satisfies

$${}_0^C \mathcal{D}_t^\alpha w - \Delta w + \gamma w \geq 0, \quad (\mathbf{x}, t) \in \Omega \times (0, T]. \quad (4.17)$$

Since  $w(\mathbf{x}, 0) = c(\mathbf{x}, 0) - c_h(0) \geq 0$  and  $\partial w / \partial \nu = 0$ , Lemma 3.1 implies  $w(\mathbf{x}, t) \geq 0$ , i.e.,  $c(\mathbf{x}, t) \geq c_h(t)$  for all  $\mathbf{x} \in \Omega$  and  $t \geq 0$ . Using the standard lower bound for the Mittag-Leffler function (valid for  $\gamma > 0$ ,  $\alpha \in (0, 1)$ ),

$$E_{\alpha,1}(-\gamma t^\alpha) \geq \frac{1}{1 + \gamma \Gamma(1-\alpha) t^\alpha}, \quad (4.18)$$

we obtain  $c(\mathbf{x}, t) \geq m_0 E_{\alpha,1}(-\gamma t^\alpha) \geq \frac{t^{-\alpha}}{t^{-\alpha} + \gamma \Gamma(1-\alpha)} m_0$ . This yields the desired estimate (4.16). Since  $E_{\alpha,1}(-z) > 0$  for all  $z \geq 0$ , the strict positivity of  $c$  follows immediately.

It remains to prove (ii), i.e.,  $c(\mathbf{x}, t)$  admits a strictly positive lower bound  $C_* > 0$  for all  $t \in [0, \infty)$ . To establish this lower bound as  $t \rightarrow \infty$ , we analyze the continuous contribution of the source term  $n(\mathbf{x}, t)$ , expressed as  $\mathcal{K}(\mathbf{x}, t) := \int_0^t (t-s)^{\alpha-1} E_{\alpha,\alpha}(-(t-s)^\alpha \mathcal{A}_\gamma) n(\mathbf{x}, s) \, ds$  in (4.10), and split the time axis into two regimes.

- **Short time interval**  $[0, 1]$ : For  $t \in [0, 1]$ , by Lemma 4.1 and from (i) with the lower bound (4.16), it holds that  $c(\mathbf{x}, t) \geq \min_{t \in [0, 1]} m_0 E_{\alpha, 1}(-\gamma t^\alpha) \geq m_0 E_{\alpha, 1}(-\gamma) := C_1 > 0$ .
- **Long time interval**  $(1, \infty)$ : For  $t > 1$ , we consider the integral contribution in  $\mathcal{K}(\mathbf{x}, t)$  specifically over the recent history window  $s \in [t - 1, t - \frac{1}{2}]$ . In this interval,  $\tau = t - s \in [\frac{1}{2}, 1]$ , and  $\tau^{\alpha-1} \geq 1$  since  $\alpha \in (0, 1)$ , we have

$$\begin{aligned} c(\mathbf{x}, t) &\geq \int_{t-1}^{t-1/2} (t-s)^{\alpha-1} E_{\alpha, \alpha}(-(t-s)^\alpha \mathcal{A}_\gamma) n(\mathbf{x}, s) ds \\ &\geq \int_{t-1}^{t-1/2} 1 \cdot (\eta_0 \tilde{M}) ds = \frac{1}{2} \eta_0 \tilde{M} := C_2 > 0. \end{aligned} \quad (4.19)$$

The constant  $C_2$  is strictly positive and independent of  $t$ .

In the last inequality in (4.19) is established by leveraging the subordination principle for the Mittag-Leffler operator. Specifically, we have

$$[E_{\alpha, \alpha}(-\tau^\alpha \mathcal{A}_\gamma) n](\mathbf{x}, t) = \int_0^\infty \alpha z M_\alpha(z) e^{-\gamma z \tau^\alpha} \left( \int_\Omega p(\mathbf{x}, \mathbf{y}, z \tau^\alpha) n(\mathbf{y}, t - \tau) d\mathbf{y} \right) dz,$$

where  $p(\mathbf{x}, \mathbf{y}, \theta)$  is the Neumann heat kernel on  $\Omega$ . For bounded connected domains  $\Omega$  satisfying the uniform interior cone condition, it is well-established that the Neumann heat kernel admits the Gaussian lower bound (see, e.g., Thm. 3.10 in Ref. 48). For any  $\theta > 0$ , there exist constants  $m_1 > 0$  and  $m_2 > 0$  such that

$$p(\mathbf{x}, \mathbf{y}, \theta) \geq \frac{m_1}{|\Omega|} \exp\left(-\frac{m_2 \text{diam}(\Omega)^2}{\theta}\right) := p_*(\theta) > 0,$$

with  $\text{diam}(\Omega) = \sup_{\mathbf{x}, \mathbf{y} \in \Omega} |\mathbf{x} - \mathbf{y}| < \infty$  is the finite diameter of the domain. This estimate provides a uniform lower bound for the heat kernel that is independent of the spatial coordinates  $\mathbf{x}, \mathbf{y}$ . Consequently, by utilizing the mass conservation law  $\int_\Omega n(\mathbf{y}, \cdot) d\mathbf{y} = \tilde{M}$ , we can bound the inner spatial integral as

$$\int_\Omega p(\mathbf{x}, \mathbf{y}, z \tau^\alpha) n(\mathbf{y}, t - \tau) d\mathbf{y} \geq p_*(z \tau^\alpha) \tilde{M}. \quad (4.20)$$

Define the auxiliary function  $\mathcal{H}(\tau) := \alpha \tilde{M} \int_0^\infty z M_\alpha(z) e^{-\gamma z \tau^\alpha} p_*(z \tau^\alpha) dz$ . Note that  $M_\alpha(z) > 0$  for all  $z > 0$ , and the exponential structure of the Gaussian bound  $p_*$  ensures that the integrand is strictly positive on  $(0, \infty)$ . Furthermore, the Mainardi function  $M_\alpha(z)$  exhibits super-exponential decay as  $z \rightarrow 0^+$  (specifically,  $M_\alpha(z) \sim \exp(-z^{-\frac{1}{1-\alpha}})$ , see e.g., Thm.3.8 (iv) in Ref. 62), which effectively counteracts the singularity potentially arising from the term  $\exp(-1/z)$  in the heat kernel estimate. By the Lebesgue dominated convergence theorem,  $\mathcal{H}(\tau)$  is continuous on the compact interval  $\tau \in [\frac{1}{2}, 1]$ . Applying the Weierstrass extreme value theorem, we conclude that  $\mathcal{H}(\tau)$  attains a strictly positive minimum

$$\min_{\tau \in [1/2, 1]} \mathcal{H}(\tau) := \eta_0 > 0.$$

Substitute this uniform bound into the temporal integral, (4.19) holds directly.

Finally, setting  $C_* = \min\{C_1, C_2\} > 0$  yields  $c(\mathbf{x}, t) \geq C_*$  for all  $\mathbf{x} \in \Omega$  and  $t \geq 0$ . This completes the proof.  $\square$

**Remark 4.1.** Combing Lemmas 4.4 and 4.5 yields the non-negativity of  $n(\mathbf{x}, t)$  and the strict positivity of  $c(\mathbf{x}, t) > 0$  almost everywhere on  $(\mathbf{x}, t) \in \Omega \times [0, T]$ . In particular, the lower bound

established in Lemma 4.5 guarantees the well-posedness of the logarithmic chemotaxis term and will be frequently invoked in the forthcoming analysis.

**Lemma 4.6.** *Let  $T > 0$ ,  $d \geq 2$  and  $1 \leq p, q \leq \infty$ . Suppose the initial data  $n_0(\mathbf{x})$  and  $c_0(\mathbf{x})$  satisfy (3.4). Then the following estimates hold for  $t \in (0, T]$ :*

(i) *If  $\frac{1}{q} - \frac{1}{p} < \frac{2}{d}$ , there exists a positive constant  $C$  such that*

$$\|c(\mathbf{x}, t)\|_{L^p} \leq C \left( 1 + \max \left\{ T^\alpha, T^{\alpha - \frac{\alpha d}{2} \max\{0, \frac{1}{q} - \frac{1}{p}\}} \right\} \sup_{t \in (0, T)} \|n(\mathbf{x}, t)\|_{L^q} \right). \quad (4.21)$$

(ii) *If  $\frac{1}{q} - \frac{1}{p} < \frac{1}{d}$ , there exists a positive constant  $C$  such that*

$$\|c(\mathbf{x}, t)\|_{W^{1,p}} \leq C \left( 1 + \max \left\{ T^\alpha, T^{\frac{\alpha}{2} - \frac{\alpha d}{2} \max\{0, \frac{1}{q} - \frac{1}{p}\}} \right\} \sup_{t \in (0, T)} \|n(\mathbf{x}, t)\|_{L^q} \right). \quad (4.22)$$

**Proof.** We divide the proof of (i) into two distinct cases:  $p \geq q$  and  $p < q$ .

**Case 1:**  $p \geq q$ . Apply estimates (4.4) and (4.7) from Lemma 4.2, together with Hölder's inequality, yields, for  $t > 0$

$$\begin{aligned} \|c(\mathbf{x}, t)\|_{L^p} &\leq \|E_\alpha(-t^\alpha \mathcal{A})c_0\|_{L^p} + \int_0^t (t-s)^{\alpha-1} \|E_{\alpha,\alpha}(-(t-s)^\alpha \mathcal{A}_\gamma)n(\mathbf{x}, s)\|_{L^p} ds \\ &\leq |\Omega|^{1/p} \|E_\alpha(-t^\alpha \mathcal{A})c_0\|_{L^\infty} + C \int_0^t (t-s)^{\alpha-1} \|n(\mathbf{x}, s)\|_{L^q} ds \\ &\quad + C \int_0^t (t-s)^{\alpha-1 - \frac{\alpha d}{2}(\frac{1}{q} - \frac{1}{p})} \|n(\mathbf{x}, s)\|_{L^q} ds \\ &\leq C \|c_0\|_{L^\infty} + C \max \left\{ T^\alpha, T^{\alpha - \frac{\alpha d}{2}(\frac{1}{q} - \frac{1}{p})} \right\} \sup_{t \in (0, T)} \|n(\mathbf{x}, t)\|_{L^q}. \end{aligned} \quad (4.23)$$

In the last inequality, we used the fact that if  $0 \leq \frac{1}{q} - \frac{1}{p} < \frac{2}{d}$ ,  $0 < 1 - \alpha + \frac{\alpha d}{2}(\frac{1}{q} - \frac{1}{p}) < 1$ , then the second integral is convergent and bounded as above.

**Case 2:**  $p < q$ . The estimate follows directly from Hölder's inequality. Combining the two cases gives (4.23) for all  $1 \leq p, q \leq \infty$ . Under the assumptions in (3.4), the estimate (4.21) follows immediately.

For the gradient estimate in (ii), we use a similar argument together with the commutator identity  $\mathcal{A}^{1/2} E_\alpha(-t^\alpha \mathcal{A})c_0 = E_\alpha(-t^\alpha \mathcal{A})\mathcal{A}^{1/2}c_0$ , which follows from the corresponding identity for the heat semigroup  $\mathcal{A}^{1/2} e^{t\Delta} c_0 = e^{t\Delta} \mathcal{A}^{1/2} c_0$ . Applying the estimates (4.4) and (4.9) from Lemma 4.2, and noting that the condition  $0 \leq \frac{1}{q} - \frac{1}{p} < \frac{1}{d}$  implies  $1 - \frac{\alpha}{2} + \frac{\alpha d}{2}(\frac{1}{q} - \frac{1}{p}) < 1$ , we obtain (4.22). This completes the proof of the lemma.  $\square$

**Remark 4.2.** Lemma 4.6 requires the exponents  $p, q$  to satisfy  $1 \leq p, q \leq \infty$  and  $\frac{1}{q} - \frac{1}{p} < \frac{1}{d}$  with  $d \geq 2$ . Without loss of generality, we may make  $q \in [\frac{d}{2}, d)$ , which implies  $\frac{dq}{d-q} > d$ . This allows us to choose  $p > d$  with  $p < \frac{dq}{d-q}$ . Such a choice simultaneously satisfies the hypotheses of Lemma 4.6 and the assumptions needed in Theorem 3.2.

The proofs of these lemmas are based on standard arguments, yet their results reveal a clear departure from the classical logarithmic Keller–Segel system. This distinction provides new insight into the time-nonlocal system (1.1).

### 5. Local Well-Posedness of Mild Solution in Arbitrary Dimensions

Let  $\Omega \subset \mathbb{R}^d$  ( $d \geq 2$ ) be a bounded domain with smooth boundary. Following the framework adopted in, e.g., Refs. 64, 129, 134, we introduce the Banach space

$$\mathbb{X} := C([0, T]; L^\infty(\Omega)) \times C([0, T]; W^{1,p}(\Omega)), \quad \text{for } p > d \geq 2, \quad (5.1)$$

endowed with the norm

$$\|(n, c)\|_{\mathbb{X}} := \|n\|_{C([0, T]; L^\infty(\Omega))} + \|c\|_{C([0, T]; W^{1,p}(\Omega))}. \quad (5.2)$$

Since  $p > d \geq 2$ , the Sobolev embedding theorem ensures that  $W^{1,p}(\Omega) \hookrightarrow C(\overline{\Omega})$ . This continuity allows us to define pointwise bounds for  $c(\mathbf{x}, t)$ , which is further justified by Lemma 4.5. For fixed constants  $\mathcal{R} > 0$  and  $C_* > 0$ , we define the closed subset  $\mathfrak{B}$  as follows,

$$\mathfrak{B} := \left\{ (n, c) \in \mathbb{X} \left| \begin{array}{l} \|(n, c)\|_{\mathbb{X}} \leq \mathcal{R}, \quad n \geq 0, \quad c \geq C_* \text{ in } \Omega \times [0, T], \\ \partial_\nu n = \partial_\nu c = 0 \text{ on } \partial\Omega \end{array} \right. \right\}. \quad (5.3)$$

We focus on the mapping  $\mathcal{M}(n, c) := (\mathcal{M}_1(n, c), \mathcal{M}_2(n, c))$ , defined for  $t \in (0, T]$  by

$$\begin{cases} \mathcal{M}_1(n, c) = E_\alpha(-t^\alpha \mathcal{A})n_0 - \chi \int_0^t (t-s)^{\alpha-1} E_{\alpha,\alpha}(-(t-s)^\alpha \mathcal{A}) \nabla \cdot \left( \frac{n}{c} \nabla c \right) (s) \, ds, \\ \mathcal{M}_2(n, c) = E_\alpha(-t^\alpha \mathcal{A}_\gamma)c_0 + \int_0^t (t-s)^{\alpha-1} E_{\alpha,\alpha}(-(t-s)^\alpha \mathcal{A}_\gamma)n(s) \, ds. \end{cases} \quad (5.4)$$

These components satisfy

$$\begin{cases} {}_0^C \mathcal{D}_t^\alpha \mathcal{M}_1(n, c)(\mathbf{x}, t) = \mathcal{D} \Delta \mathcal{M}_1(n, c)(\mathbf{x}, t) - \mathcal{D} \chi \nabla \cdot \left( \frac{n}{c} \nabla c \right) (\mathbf{x}, t), \\ {}_0^C \mathcal{D}_t^\alpha \mathcal{M}_2(n, c)(\mathbf{x}, t) = \mathcal{D} \Delta \mathcal{M}_2(n, c)(\mathbf{x}, t) - \gamma \mathcal{M}_2(n, c)(\mathbf{x}, t) + n(\mathbf{x}, t), \\ \mathcal{M}_1(n, c)(\mathbf{x}, 0) = n_0(\mathbf{x}), \quad \mathcal{M}_2(n, c)(\mathbf{x}, 0) = c_0(\mathbf{x}), \\ \partial_\nu \mathcal{M}_1(n, c)(\mathbf{x}, t) = 0, \quad \partial_\nu \mathcal{M}_2(n, c)(\mathbf{x}, t) = 0. \end{cases} \quad (5.5)$$

Our goal is to establish the following properties of  $\mathcal{M}$ :

- $\mathcal{M}(n, c) \in \mathbb{X}$  for all  $(n, c) \in \mathbb{X}$ ,  $t \in (0, T]$ ;
- for sufficiently large  $\mathcal{R} > 0$  and appropriately small  $T > 0$ ,  $\mathcal{M}$  maps  $\mathfrak{B}$  into itself; and
- under the same conditions,  $\mathcal{M}$  is a contraction on  $\mathfrak{B}$ .

We first show that  $\mathcal{M}$  is well-defined on  $\mathfrak{B}$  and, under suitable assumptions, is self-mapping.

**Lemma 5.1.** *Let the initial data  $n_0(\mathbf{x})$  and  $c_0(\mathbf{x})$  satisfy (3.4) and let  $\chi > 0$ . Define the mapping  $\mathcal{M}(n, c) := (\mathcal{M}_1(n, c), \mathcal{M}_2(n, c))$  by (5.4). Then  $\mathcal{M}(n, c) \in \mathbb{X}$  for all  $(n, c) \in \mathbb{X}$ . Moreover, for any  $t \in (0, T]$ , if  $\mathcal{R} > 0$  is suitably large and  $T > 0$  is appropriately small, the mapping  $\mathcal{M}$  is well-defined on the closed subset  $\mathfrak{B}$  and maps  $\mathfrak{B}$  into itself, i.e.,  $\mathcal{M} : \mathfrak{B} \rightarrow \mathfrak{B}$ .*

**Proof.** We assume without loss of generality that  $t \in (0, T]$  with  $T < 1$  and  $p > d$ . For any  $(n, c) \in \mathfrak{B}$ , we have  $n(t, x) \geq 0$  and  $c(x, t) \geq C_*$  on  $\Omega \times (0, T)$ . Applying estimates (4.4) and (4.5)

from Lemma 4.2, together with Hölder's inequality, yields

$$\begin{aligned}
 \|\mathcal{M}_1(n, c)\|_{L^\infty} &\leq C\|n_0\|_{L^\infty} + \chi \int_0^t s^{\alpha-1} \left\| E_{\alpha, \alpha}(-s^\alpha \mathcal{A}) \nabla \cdot \left( \frac{n}{c} \nabla c \right) (t-s) \right\|_{L^\infty} ds \\
 &\leq C\|n_0\|_{L^\infty} + C \int_0^t (t-s)^{\frac{\alpha}{2} - \frac{\alpha d}{2p} - 1} \|c(s)^{-1}\|_{L^\infty} \|n(s) \nabla c(s)\|_{L^p} ds \\
 &\leq C\|n_0\|_{L^\infty} + \frac{C}{C_*} \int_0^t (t-s)^{\frac{\alpha}{2} - \frac{\alpha d}{2p} - 1} \|n(s)\|_{L^\infty} \|\nabla c(s)\|_{L^p} ds \\
 &\leq C\|n_0\|_{L^\infty} + C\mathcal{R}^2 \int_0^t (t-s)^{\frac{\alpha}{2} - \frac{\alpha d}{2p} - 1} ds \\
 &\leq C\|n_0\|_{L^\infty} + C\mathcal{R}^2 T^{\frac{\alpha}{2}(1-\frac{d}{p})}.
 \end{aligned}$$

Choosing  $\mathcal{R} > 0$  suitably large and  $T > 0$  appropriately small (depending on  $n_0$  and  $c_0$  only through their norms in  $L^\infty(\Omega)$  and  $W^{1,p}(\Omega)$ ), we obtain

$$\sup_{t \in [0, T]} \|\mathcal{M}_1(n, c)\|_{L^\infty} \leq \mathcal{R}/2. \quad (5.6)$$

Similarly, using estimates (4.4) and (4.9) from Lemma 4.2, for  $p > d$ , we have

$$\begin{aligned}
 \|\mathcal{A}^{1/2} \mathcal{M}_2(n, c)\|_{L^p} &\leq \left\| E_\alpha(-t^\alpha \mathcal{A}_\gamma) \mathcal{A}^{1/2} c_0 \right\|_{L^p} + \int_0^t s^{\alpha-1} \left\| \mathcal{A}^{1/2} E_{\alpha, \alpha}(-s^\alpha \mathcal{A}_\gamma) n(t-s) \right\|_{L^p} ds \\
 &\leq C\|\nabla c_0\|_{L^\infty} + C \int_0^t (t-s)^{\frac{\alpha}{2}-1} \|n(s)\|_{L^p} ds \\
 &\leq C\|\nabla c_0\|_{L^\infty} + CT^{\frac{\alpha}{2}} \mathcal{R},
 \end{aligned} \quad (5.7)$$

and

$$\|\mathcal{M}_2(n, c)\|_{L^p} \leq C\|c_0\|_{L^\infty} + CT^\alpha \mathcal{R}. \quad (5.8)$$

Thus, for  $\mathcal{R}$  and  $T$  chosen as above, we get

$$\sup_{t \in [0, T]} \|\mathcal{M}_2(n, c)\|_{W^{1,p}} \leq \mathcal{R}/2. \quad (5.9)$$

Combining (5.6) and (5.9), we conclude that for all  $t \geq 0$ ,

$$\|\mathcal{M}(n, c)\|_{\mathfrak{X}} \leq \mathcal{R}, \quad \forall (n, c) \in \mathfrak{B}.$$

To complete the proof that  $\mathcal{M}(\mathfrak{B}) \subset \mathfrak{B}$ , it remains to verify that  $\mathcal{M}_1$  preserves the non-negativity of elements in  $\mathfrak{B}$  (i.e.,  $\mathcal{M}_1 \geq 0$ ), and that  $\mathcal{M}_2$  preserves the lower bound constraint  $c \geq C_* > 0$  that defines  $\mathfrak{B}$ . This is done by adapting the technique from the proofs of Lemmas 4.4 and 4.5.

**Non-negativity of  $\mathcal{M}_1$ .** Following the argument in Lemma 4.4, Multiply the first equation in (5.5) by  $\text{sgn}(\mathcal{M}_1)$ , integrate over  $\Omega$ , and apply the Neumann boundary conditions. This yields

$${}_0^C \mathfrak{D}_t^\alpha \int_\Omega |\mathcal{M}_1| dx \leq 0.$$

On the other hand, mass conservation (derived from the same equation) gives  ${}_0^C \mathfrak{D}_t^\alpha \int_\Omega \mathcal{M}_1 dx = 0$ . Subtracting yields

$${}_0^C \mathfrak{D}_t^\alpha \int_\Omega (|\mathcal{M}_1| - \mathcal{M}_1) dx \leq 0.$$

Since  $|\mathcal{M}_1| - \mathcal{M}_1 \geq 0$  and vanishes at  $t = 0$ , it follows that  $|\mathcal{M}_1| - \mathcal{M}_1 \equiv 0$ , i.e.,  $\mathcal{M}_1(n, c) \geq 0$  for all  $(n, c) \in \mathfrak{B}$ .

**Lower bound for  $\mathcal{M}_2$ .** Recall from Lemma 4.5 that

$$C_* = \min\{C_1, C_2\} > 0, \quad C_1 = m_0 E_{\alpha,1}(-\gamma), \quad m_0 = \inf_{\Omega} c_0(\mathbf{x}) > 0, \quad (5.10)$$

satisfies  $c(\mathbf{x}, t) \geq C_*$  for the original solution. We show the same for  $\mathcal{M}_2(n, c)$ . Using the mild representation of  $\mathcal{M}_2$ , we have

$$\mathcal{M}_2(n, c)(\mathbf{x}, t) = E_{\alpha}(-t^{\alpha} \mathcal{A}_{\gamma}) c_0(\mathbf{x}) + \int_0^t (t-s)^{\alpha-1} E_{\alpha,\alpha}(-(t-s)^{\alpha} \mathcal{A}_{\gamma}) n(\mathbf{x}, s) ds.$$

Since  $(n, c) \in \mathfrak{B}$  implies  $n \geq 0$  and the Mittag-Leffler operators  $E_{\alpha}(-t^{\alpha} \mathcal{A}_{\gamma})$ ,  $E_{\alpha,\alpha}(-t^{\alpha} \mathcal{A}_{\gamma})$  are positivity-preserving (see, e.g., Ref. 127), the integral term is non-negative. Hence,

$$\mathcal{M}_2(n, c)(\mathbf{x}, t) \geq E_{\alpha}(-t^{\alpha} \mathcal{A}_{\gamma}) c_0(\mathbf{x}).$$

Combining the lower bound  $c_0 \geq m_0$  with the positivity-preserving property, we obtain

$$E_{\alpha}(-t^{\alpha} \mathcal{A}_{\gamma}) c_0 \geq m_0 E_{\alpha}(-t^{\alpha} \mathcal{A}_{\gamma}) 1.$$

Using the eigenfunction expansion and the identity  $\mathcal{A}_{\gamma} 1 = \gamma 1$ , it follows that  $E_{\alpha}(-t^{\alpha} \mathcal{A}_{\gamma}) 1 = E_{\alpha,1}(-\gamma t^{\alpha}) 1$ . Thus,

$$\mathcal{M}_2(n, c)(\mathbf{x}, t) \geq m_0 E_{\alpha,1}(-\gamma t^{\alpha}), \quad (\mathbf{x}, t) \in \Omega \times [0, T]. \quad (5.11)$$

In the present local existence argument we may assume without loss of generality that  $T \leq 1$  (indeed the statement already restricts to  $T < 1$ ). Since the Mittag-Leffler function  $E_{\alpha,1}(-x)$  is strictly decreasing on  $[0, \infty)$  and  $t^{\alpha} \leq 1$ , we have

$$m_0 E_{\alpha,1}(-\gamma t^{\alpha}) \geq m_0 E_{\alpha,1}(-\gamma T^{\alpha}) \geq m_0 E_{\alpha,1}(-\gamma) = C_1 \geq C_*.$$

Combining this with (5.11) yields

$$\mathcal{M}_2(n, c)(\mathbf{x}, t) \geq C_*, \quad (\mathbf{x}, t) \in \Omega \times [0, T]. \quad (5.12)$$

Thus  $\mathcal{M}_2 \geq C_*$ , and the constant  $C_*$  here coincides with that obtained in Lemma 4.5.

Combining the non-negativity of  $\mathcal{M}_1$ , the uniform positive lower bound of  $\mathcal{M}_2$  established in (5.12), and the norm bounds (5.6)–(5.9), we conclude that  $\mathcal{M}(\mathfrak{B}) \subset \mathfrak{B}$ . Moreover, the estimates (5.6)–(5.8) already guarantee that  $\mathcal{M}(n, c)(t) \in \mathbb{X}$  for all  $(n, c) \in \mathfrak{B}$ .

Finally, the continuity of  $\mathcal{M}(n, c)$  in  $t \in [0, T]$  follows from strong continuity of the Mittag-Leffler operator (see Lemma 4.1) and the elementary properties of the Neumann heat semigroup. With this, it immediately follows that for any  $t_1, t_2 \in [0, T]$  with  $t_1 < t_2$ ,  $\lim_{t_1 \rightarrow t_2^-} \|\mathcal{M}(n, c)(t_1) - \mathcal{M}(n, c)(t_2)\|_{\mathbb{X}} = 0$ , which implies  $\mathcal{M}(n, c) \in C([0, T]; L^{\infty}(\Omega))$ . In establishing this continuity result, we also naturally prove that  $n(\mathbf{x}, t) \in C([0, T]; L^{\infty}(\Omega))$ ,  $c(\mathbf{x}, t) \in C([0, T]; W^{1,p}(\Omega))$ ,  $p > d$ . Since this argument is standard (see, e.g., Refs. 27, 88), the detailed verification is omitted. The proof is now complete.  $\square$

**Lemma 5.2 (Contraction mapping).** *Under the assumptions of Lemma 5.1, the mapping  $\mathcal{M}(n, c) : \mathfrak{B} \rightarrow \mathfrak{B}$  is a contraction for all  $t \in (0, T]$ , provided  $\mathcal{R} > 0$  is suitably large and  $T > 0$  is appropriately small.*

**Proof.** Let  $(n, c)$  and  $(\tilde{n}, \tilde{c})$  belong to  $\mathfrak{B}$ . Applying estimates (4.5) from Lemma 4.2, together with Lemma 4.5 and Hölder's inequality, we obtain the following bound

$$\begin{aligned}
 & \|\mathcal{M}_1(n, c) - \mathcal{M}_1(\tilde{n}, \tilde{c})\|_{L^\infty} \\
 & \leq \chi \int_0^t (t-s)^{\alpha-1} \left\| E_{\alpha, \alpha}(- (t-s)^\alpha \mathcal{A}) \nabla \cdot \left( \frac{n}{c} \nabla c - \frac{\tilde{n}}{\tilde{c}} \nabla \tilde{c} \right) (s) \right\|_{L^\infty} ds \\
 & \leq C \int_0^t (t-s)^{\frac{\alpha}{2} - \frac{\alpha d}{2p} - 1} \left\| \left( \frac{n}{c} \nabla c - \frac{\tilde{n}}{\tilde{c}} \nabla \tilde{c} \right) (s) \right\|_{L^p} ds \\
 & \leq C \int_0^t (t-s)^{\frac{\alpha}{2} - \frac{\alpha d}{2p} - 1} \left\{ \|(n - \tilde{n})(s)\|_{L^\infty} \|c(s)\|_{L^\infty}^{-1} \|\nabla c(s)\|_{L^p} \right. \\
 & \quad + \|\tilde{n}(s)\|_{L^\infty} \|c(s)\|_{L^\infty}^{-1} \|(\nabla c - \nabla \tilde{c})(s)\|_{L^p} \\
 & \quad \left. + \|\tilde{n}(s)\|_{L^\infty} \|(1/c - 1/\tilde{c})(s)\|_{L^p} \|\nabla c(s)\|_{L^p} \right\} ds \\
 & \leq (C\mathcal{R}/C_*) (1 + (\mathcal{R}/C_*)) T^{\frac{\alpha}{2}(1 - \frac{d}{p})} \|(n, c) - (\tilde{n}, \tilde{c})\|_{\mathbb{X}}.
 \end{aligned}$$

Hence,

$$\sup_{t \in (0, T]} \|\mathcal{M}_1(n, c) - \mathcal{M}_1(\tilde{n}, \tilde{c})\|_{L^\infty(\Omega)} \leq C\mathcal{R}^2 T^{\frac{\alpha}{2}(1 - \frac{d}{p})} \|(n, c) - (\tilde{n}, \tilde{c})\|_{\mathbb{X}}. \quad (5.13)$$

Similarly, using estimate (4.9) from Lemma 4.2, we obtain, for  $t \in (0, T]$ ,

$$\begin{aligned}
 \|\mathcal{A}^{1/2}(\mathcal{M}_2(n, c) - \mathcal{M}_2(\tilde{n}, \tilde{c}))\|_{L^p} & \leq \int_0^t (t-s)^{\alpha-1} \left\| \mathcal{A}^{1/2} E_{\alpha, \alpha}(- (t-s)^\alpha \mathcal{A}_\gamma) (n(s) - \tilde{n}(s)) \right\|_{L^p} ds \\
 & \leq C \int_0^t (t-s)^{\frac{\alpha}{2} - 1} \|n(s) - \tilde{n}(s)\|_{L^p} ds \leq CT^{\frac{\alpha}{2}} \|(n, c) - (\tilde{n}, \tilde{c})\|_{\mathbb{X}},
 \end{aligned}$$

and

$$\|\mathcal{M}_2(n, c) - \mathcal{M}_2(\tilde{n}, \tilde{c})\|_{L^p} \leq CT^\alpha \|(n, c) - (\tilde{n}, \tilde{c})\|_{\mathbb{X}}.$$

Combining these two bounds yields

$$\sup_{t \in (0, T]} \|\mathcal{M}_2(n, c) - \mathcal{M}_2(\tilde{n}, \tilde{c})\|_{W^{1,p}} \leq C \max\{T^{\alpha/2}, T^\alpha\} \|(n, c) - (\tilde{n}, \tilde{c})\|_{\mathbb{X}}. \quad (5.14)$$

By integrating the estimates (5.13) and (5.14), we can establish that choosing a suitably small  $T > 0$  and an appropriately large radius  $\mathcal{R} > 0$  ensures the following result holds, for all  $t \in (0, T]$ ,

$$\|\mathcal{M}(n, c) - \mathcal{M}(\tilde{n}, \tilde{c})\|_{\mathbb{X}} \leq C_{\mathfrak{B}} \|(n, c) - (\tilde{n}, \tilde{c})\|_{\mathbb{X}},$$

where the contractive constant  $C_{\mathfrak{B}}$  is defined as

$$C_{\mathfrak{B}} := C \max\left\{ \mathcal{R}^2 T^{\frac{\alpha}{2}(1 - \frac{d}{p})}, T^{\frac{\alpha}{2}}, T^\alpha \right\} < 1.$$

As a result, the mapping  $\mathcal{M}$  is a contraction on the closed subset  $\mathfrak{B}$ .  $\square$

**Theorem 5.1.** *Let the initial data  $n_0(\mathbf{x})$ ,  $c_0(\mathbf{x})$  satisfy (3.4). Then there exists an appropriately small  $T > 0$  such that system (1.1) admits a unique local mild solution  $(n, c) \in \mathfrak{B}$  for  $t \in [0, T]$ , satisfying*

$$n(\mathbf{x}, t) \in C([0, T]; L^\infty(\Omega)), \quad c(\mathbf{x}, t) \in C([0, T]; W^{1,p}(\Omega)), \quad p > d \geq 2. \quad (5.15)$$

Furthermore, for  $p > d$ , as  $t \rightarrow 0^+$ , it holds that

$$\lim_{t \rightarrow 0^+} \|n(\mathbf{x}, t) - n_0(\mathbf{x})\|_{L^p} \rightarrow 0, \quad \lim_{t \rightarrow 0^+} \|c(\mathbf{x}, t) - c_0(\mathbf{x})\|_{W^{1,p}} \rightarrow 0. \quad (5.16)$$

**Proof.** By Lemmas 5.1 and 5.2, the mapping  $\mathcal{M}(n, c)(t) : \mathfrak{B} \rightarrow \mathfrak{B}$  defined in (5.4) is well-defined and strictly contractive on the complete metric space  $\mathfrak{B}$  for all  $t \in (0, T]$ , with  $T > 0$  appropriately small. The Banach fixed-point theorem (see Theorem. 5.7 in Ref. 20) then guarantees a unique fixed point  $(n, c) \in \mathfrak{B}$ , which yields the unique local mild solution to (1.1) on  $[0, T]$ . This establishes the local well-posedness.

We now verify the initial data attainment. By applying the estimates from Lemma 4.2, we directly derive

$$\begin{aligned} \|n(\cdot, t) - n_0\|_{L^p} &\leq \|E_\alpha(-t^\alpha \mathcal{A})n_0 - n_0\|_{L^p} + \chi \int_0^t s^{\alpha-1} \left\| E_{\alpha,\alpha}(-s^\alpha \mathcal{A}) \nabla \cdot \left( \frac{n}{c} \nabla c \right) (t-s) \right\|_{L^p} ds \\ &\leq |\Omega|^{1/p} \|E_\alpha(-t^\alpha \mathcal{A})n_0 - n_0\|_{L^\infty} + \frac{C}{C_*} \int_0^t (t-s)^{\frac{\alpha}{2} - \frac{\alpha d}{2p} - 1} ds \|(n, c)\|_{\mathbb{X}}^2 \\ &\leq |\Omega|^{1/p} \|E_\alpha(-t^\alpha \mathcal{A})n_0 - n_0\|_{L^\infty} + Ct^{\frac{\alpha}{2}(1-\frac{d}{p})} \|(n, c)\|_{\mathbb{X}}^2. \end{aligned}$$

By the strong continuity of the Mittag-Leffler operator (Lemma 4.1),  $\|n(\cdot, t) - n(\cdot, 0)\|_{L^p} \rightarrow 0$  as  $t \rightarrow 0^+$ . Hence  $\|n(\cdot, t) - n_0\|_{L^p} \rightarrow 0$ .

Similarly, for the gradient part of  $c$

$$\begin{aligned} \|\mathcal{A}^{1/2}c(\cdot, t) - \mathcal{A}^{1/2}c_0\|_{L^p} &\leq \|\mathcal{A}^{1/2}E_\alpha(-t^\alpha \mathcal{A}_\gamma)c_0 - \mathcal{A}^{1/2}c_0\|_{L^p} \\ &\quad + \int_0^t s^{\alpha-1} \|\mathcal{A}^{1/2}E_{\alpha,\alpha}(-s^\alpha \mathcal{A}_\gamma)n(t-s)\|_{L^p} ds \\ &\leq \|E_\alpha(-t^\alpha \mathcal{A}_\gamma)\mathcal{A}^{1/2}c_0 - \mathcal{A}^{1/2}c_0\|_{L^p} + C \int_0^t (t-s)^{\frac{\alpha}{2} - \frac{\alpha d}{2p} - 1} \|n(s)\|_{L^\infty} ds \\ &\leq \|E_\alpha(-t^\alpha \mathcal{A}_\gamma)\mathcal{A}^{1/2}c_0 - \mathcal{A}^{1/2}c_0\|_{L^p} + Ct^{\frac{\alpha}{2}(1-\frac{d}{p})} \|(n, c)\|_{\mathbb{X}} \rightarrow 0, \end{aligned}$$

as  $t \rightarrow 0^+$ , where we used the commutativity  $\mathcal{A}^{1/2}E_\alpha(-t^\alpha \mathcal{A}_\gamma) = E_\alpha(-t^\alpha \mathcal{A}_\gamma)\mathcal{A}^{1/2}$  and the strong continuity of the semigroup.

For the  $L^p$ -norm of  $c$ , we similarly obtain

$$\|c(\cdot, t) - c_0\|_{L^p} \leq \|E_\alpha(-t^\alpha \mathcal{A}_\gamma)c_0 - c_0\|_{L^p} + Ct^{\alpha(1-\frac{d}{2p})} \|(n, c)\|_{\mathbb{X}} \rightarrow 0, \quad t \rightarrow 0^+.$$

Combining the above convergence results yields (5.16). This completes the proof.  $\square$

Theorem 5.1 establishes local well-posedness of system (4.10) in  $\mathbb{X}$ , and provides the key estimate (5.16) for solutions  $(n, c)(\cdot, t)$ , which guarantees continuous dependence on initial data.

We now aim to improve the temporal and spatial regularity of this mild solution. To facilitate the analysis, we introduce the shorthand  $\mathcal{G}(s) := \nabla \cdot \left( \frac{n(\mathbf{x}, s)}{c(\mathbf{x}, s)} \nabla c(\mathbf{x}, s) \right)$ , together with the Mittag-Leffler families

$$\begin{cases} \mathcal{S}_\alpha(t) := E_\alpha(-t^\alpha \mathcal{A}), & \mathcal{P}_\alpha(t) := t^{\alpha-1} E_{\alpha,\alpha}(-t^\alpha \mathcal{A}), \\ \mathcal{S}_\alpha^\gamma(t) := E_\alpha(-t^\alpha \mathcal{A}_\gamma), & \mathcal{P}_\alpha^\gamma(t) := t^{\alpha-1} E_{\alpha,\alpha}(-t^\alpha \mathcal{A}_\gamma). \end{cases} \quad (5.17)$$

Estimates for these operators are collected in Lemma Appendix A.2. With these tools in hand, we present the following lemmas on enhanced regularity.

**Lemma 5.3 (Improved temporal regularity).** *Suppose  $p > d \geq 2$  and  $T > \tau > 0$ , where  $T$  is appropriately small. Let  $(n, c)$  be the local mild solution obtained in Theorem 5.1 for Problem (1.1). Then, for  $\alpha \in (0, 1)$ , the following regularity properties hold on  $[\tau, T]$ ,*

$$\begin{aligned} c(\mathbf{x}, t) &\in L^\infty([\tau, T]; W^{2,p}(\Omega)) \cap C^{0,\alpha/2}([\tau, T]; W^{2,p}(\Omega)), \\ n(\mathbf{x}, t) &\in L^\infty([\tau, T]; W^{1,p}(\Omega)) \cap C^{0,\alpha}([\tau, T]; L^p(\Omega)). \end{aligned}$$

Moreover, for any  $\tau > 0$ , there also hold

$$\sup_{t \in [\tau, T]} \left( \|n(\mathbf{x}, t)\|_{L^\infty} + \|\nabla n(\mathbf{x}, t)\|_{L^p} + \|c(\mathbf{x}, t)\|_{L^\infty} + \|\nabla c(\mathbf{x}, t)\|_{L^\infty} \right) < \infty.$$

**Proof.** To help navigate the proof, we provide a schematic diagram in Fig.4 that outlines the logical flow of the regularity improvements.

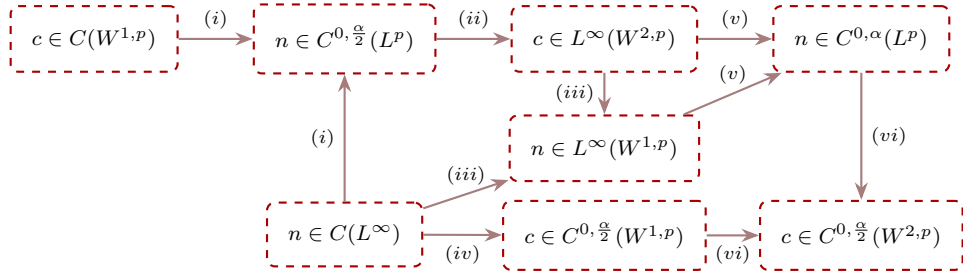


Fig. 4: The diagram for illustrating the proof of improved regularity of  $(n, c)$ .

Recall that  $\mathcal{A} = -\Delta$  is the Neumann Laplacian on  $L^p(\Omega)$ ,  $1 < p < \infty$ , and  $\mathcal{A}_\gamma = \mathcal{A} + \gamma I$  is the damped Neumann Laplacian with  $\gamma > 0$ . Since  $\gamma I$  is bounded on  $L^p(\Omega)$ , we have  $D(\mathcal{A}_\gamma) = D(\mathcal{A})$  and the norm equivalence  $\|u\|_{W^{2,p}} \simeq \|\mathcal{A}u\|_{L^p} + \|u\|_{L^p} \simeq \|\mathcal{A}_\gamma u\|_{L^p} + \|u\|_{L^p}$  (see, e.g., Ref. 82). We also recall the notation  $\mathcal{G}(s) := \nabla \cdot \left( \frac{n(\mathbf{x}, s)}{c(\mathbf{x}, s)} \nabla c(\mathbf{x}, s) \right)$  and the Mittag-Leffler families defined in (5.17). With these preparations, we prove the lemma in the following steps.

- **Step (i):**  $C^{0,\alpha/2}([\tau, T]; L^p(\Omega))$ -regularity of  $n$ .

We first establish a temporal regularity estimate for  $n$ , using the already available bounds  $n \in L^\infty((0, T) \times \Omega)$  and  $c \in L^\infty([\tau, T]; W^{1,p}(\Omega))$  from Theorem 5.1. Since  $p > d \geq 2$ , Sobolev embedding gives  $c \in L^\infty([\tau, T]; L^\infty(\Omega))$ . Together with the lower bound  $c \geq C_* > 0$  (Lemma 4.5), this implies  $F := -n \frac{\nabla c}{c}$  belongs to  $L^\infty([\tau, T]; L^p(\Omega))$ . Recalling  $\mathcal{G} = \nabla \cdot F$ , the mild solution for  $n$  reads

$$n(t) = \mathcal{S}_\alpha(t)n_0 + \int_0^t \mathcal{P}_\alpha(t-s)\mathcal{G}(s) ds.$$

Let  $\tau \leq t_1 < t_2 \leq T$ . We decompose the difference  $n(t_2) - n(t_1) = \mathcal{J}_1 + \mathcal{J}_2 + \mathcal{J}_3$ , where

$$\begin{cases} \mathcal{J}_1 := (\mathcal{S}_\alpha(t_2) - \mathcal{S}_\alpha(t_1))n_0, \\ \mathcal{J}_2 := \int_0^{t_1} (\mathcal{P}_\alpha(t_2-s) - \mathcal{P}_\alpha(t_1-s))\mathcal{G}(s) ds, \\ \mathcal{J}_3 := \int_{t_1}^{t_2} \mathcal{P}_\alpha(t_2-s)\mathcal{G}(s) ds. \end{cases} \quad (5.18)$$

For  $\mathcal{J}_3$ , using the kernel bound  $\|\mathcal{P}_\alpha(t)\nabla \cdot f\|_{L^p} \leq Ct^{\frac{\alpha}{2}-1}\|f\|_{L^p}$ , we estimate

$$\|J_3\|_{L^p} \leq C \int_{t_1}^{t_2} (t_2 - s)^{\alpha/2-1} \|F(s)\|_{L^p} ds \leq C|t_2 - t_1|^{\alpha/2}.$$

For  $\mathcal{J}_2$ , applying the fundamental theorem of calculus yields

$$\|J_2\|_{L^p} \leq C \int_{t_1}^{t_2} \int_0^{t_1} (r - s)^{\frac{\alpha}{2}-2} \|F(s)\|_{L^p} ds dr \leq C \int_{t_1}^{t_2} (r - t_1)^{\frac{\alpha}{2}-1} dr = C|t_2 - t_1|^{\frac{\alpha}{2}}.$$

For  $J_1$ , the continuous differentiability of the operator  $\mathcal{S}_\alpha(t)$  for  $t > 0$  gives  $\|J_1\|_{L^p} \leq C_\tau|t_2 - t_1|$ . Combining the estimates for  $J_1$ ,  $J_2$ , and  $J_3$ , we conclude that

$$\|n(t_2) - n(t_1)\|_{L^p} \leq C|t_2 - t_1|^{\frac{\alpha}{2}}, \quad \forall \tau \leq t_1 < t_2 \leq T.$$

Therefore, the desired Hölder regularity has been established, that is  $n \in C^{0, \frac{\alpha}{2}}([\tau, T]; L^p(\Omega))$ .

- **Step (ii):**  $L^\infty([\tau, T]; W^{2,p}(\Omega))$ -regularity of  $c$ .

For  $t \in [\tau, T]$ , applying the shifted operator  $\mathcal{A}_\gamma$  to the mild formulation of  $c$  yields

$$\|\mathcal{A}_\gamma c(\mathbf{x}, t)\|_{L^p} \leq \|\mathcal{A}_\gamma \mathcal{S}_\alpha^\gamma(t)c_0\|_{L^p} + \int_0^t \|\mathcal{A}_\gamma \mathcal{P}_\alpha^\gamma(t-s)n(\mathbf{x}, s)\|_{L^p} ds.$$

From the resolvent estimate for the Mittag-Leffler family (see Lemma 4.2), for  $t > 0$ , we have  $\|\mathcal{A}_\gamma \mathcal{S}_\alpha^\gamma(t)\|_{L^p \rightarrow L^p} \leq Ct^{-\alpha}$ . Hence, for  $t \geq \tau > 0$ ,

$$\|\mathcal{A}_\gamma \mathcal{S}_\alpha^\gamma(t)c_0\|_{L^p} \leq Ct^{-\alpha}\|c_0\|_{L^p} \leq C(\tau)\|c_0\|_{L^p}.$$

For the convolution term, write  $n(\mathbf{x}, s) = n(\mathbf{x}, t) + (n(\mathbf{x}, s) - n(\mathbf{x}, t))$ . Then

$$\begin{aligned} \int_0^t \mathcal{A}_\gamma \mathcal{P}_\alpha^\gamma(t-s)n(\mathbf{x}, s) ds &= \int_0^t \mathcal{A}_\gamma \mathcal{P}_\alpha^\gamma(t-s)(n(\mathbf{x}, s) - n(\mathbf{x}, t)) ds \\ &\quad + \left( \int_0^t \mathcal{A}_\gamma \mathcal{P}_\alpha^\gamma(t-s) ds \right) n(\mathbf{x}, t). \end{aligned}$$

Using the resolvent identity  $\int_0^t \mathcal{A}_\gamma \mathcal{P}_\alpha^\gamma(r) dr = I - \mathcal{S}_\alpha^\gamma(t)$ , we obtain

$$\mathcal{A}_\gamma c(\mathbf{x}, t) = \mathcal{A}_\gamma \mathcal{S}_\alpha^\gamma(t)c_0 + (I - \mathcal{S}_\alpha^\gamma(t))n(\mathbf{x}, t) + \int_0^t \mathcal{A}_\gamma \mathcal{P}_\alpha^\gamma(t-s)(n(\mathbf{x}, s) - n(\mathbf{x}, t)) ds.$$

By Lemma 4.2, we obtain  $\|\mathcal{S}_\alpha^\gamma(t)\|_{L^p \rightarrow L^p} \leq C$ . Since  $n(\mathbf{x}, t) \in C([0, T]; L^p(\Omega))$  from Theorem 5.1, the second term remains uniformly bounded on  $[\tau, T]$ . Moreover, Lemma Appendix A.2 gives  $\|\mathcal{A}_\gamma \mathcal{P}_\alpha^\gamma(t)\|_{L^p \rightarrow L^p} \leq Ct^{-1}(1+t^\alpha)^{-1}$ . Thus, for the third term, by the temporal Hölder continuity  $n \in C^{0, \alpha/2}([\tau, T]; L^p)$ , we have, for some  $\theta \in (0, \alpha/2]$ ,

$$\begin{aligned} &\int_0^t \|\mathcal{A}_\gamma \mathcal{P}_\alpha^\gamma(t-s)(n(\mathbf{x}, s) - n(\mathbf{x}, t))\|_{L^p} ds \\ &\leq C \int_0^t \frac{\|n(\mathbf{x}, s) - n(\mathbf{x}, t)\|_{L^p}}{(t-s)(1+(t-s)^\alpha)} ds \leq C \int_0^t \frac{|t-s|^\theta}{(t-s)(1+(t-s)^\alpha)} ds. \end{aligned}$$

Letting  $r = t-s$ , we obtain  $\int_0^t \frac{r^{\theta-1}}{1+r^\alpha} dr \leq \int_0^T r^{\theta-1} dr = \frac{T^\theta}{\theta} < \infty$ , since  $t \leq T$  and  $\theta > 0$ . Therefore the convolution term is uniformly bounded in  $t \in [\tau, T]$ , and we conclude

$$\sup_{t \in [\tau, T]} \|\mathcal{A}_\gamma c(\mathbf{x}, t)\|_{L^p} < \infty.$$

Elliptic regularity for the Neumann Laplacian implies  $\|c(\mathbf{x}, t)\|_{W^{2,p}} \simeq \|\mathcal{A}_\gamma c(\mathbf{x}, t)\|_{L^p} + \|c(\mathbf{x}, t)\|_{L^p}$  (see, e.g., Ref. 82). Since  $c(\mathbf{x}, t) \in C([0, T]; L^p(\Omega))$  from Theorem 5.1, we conclude  $c(\mathbf{x}, t) \in L^\infty([\tau, T]; W^{2,p}(\Omega))$ . Moreover, since  $p > d$ , the embedding  $W^{2,p}(\Omega) \hookrightarrow W^{1,\infty}(\Omega)$  yields

$$\sup_{t \in [\tau, T]} \left( \|c(\mathbf{x}, t)\|_{L^\infty} + \|\nabla c(\mathbf{x}, t)\|_{L^\infty} \right) < \infty. \quad (5.19)$$

- **Step (iii):**  $L^\infty([\tau, T]; W^{1,p})$ -regularity of  $n$ .

Expanding the chemotaxis term  $\mathcal{G}(t) := \nabla \cdot \left( \frac{n}{c} \nabla c \right)$ , a direct expansion gives

$$\mathcal{G} = \frac{1}{c} \nabla n \cdot \nabla c - \frac{n}{c^2} |\nabla c|^2 + \frac{n}{c} \Delta c.$$

By Lemma 4.5,  $c$  is uniformly positive on  $[\tau, T]$ , i.e.,  $c \geq C_* > 0$ . Combined with  $n \in C([\tau, T]; L^\infty(\Omega))$  and  $c \in L^\infty([\tau, T]; W^{2,p}(\Omega))$  from Theorem 5.1, along with the embedding  $W^{2,p}(\Omega) \hookrightarrow W^{1,\infty}(\Omega)$  for  $p > d \geq 2$  and the uniform bound  $\|n(t)\|_{L^\infty} \leq C_\tau$ , we establish the estimate, for all  $t \in [\tau, T]$ ,

$$\begin{aligned} \|\mathcal{G}(t)\|_{L^p} &\leq C \left( \|\nabla n(t)\|_{L^p} \|\nabla c(t)\|_{L^\infty} + \|n(t)\|_{L^\infty} \|\nabla c(t)\|_{L^\infty}^2 + \|n(t)\|_{L^\infty} \|\Delta c(t)\|_{L^p} \right) \\ &\leq C_\tau (1 + \|\nabla n(t)\|_{L^p}). \end{aligned} \quad (5.20)$$

Returning to the integral representation of  $n$  prescribed in (4.10), applying the gradient operator and using the smoothing property of the resolvent family given by Lemma Appendix A.2, namely  $\|\mathcal{A}^{1/2} \mathcal{P}_\alpha(t)\|_{L^p \rightarrow L^p} \leq C t^{\frac{\alpha}{2}-1}$ , we obtain

$$\begin{aligned} \|\mathcal{A}^{1/2} n(t)\|_{L^p} &\leq \|\mathcal{A}^{1/2} \mathcal{S}_\alpha(t) n_0\|_{L^p} + C \int_0^t (t-s)^{\frac{\alpha}{2}-1} \|\mathcal{G}(s)\|_{L^p} ds \\ &\leq C_\tau + C_\tau \int_0^t (t-s)^{\frac{\alpha}{2}-1} \|\mathcal{A}^{1/2} n(s)\|_{L^p} ds, \end{aligned}$$

where we used estimate (5.20). Setting  $u(t) := \|\mathcal{A}^{1/2} n(\mathbf{x}, t)\|_{L^p(\Omega)}$ , we form the Volterra-type inequality for  $t \in [\tau, T]$ ,

$$u(t) \leq C_\tau + C_\tau \int_0^t (t-s)^{\frac{\alpha}{2}-1} u(s) ds, \quad (5.21)$$

Since the kernel  $k(t) = C_2 t^{\frac{\alpha}{2}-1} \in L^1(0, T)$  for any  $\alpha > 0$ . Applying the Volterra-type Grönwall inequality (see Lemma 8.2 in Chapter 9 of Ref. 43) to (5.21) yields

$$u(t) = \|\mathcal{A}^{1/2} n(\mathbf{x}, t)\|_{L^p} \leq C, \quad \forall t \in [\tau, T]. \quad (5.22)$$

Combined with the already established bound  $\|n(\mathbf{x}, t)\|_{L^p} \leq C$ , it follows that  $n \in L^\infty([\tau, T]; W^{1,p}(\Omega))$ . Since  $p > d$ , the Sobolev embedding  $W^{1,p}(\Omega) \hookrightarrow L^\infty(\Omega)$  holds. Together with the uniform estimate of  $\|n(t)\|_{W^{1,p}}$  obtained above, we conclude that  $n$  is pointwise bounded on  $[\tau, T]$ , i.e.,

$$\sup_{t \in [\tau, T]} \|n(t)\|_{L^\infty} < \infty.$$

- **Step (iv):**  $C^{0,\alpha/2}([\tau, T]; W^{1,p}(\Omega))$ -regularity of  $c$ .

Let  $\tau \leq t_1 < t_2 \leq T$ . Leveraging the mild formulation of  $c(\mathbf{x}, t)$ , we decompose

$$c(\mathbf{x}, t_2) - c(\mathbf{x}, t_1) = (\mathcal{S}_\alpha^\gamma(t_2) - \mathcal{S}_\alpha^\gamma(t_1))c_0 + \int_0^{t_1} (\mathcal{P}_\alpha^\gamma(t_2 - s) - \mathcal{P}_\alpha^\gamma(t_1 - s))n(\mathbf{x}, s) ds$$

$$+ \int_{t_1}^{t_2} \mathcal{P}_\alpha^\gamma(t_2 - s)n(\mathbf{x}, s)ds =: \mathcal{K}_1 + \mathcal{K}_2 + \mathcal{K}_3.$$

We estimate each term in  $W^{1,p}(\Omega)$ .

For term  $\mathcal{K}_1$ , since  $\mathcal{S}_\alpha^\gamma(t)$  is differentiable on  $(0, \infty)$  as a bounded operator on  $L^p(\Omega)$  with  $1 < p < \infty$ , we obtain

$$\mathcal{K}_1 = (\mathcal{S}_\alpha^\gamma(t_2) - \mathcal{S}_\alpha^\gamma(t_1))c_0 = \int_{t_1}^{t_2} \partial_s \mathcal{S}_\alpha^\gamma(s) c_0 ds. \quad (5.23)$$

By taking the  $W^{1,p}$ -norm and applying Minkowski's inequality,

$$\|\mathcal{K}_1\|_{W^{1,p}} \leq \int_{t_1}^{t_2} \|\partial_s \mathcal{S}_\alpha^\gamma(s) c_0\|_{W^{1,p}} ds. \quad (5.24)$$

Recall the derivative identity (see, e.g., Ref. 104)

$$\partial_s \mathcal{S}_\alpha^\gamma(s) = \partial_s E_\alpha(-s^\alpha \mathcal{A}_\gamma) = -s^{\alpha-1} \mathcal{A}_\gamma E_{\alpha,\alpha}(-s^\alpha \mathcal{A}_\gamma) = -\mathcal{A}_\gamma \mathcal{P}_\alpha^\gamma(s). \quad (5.25)$$

Using the norm equivalence  $\|u\|_{W^{1,p}} \leq C(\|\mathcal{A}_\gamma^{1/2}u\|_{L^p} + \|u\|_{L^p})$ , and the commutativity of  $\mathcal{A}_\gamma^{1/2}$  with  $\mathcal{A}_\gamma \mathcal{P}_\alpha^\gamma(s)$ , we get

$$\|\partial_s \mathcal{S}_\alpha^\gamma(s)c_0\|_{W^{1,p}} = \|\mathcal{A}_\gamma \mathcal{P}_\alpha^\gamma(s)c_0\|_{W^{1,p}} \leq C \left( \|\mathcal{A}_\gamma \mathcal{P}_\alpha^\gamma(s)\mathcal{A}_\gamma^{1/2}c_0\|_{L^p} + \|\mathcal{A}_\gamma \mathcal{P}_\alpha^\gamma(s)c_0\|_{L^p} \right).$$

By employing the explicit resolvent-type estimate from Lemma Appendix A.2, which provides  $\|\mathcal{A}_\gamma \mathcal{P}_\alpha^\gamma(s)\|_{L^p \rightarrow L^p} \leq Cs^{-1}(1+s^\alpha)^{-1}$ , we obtain

$$\begin{aligned} \|\partial_s \mathcal{S}_\alpha^\gamma(s)c_0\|_{W^{1,p}} &\leq Cs^{-1}(1+s^\alpha)^{-1} \left( \|\mathcal{A}_\gamma^{1/2}c_0\|_{L^p} + \|c_0\|_{L^p} \right) \\ &\leq Cs^{-1}(1+s^\alpha)^{-1} \|c_0\|_{W^{1,p}} \leq Cs^{-1} \|c_0\|_{W^{1,p}}, \end{aligned}$$

where we used the property  $(1+s^\alpha)^{-1} < 1$  for all  $s > 0$ . Substituting this bound into (5.24), we infer that

$$\|\mathcal{K}_1\|_{W^{1,p}} \leq C \|c_0\|_{W^{1,p}} \int_{t_1}^{t_2} s^{-1} ds. \quad (5.26)$$

Since  $t_1, t_2 \in [\tau, T]$  with  $\tau > 0$ , the integrand is uniformly bounded by  $\tau^{-1}$ . Thus, the integral evaluates to  $\int_{t_1}^{t_2} s^{-1} ds \leq \tau^{-1}|t_2 - t_1|$ . By the embedding  $C^{0,1} \hookrightarrow C^{0,\alpha/2}$  for any  $0 < \alpha < 1$ , we obtain

$$\|\mathcal{K}_1\|_{W^{1,p}} \leq C|t_2 - t_1|^{\alpha/2}.$$

This establishes the desired Hölder continuity on  $[\tau, T]$ .

For term  $\mathcal{K}_3$ , by applying Minkowski's integral inequality, we can decompose the estimate as follows:

$$\begin{aligned} \|\mathcal{K}_3\|_{W^{1,p}} &\leq C \left( \|\mathcal{A}_\gamma^{1/2}\mathcal{K}_3\|_{L^p} + \|\mathcal{K}_3\|_{L^p} \right) \\ &\leq C \int_{t_1}^{t_2} \left( \|\mathcal{A}_\gamma^{1/2}\mathcal{P}_\alpha^\gamma(t_2 - s)n(\cdot, s)\|_{L^p} + \|\mathcal{P}_\alpha^\gamma(t_2 - s)n(\cdot, s)\|_{L^p} \right) ds. \end{aligned}$$

Recall from Lemma Appendix A.2 that  $\|\mathcal{A}_\gamma^{1/2}\mathcal{P}_\alpha^\gamma(t)\|_{L^p \rightarrow L^p} \leq Ct^{\frac{\alpha}{2}-1}(1+t^\alpha)^{-1}$ , and the standard resolvent estimate gives  $\|\mathcal{P}_\alpha^\gamma(t)\|_{L^p \rightarrow L^p} \leq Ct^{\alpha-1}(1+t^\alpha)^{-1}$ . Since  $n \in C([\tau, T]; L^\infty(\Omega))$  according to Theorem 5.1, the source term is uniformly bounded, i.e.,  $\max_{s \in [\tau, T]} \|n(\cdot, s)\|_{L^p} \leq C_\tau$ .

Substituting these into the inequality yields

$$\begin{aligned} \|\mathcal{K}_3\|_{W^{1,p}} \leq C_\tau \int_{t_1}^{t_2} & \left[ (t_2 - s)^{\frac{\alpha}{2}-1} (1 + (t_2 - s)^\alpha)^{-1} \right. \\ & \left. + (t_2 - s)^{\alpha-1} (1 + (t_2 - s)^\alpha)^{-1} \right] ds. \end{aligned}$$

Note that for all  $s \in [t_1, t_2]$ , the bounded algebraic factors satisfy  $(1 + (t_2 - s)^\alpha)^{-1/2} \leq 1$  and  $(1 + (t_2 - s)^\alpha)^{-1} \leq 1$ . Furthermore, since  $\alpha > 0$ , the temporal exponent satisfies  $\frac{\alpha}{2} - 1 < \alpha - 1$ , meaning that the singularity  $(t_2 - s)^{\frac{\alpha}{2}-1}$  dominates as  $s \rightarrow t_2$ . Consequently, on the bounded time interval, the sum inside the bracket can be sharply capped by the more singular term, leading to

$$\|\mathcal{K}_3\|_{W^{1,p}} \leq C_\tau \int_{t_1}^{t_2} (t_2 - s)^{\frac{\alpha}{2}-1} ds = \frac{2C_\tau}{\alpha} |t_2 - t_1|^{\alpha/2}. \quad (5.27)$$

For term  $\mathcal{K}_2$ , we first apply the fundamental theorem of calculus to represent the kernel difference as  $\mathcal{P}_\alpha^\gamma(t_2 - s) - \mathcal{P}_\alpha^\gamma(t_1 - s) = \int_{t_1}^{t_2} \partial_r \mathcal{P}_\alpha^\gamma(r - s) dr$ . Hence

$$\mathcal{K}_2 = \int_0^{t_1} \int_{t_1}^{t_2} \partial_r \mathcal{P}_\alpha^\gamma(r - s) n(s) dr ds.$$

Invoking the norm equivalence  $\|u\|_{W^{1,p}} \leq C(\|\mathcal{A}_\gamma^{1/2} u\|_{L^p} + \|u\|_{L^p})$  once again, together with Minkowski's inequality, we obtain

$$\|\mathcal{K}_2\|_{W^{1,p}} \leq C \int_0^{t_1} \int_{t_1}^{t_2} \left( \|\mathcal{A}_\gamma^{1/2} \partial_r \mathcal{P}_\alpha^\gamma(r - s) n(s)\|_{L^p} + \|\partial_r \mathcal{P}_\alpha^\gamma(r - s) n(s)\|_{L^p} \right) dr ds.$$

Since  $n \in C([0, T]; L^p(\Omega))$ , there exists a constant  $\bar{M} > 0$  such that  $\|n\|_{L^p} \leq \bar{M}$  for  $0 \leq s \leq T$ . Moreover, by the standard Mittag-Leffler operator estimates,  $\|\mathcal{A}_\gamma^{1/2} \partial_r \mathcal{P}_\alpha^\gamma(t)\|_{L^p \rightarrow L^p} \leq Ct^{\alpha/2-2}$ , and  $\|\partial_t \mathcal{P}_\alpha^\gamma(t)\|_{L^p \rightarrow L^p} \leq Ct^{\alpha-2}$  (see Lemma [Appendix A.2](#)). Therefore,

$$\|\mathcal{K}_2\|_{W^{1,p}} \leq C\bar{M} \int_0^{t_1} \int_{t_1}^{t_2} \left( (r - s)^{\frac{\alpha}{2}-2} + (r - s)^{\alpha-2} \right) dr ds.$$

We first estimate the more singular contribution. By Fubini's theorem,

$$\int_0^{t_1} \int_{t_1}^{t_2} (r - s)^{\frac{\alpha}{2}-2} dr ds = \int_{t_1}^{t_2} \int_0^{t_1} (r - s)^{\frac{\alpha}{2}-2} ds dr.$$

Introducing the change of variables  $u = r - s$ , we obtain  $\int_0^{t_1} (r - s)^{\frac{\alpha}{2}-2} ds = \int_{r-t_1}^r u^{\frac{\alpha}{2}-2} du$ . Since  $\alpha/2 - 2 < -1$ , direct integration yields  $\int_{r-t_1}^r u^{\frac{\alpha}{2}-2} du = \frac{1}{1-\alpha/2} [(r - t_1)^{\alpha/2-1} - r^{\alpha/2-1}]$ . Because  $\alpha/2 - 1 < 0$ , it follows that  $\int_0^{t_1} (r - s)^{\frac{\alpha}{2}-2} ds \leq C(r - t_1)^{\alpha/2-1}$ . Integrating once more with respect to  $r$ , we arrive at  $\int_{t_1}^{t_2} (r - t_1)^{\alpha/2-1} dr = \frac{2}{\alpha} |t_2 - t_1|^{\alpha/2}$ . Hence,

$$\int_0^{t_1} \int_{t_1}^{t_2} (r - s)^{\frac{\alpha}{2}-2} dr ds \leq C |t_2 - t_1|^{\frac{\alpha}{2}}.$$

Similarly,

$$\int_0^{t_1} \int_{t_1}^{t_2} (r - s)^{\alpha-2} dr ds \leq C |t_2 - t_1|^\alpha.$$

Combining the above estimates and observing that  $|t_2 - t_1|^\alpha \leq T^{\alpha/2}|t_2 - t_1|^{\alpha/2}$ , we conclude that

$$\|\mathcal{K}_2\|_{W^{1,p}} \leq C_{\tau,T}|t_2 - t_1|^{\alpha/2}. \quad (5.28)$$

Therefore,  $\mathcal{K}_2$  satisfies the desired Hölder's regularity in  $W^{1,p}(\Omega)$ .

Collecting all of the aforementioned estimates, we may conclude that  $c(\mathbf{x}, t) \in C^{0,\alpha/2}([\tau, T]; W^{1,p}(\Omega))$  for  $\tau > 0$  and  $p > d \geq 2$ .

- **Step** (v):  $C^{0,\alpha}([\tau, T]; L^p(\Omega))$ -regularity of  $n$ .

In view of the estimates (5.20) and (5.22), with  $c \in L^\infty([\tau, T]; W^{2,p}(\Omega))$  and  $n \in L^\infty([\tau, T]; W^{1,p})$ , we now have  $\mathcal{G} \in L^\infty([\tau, T]; L^p(\Omega))$ . Based on this, to rigorously establish that  $n \in C^{0,\alpha}([\tau, T]; L^p(\Omega))$ , we choose  $\tau \leq t_1 < t_2 \leq T$  and recall the decomposition of  $n(t_2) - n(t_1)$  in (5.18).

For  $\mathcal{J}_1$ , since  $t_1 \geq \tau > 0$ , the differentiability of  $\mathcal{S}_\alpha(t)$  yields a localized Lipschitz bound  $\|\mathcal{J}_1\|_{L^p} \leq C_\tau|t_2 - t_1|$ , which algebraically embeds into  $C^{0,\alpha}$ . For  $\mathcal{J}_3$ , the standard resolvent estimate  $\|\mathcal{P}_\alpha(t)\|_{L^p \rightarrow L^p} \leq Ct^{\alpha-1}$  (see Lemma Appendix A.2) coupled with the result  $\mathcal{G} \in L^\infty([\tau, T]; L^p(\Omega))$  directly implies  $\|\mathcal{J}_3\|_{L^p} \leq C\|\mathcal{G}\|_{L^\infty} \int_{t_1}^{t_2} (t_2 - s)^{\alpha-1} ds \leq C|t_2 - t_1|^\alpha$ . Finally, for  $\mathcal{J}_2$ , we express the kernel difference as  $\int_{t_1}^{t_2} \partial_\theta \mathcal{P}_\alpha(\theta - s) d\theta$  and utilize the temporal derivative decay estimate  $\|\partial_\theta \mathcal{P}_\alpha(\theta - s)\|_{L^p \rightarrow L^p} \leq C(\theta - s)^{\alpha-2}$ . Applying Fubini's theorem to exchange the integration order over the domain yields the sharp bound  $\int_{t_1}^{t_2} \int_0^{t_1} (\theta - s)^{\alpha-2} ds d\theta = \frac{1}{1-\alpha} \int_{t_1}^{t_2} [(\theta - t_1)^{\alpha-1} - \theta^{\alpha-1}] \leq C|t_2 - t_1|^\alpha$ , thereby confirming that  $\|\mathcal{J}_2\|_{L^p} \leq C|t_2 - t_1|^\alpha$ . Combining these three bounds yields

$$\|n(t_2) - n(t_1)\|_{L^p} \leq C_{\tau,T}|t_2 - t_1|^\alpha, \quad (5.29)$$

which implies  $n \in C^{0,\alpha}([\tau, T]; L^p(\Omega))$ .

- **Step** (vi):  $C^{0,\alpha/2}([\tau, T]; W^{2,p}(\Omega))$ -regularity of  $c$ .

We now proceed to establish the temporal Hölder continuity of  $c$  in  $W^{2,p}(\Omega)$ . Recall the mild solution for  $c$  in (4.10) that

$$\mathcal{A}_\gamma c(t) = \mathcal{A}_\gamma \mathcal{S}_\alpha^\gamma(t) c_0 + (I - \mathcal{S}_\alpha^\gamma(t))n(t) + \int_0^t \mathcal{A}_\gamma \mathcal{P}_\alpha^\gamma(t-s)(n(s) - n(t)) ds.$$

For convenience, we define the three terms on the right-hand side as  $H_1(t)$ ,  $H_2(t)$ , and  $H_3(t)$ , respectively,  $H_1(t) := \mathcal{A}_\gamma \mathcal{S}_\alpha^\gamma(t) c_0$ ,  $H_2(t) := (I - \mathcal{S}_\alpha^\gamma(t))n(t)$ ,  $H_3(t) := \int_0^t \mathcal{A}_\gamma \mathcal{P}_\alpha^\gamma(t-s)(n(s) - n(t)) ds$ . Let  $\tau \leq t_1 < t_2 \leq T$ . We estimate the increments of  $H_1$ ,  $H_2$ , and  $H_3$  separately.

For  $H_1$ , if  $t_1 \geq \tau > 0$ , the operator  $\mathcal{A}_\gamma \mathcal{S}_\alpha^\gamma(t)$  is smooth in  $t$ , so  $H_1$  is Lipschitz on  $[\tau, T]$ , which implies  $\|H_1(t_2) - H_1(t_1)\|_{L^p} \leq C_\tau|t_2 - t_1| \|c_0\|_{L^p}$ .

For  $H_2$ , we write

$$H_2(t_2) - H_2(t_1) = (I - \mathcal{S}_\alpha^\gamma(t_2))(n(t_2) - n(t_1)) + (\mathcal{S}_\alpha^\gamma(t_1) - \mathcal{S}_\alpha^\gamma(t_2))n(t_1).$$

Since  $n \in C^{0,\alpha}([\tau, T]; L^p(\Omega))$  and  $\mathcal{S}_\alpha^\gamma(t)$  is uniformly bounded on  $L^p(\Omega)$ , it follows that  $\|(I - \mathcal{S}_\alpha^\gamma(t_2))(n(t_2) - n(t_1))\|_{L^p} \leq C|t_2 - t_1|^\alpha$ . Moreover, arguing as above,

$$\|(\mathcal{S}_\alpha^\gamma(t_1) - \mathcal{S}_\alpha^\gamma(t_2))n(t_1)\|_{L^p} \leq \int_{t_1}^{t_2} \|\mathcal{A}_\gamma \mathcal{P}_\alpha^\gamma(r)\|_{L^p \rightarrow L^p} dr \|n(t_1)\|_{L^p} \leq C_\tau|t_2 - t_1|.$$

Therefore,

$$\|H_2(t_2) - H_2(t_1)\|_{L^p} \leq C|t_2 - t_1|^\alpha.$$

We now proceed to estimate  $H_3$ . To this end, we decompose the increment as  $H_3(t_2) - H_3(t_1) = I_1 + I_2$ , where

$$I_2 = \int_{t_1}^{t_2} \mathcal{A}_\gamma \mathcal{P}_\alpha^\gamma(t_2 - s)(n(s) - n(t_2)) ds,$$

and

$$I_1 = \int_0^{t_1} [\mathcal{A}_\gamma \mathcal{P}_\alpha^\gamma(t_2 - s)(n(s) - n(t_2)) - \mathcal{A}_\gamma \mathcal{P}_\alpha^\gamma(t_1 - s)(n(s) - n(t_1))] ds.$$

For the term  $I_2$ , we employ the Hölder continuity of  $n$  to obtain

$$\begin{aligned} \|I_2\|_{L^p} &\leq C \int_{t_1}^{t_2} (t_2 - s)^{-1} \|n(s) - n(t_2)\|_{L^p} ds \\ &\leq C \int_{t_1}^{t_2} (t_2 - s)^{\alpha-1} ds \leq C|t_2 - t_1|^\alpha. \end{aligned}$$

To estimate  $I_1$ , we further split it as  $I_1 = I_{11} + I_{12}$ , where

$$\begin{cases} I_{11} = \int_0^{t_1} (\mathcal{A}_\gamma \mathcal{P}_\alpha^\gamma(t_2 - s) - \mathcal{A}_\gamma \mathcal{P}_\alpha^\gamma(t_1 - s))(n(s) - n(t_1)) ds, \\ I_{12} = \int_0^{t_1} \mathcal{A}_\gamma \mathcal{P}_\alpha^\gamma(t_2 - s)(n(t_1) - n(t_2)) ds. \end{cases}$$

For  $I_{11}$ , applying the fundamental theorem of calculus yields

$$\mathcal{A}_\gamma \mathcal{P}_\alpha^\gamma(t_2 - s) - \mathcal{A}_\gamma \mathcal{P}_\alpha^\gamma(t_1 - s) = \int_{t_1}^{t_2} \partial_r (\mathcal{A}_\gamma \mathcal{P}_\alpha^\gamma(r - s)) dr.$$

By Lemma [Appendix A.2](#), we have  $\|\partial_r (\mathcal{A}_\gamma \mathcal{P}_\alpha^\gamma(r - s))\|_{L^p \rightarrow L^p} \leq C(r - s)^{-2}$ . Therefore,

$$\begin{aligned} \|I_{11}\|_{L^p} &\leq C \int_{t_1}^{t_2} \int_0^{t_1} (r - s)^{-2} \|n(s) - n(t_1)\|_{L^p} ds dr \\ &\leq C \int_{t_1}^{t_2} \int_0^{t_1} (r - s)^{-2} (t_1 - s)^\alpha ds dr. \end{aligned}$$

By introducing the change of variables  $u = t_1 - s$ , we have  $r - s = (r - t_1) + u$ . This allows us to estimate the inner integral as follows

$$\begin{aligned} \int_0^{t_1} (r - s)^{-2} (t_1 - s)^\alpha ds &= \int_0^{t_1} ((r - t_1) + u)^{-2} u^\alpha du \\ &\leq \int_0^\infty ((r - t_1) + u)^{-2} u^\alpha du = C(r - t_1)^{\alpha-1}. \end{aligned}$$

Consequently,

$$\|I_{11}\|_{L^p} \leq C \int_{t_1}^{t_2} (r - t_1)^{\alpha-1} dr \leq C|t_2 - t_1|^\alpha.$$

For  $I_{12}$ , we use the identity  $\int_0^{t_1} \mathcal{A}_\gamma \mathcal{P}_\alpha^\gamma(t_2 - s) ds = \mathcal{S}_\alpha^\gamma(t_2 - t_1) - \mathcal{S}_\alpha^\gamma(t_2)$  to explicitly evaluate it as  $I_{12} = (\mathcal{S}_\alpha^\gamma(t_2 - t_1) - \mathcal{S}_\alpha^\gamma(t_2))(n(t_1) - n(t_2))$ . Since the operator  $\mathcal{S}_\alpha^\gamma(t)$  is uniformly bounded on  $L^p(\Omega)$ , we obtain the estimate

$$\|I_{12}\|_{L^p} \leq C \|n(t_1) - n(t_2)\|_{L^p} \leq C |t_2 - t_1|^\alpha.$$

Combining the bounds for  $I_{11}$ ,  $I_{12}$ , and  $I_2$ , we conclude that

$$\|H_3(t_2) - H_3(t_1)\|_{L^p} \leq C |t_2 - t_1|^\alpha.$$

Furthermore, aggregating the estimates for  $H_1$ ,  $H_2$ , and  $H_3$  yields

$$\|\mathcal{A}_\gamma c(t_2) - \mathcal{A}_\gamma c(t_1)\|_{L^p} \leq C |t_2 - t_1|^\alpha,$$

which implies that  $\mathcal{A}_\gamma c \in C^{0,\alpha/2}([\tau, T]; L^p(\Omega))$ . On the other hand, it has been established in Step (iv) that  $c \in C^{0,\alpha/2}([\tau, T]; W^{1,p}(\Omega))$ . Leveraging the continuous embedding  $W^{1,p}(\Omega) \hookrightarrow L^p(\Omega)$ , we deduce

$$\|c(t_2) - c(t_1)\|_{L^p} \leq C |t_2 - t_1|^{\alpha/2}.$$

Finally, utilizing the norm equivalence  $\|u\|_{W^{2,p}(\Omega)} \leq C(\|\mathcal{A}_\gamma u\|_{L^p(\Omega)} + \|u\|_{L^p(\Omega)})$  for  $u \in D(\mathcal{A}_\gamma)$ , we obtain

$$\|c(t_2) - c(t_1)\|_{W^{2,p}} \leq C \|\mathcal{A}_\gamma(c(t_2) - c(t_1))\|_{L^p} + C \|c(t_2) - c(t_1)\|_{L^p} \leq C |t_2 - t_1|^{\alpha/2}.$$

Hence,  $c \in C^{0,\alpha}([\tau, T]; W^{2,p}(\Omega))$ . In particular,  $D^2 c \in C^{0,\alpha/2}([\tau, T]; L^p(\Omega))$ . This completes the proof.  $\square$

**Lemma 5.4 (Improved spatial regularity).** *Let  $T > 0$  be appropriately small and let  $(n, c)$  be the local mild solution of System (1.1). Then  $n(\mathbf{x}, t) \in C^{0,\alpha/2}((0, T]; W^{1,p}(\Omega)) \cap C((0, T]; D(\mathcal{A}))$  and  $c(\mathbf{x}, t) \in C((0, T]; D(\mathcal{A}))$  for  $p > d \geq 2$ .*

**Proof.** Let  $\mathcal{A} := -\Delta$  be the Neumann Laplacian on  $L^p(\Omega)$ . To establish the desired temporal continuity in  $D(\mathcal{A})$ , it suffices to show that  $n, c \in C([\tau, T]; D(\mathcal{A}))$  for every  $\tau > 0$ .

The spatial regularity of  $c$  follows directly from Lemma 5.3, which guarantees that  $c \in C^{0,\alpha}([\tau, T]; W^{2,p}(\Omega)) \subset C([\tau, T]; W^{2,p}(\Omega))$ . Since  $c$  satisfies the Neumann boundary condition,  $c(t) \in D(\mathcal{A}_\gamma) = D(\mathcal{A})$ . The equivalence between the graph norm of  $D(\mathcal{A})$  and the  $W^{2,p}(\Omega)$  norm, then yields  $c \in C([\tau, T]; D(\mathcal{A}))$ .

For the regularity of  $n$ , we use the mild formulation

$$n(t) = \mathcal{S}_\alpha(t)n_0 + \int_0^t \mathcal{P}_\alpha(t-s)\mathcal{G}(s)ds,$$

where  $\mathcal{G} := \chi(\frac{1}{c}\nabla n \cdot \nabla c - \frac{n}{c^2}|\nabla c|^2 + \frac{n}{c}\Delta c)$ . From Lemma 5.3, we know  $\mathcal{G} \in L^\infty((0, T]; L^p(\Omega))$ . Fix  $\tau > 0$  and introduce a strict time-truncation parameter  $\delta := \tau/2 > 0$ . The proof proceeds in the following sequential stages.

- **Step (i):** The Hölder continuity of  $n$  bounded away from  $t = 0$ .

To this end, we estimate the regularity of  $n(t)$  for  $t \in [\delta, T]$ . Since  $t \geq \delta > 0$ , the initial value term satisfies  $\mathcal{S}_\alpha(t)n_0 \in C^\infty([\delta, T]; D(\mathcal{A}))$ . For the convolution integral, utilizing the estimate  $\|\mathcal{A}^{1/2}\mathcal{P}_\alpha(t)\|_{L^p \rightarrow L^p} \leq Ct^{\alpha/2-1}$  from Lemma Appendix A.2 and arguing exactly as in Step (iii) of Lemma 5.3, we rigorously deduce that  $\mathcal{A}^{1/2}n \in C^{0,\alpha/2}([\delta, T]; L^p(\Omega))$ . Therefore, via domain characterization, we obtain  $n \in C^{0,\alpha/2}([\delta, T]; W^{1,p}(\Omega))$ .

- **Step (ii):** The Hölder continuity of the forcing term  $\mathcal{G}$ .

Since  $p > d \geq 2$ , the embeddings  $W^{1,p}(\Omega) \hookrightarrow L^\infty(\Omega)$  and  $W^{2,p}(\Omega) \hookrightarrow W^{1,\infty}(\Omega)$  hold. We collect the regularities on the restricted interval  $[\delta, T]$ :  $c \in C^{0,\alpha}([\delta, T]; W^{2,p}(\Omega))$ , which gives  $\Delta c \in C^{0,\alpha}([\delta, T]; L^p(\Omega))$  and  $\nabla c, c^{-1} \in C^{0,\alpha}([\delta, T]; L^\infty(\Omega))$ .  $n \in C^{0,\alpha/2}([\delta, T]; W^{1,p}(\Omega))$ , which gives  $\nabla n \in C^{0,\alpha/2}([\delta, T]; L^p(\Omega))$  and  $n \in C^{0,\alpha/2}([\delta, T]; L^\infty(\Omega))$ . Applying standard product rules for Hölder spaces, we deduce that each nonlinear component of  $\mathcal{G}$  is Hölder continuous. Consequently  $\mathcal{G} \in C^{0,\alpha/2}([\delta, T]; L^p(\Omega))$ .

- **Step (iii):** The continuity of  $\mathcal{A}n$ .

Define  $\mathcal{J}(t) = \int_0^t \mathcal{P}_\alpha(t-s)\mathcal{G}(s)ds$ . To rigorously justify that  $\mathcal{J}(t) \in D(\mathcal{A})$  and  $\mathcal{A}\mathcal{J}(t)$  is continuous, we split  $\mathcal{J}(t)$  into a regular history part and a singular local part, namely

$$\mathcal{J}(t) = \int_0^{t-\delta} \mathcal{P}_\alpha(t-s)\mathcal{G}(s)ds + \int_{t-\delta}^t \mathcal{P}_\alpha(t-s)\mathcal{G}(s)ds := \mathcal{J}_1(t) + \mathcal{J}_2(t). \quad (5.30)$$

For  $\mathcal{J}_1(t)$ , the temporal variable  $s$  is strictly separated from  $t$  such that  $t-s \geq \delta > 0$ . In this regime,  $\mathcal{A}\mathcal{P}_\alpha(t-s)$  is uniformly bounded and differentiable. Thus,  $\mathcal{A}$  is allowed to pass through the integral, yielding

$$\mathcal{I}_1(t) := \mathcal{A}\mathcal{J}_1(t) \in C([\tau, T]; L^p(\Omega)).$$

For  $\mathcal{J}_2(t)$ , the operator  $\mathcal{A}$  cannot be directly pulled inside the singular integral. Instead, we rewrite  $\mathcal{J}_2(t)$  by adding and subtracting  $\mathcal{G}$ , i.e.,

$$\mathcal{J}_2(t) = \int_{t-\delta}^t \mathcal{P}_\alpha(t-s)(\mathcal{G}(s) - \mathcal{G}(t))ds + \left( \int_0^\delta \mathcal{P}_\alpha(r)dr \right) \mathcal{G}(t).$$

Applying  $\mathcal{A}$  to this expression is now mathematically well-defined. Using the fundamental relation  $\frac{d}{dt}\mathcal{S}_\alpha(t) = -\mathcal{A}\mathcal{P}_\alpha(t)$ , we have  $\mathcal{A} \int_0^\delta \mathcal{P}_\alpha(r)dr = I - \mathcal{S}_\alpha(\delta)$ . Therefore, we obtain

$$\mathcal{I}_2(t) := \mathcal{A}\mathcal{J}_2(t) = \int_{t-\delta}^t \mathcal{A}\mathcal{P}_\alpha(t-s)(\mathcal{G}(s) - \mathcal{G}(t))ds + (I - \mathcal{S}_\alpha(\delta))\mathcal{G}(t).$$

The boundary term  $(I - \mathcal{S}_\alpha(\delta))\mathcal{G}(t)$  is continuous since  $\mathcal{G} \in C([\delta, T]; L^p)$  and  $I - \mathcal{S}_\alpha(\delta)$  is a bounded operator. For the convolution integral, since both  $s$  and  $t$  lie within  $[\delta, T]$ , we apply the Hölder continuity of  $\mathcal{G}$  established as before, and thus there is

$$\|\mathcal{A}\mathcal{P}_\alpha(t-s)(\mathcal{G}(s) - \mathcal{G}(t))\|_{L^p} \leq C(t-s)^{-1}|t-s|^\gamma = C(t-s)^{\gamma-1}.$$

Since  $(t-s)^{\gamma-1} \in L^1(0, \delta)$  for  $\gamma > 0$ , the integral converges absolutely. Moreover, the integrand depends continuously on  $t$  and is dominated by the integrable function  $C(t-s)^{\gamma-1}$ . Hence the continuity of the integral follows from the Lebesgue dominated convergence theorem. Thus,  $\mathcal{I}_2 \in C([\tau, T]; L^p(\Omega))$ .

Combining the above estimates yields  $\mathcal{A}n(t) \in C([\tau, T]; L^p(\Omega))$ . Since the mild formulation already ensures  $n \in C([\tau, T]; L^p(\Omega))$ , it follows from the graph norm characterization of  $D(\mathcal{A})$  that  $n \in C([\tau, T]; D(\mathcal{A}))$  for every  $\tau > 0$ . Therefore, we conclude  $n \in C((0, T]; D(\mathcal{A}))$ . The proof is complete.  $\square$

**Theorem 5.2.** *Let  $\Omega \subset \mathbb{R}^d$  ( $d \geq 2$ ) be a bounded domain with smooth boundary  $\partial\Omega$ . If the initial data  $n_0(\mathbf{x})$  and  $c_0(\mathbf{x})$  satisfy the conditions specified in (3.4), then for  $p > d$ , there exists  $T > 0$*

properly small such that Problem (1.1) admits a unique local mild solution  $(n, c)(\mathbf{x}, t)$  satisfying

$$\begin{cases} n(\mathbf{x}, t) \in C([0, T]; L^\infty(\Omega)) \cap C^{0, \alpha/2}((0, T]; W^{1, p}(\Omega)) \cap C((0, T]; D(\mathcal{A})), \\ c(\mathbf{x}, t) \in C([0, T]; W^{1, p}(\Omega)) \cap C^{0, \alpha/2}((0, T]; W^{2, p}(\Omega)) \cap C((0, T]; D(\mathcal{A})). \end{cases}$$

Furthermore, the solution components  $n$  and  $c$  satisfy  $n(\cdot, t) \geq 0$  and  $c(\cdot, t) > 0$  for all  $t > 0$ , respectively.

**Proof.** By Theorem 5.1, problem (1.1) admits a unique local mild solution  $(n, c)$  on the time interval  $[0, T]$  for some  $T > 0$ . Higher-order temporal and spatial regularity is subsequently established via a bootstrap argument in Lemmas 5.3 and 5.4. What's more, the non-negativity of  $n(\mathbf{x}, t)$  and the strict positivity of  $c(\mathbf{x}, t)$  are rigorously guaranteed by Lemmas 4.4 and 4.6, respectively.  $\square$

## 6. Global Well-Posedness of Mild Solutions for Two- and Three-Dimensional Systems

### 6.1. A novel Lyapunov functional

We establish a conditional energy functional method to prove the global boundedness of solutions to system (1.1). Motivated by previous works on chemotaxis systems (see, e.g., 24, 30, 64, 103), the core idea of this approach lies in constructing and analyzing a carefully designed time-dependent energy functional whose dissipation controls the growth of the solution, thereby preventing finite-time blow-up. However, the classical logarithmic sensitivity model is not directly applicable to Problem (1.1), and the analysis is further complicated by the lack of available theoretical results for time-nonlocal KS models with logarithmic sensitivity.

To address the aforementioned difficulties, we adopt the strategy of Ref. 106 for time-fractional phase-field equations, which resolves the issue of constructing a dissipation-preserving energy functional for Caputo fractional derivatives. Inspired by their use of a time-weighted average of the classical energy, we introduce the following novel Lyapunov functional for our problem:

$$\mathcal{E}[(n, c)](t) := \int_0^t (t-s)^{\alpha-1} \mathcal{F}(s) ds, \quad t > 0, \quad (6.1)$$

where  $\mathcal{F}(\cdot)$  is a jointly convex function defined by

$$\mathcal{F}(t) := \mathcal{F}[(n, c)](t) = \underbrace{\int_{\Omega} n \log \left( \frac{n}{\bar{n}} \right) d\mathbf{x}}_{:= \mathcal{F}_1(n)} + \theta \underbrace{\int_{\Omega} \frac{|\nabla c|^2}{c} d\mathbf{x}}_{:= \mathcal{F}_2(c, \nabla c)}, \quad (6.2)$$

with  $\bar{n} := \frac{1}{|\Omega|} \int_{\Omega} n d\mathbf{x}$  and  $\theta > 0$  a constant. The non-negativity of  $\mathcal{F}(t)$  is fundamental to our analysis. Indeed, since  $\varphi(n) = n \log n$  is strictly convex, Jensen's inequality gives  $\int_{\Omega} n \log n d\mathbf{x} \geq |\Omega| \bar{n} \log \bar{n}$ , which ensures  $\mathcal{F}_1(n) \geq 0$ . Combined with the obvious non-negativity of the term  $\mathcal{F}_2(c, \nabla c)$ , we conclude  $\mathcal{F}(t) \geq 0$  for all  $t > 0$ . The non-negativity of  $\mathcal{F}(t)$  on  $[0, T]$  ensures that  $\mathcal{E}(t) \geq 0$  as a direct consequence of the positivity of the integral kernel  $(t-s)^{\alpha-1}$ .

**Remark 6.1.** The Lyapunov functional (6.1) is defined as a time-convolution of the free energy (6.2) with the positive kernel  $(t-s)^{\alpha-1}$ . This structure captures history-dependent energy accumulation associated with the evolution of system (1.1). It tracks the cumulative effect of the instantaneous free energy over time, rather than relying solely on pointwise-in-time estimates, and provides a convenient framework for establishing boundedness of mild solutions.

Let  $\phi(n) := n \log\left(\frac{n}{\bar{n}}\right)$  for  $n \in [0, \infty)$ . The functional  $\mathcal{F}_1(n)$  is strictly convex on the set  $\{n \in L^1(\Omega) : n \geq 0; \int_{\Omega} n d\mathbf{x} = \tilde{M}\}$ . Defining  $\phi(0) := 0$  and using  $\lim_{n \rightarrow 0^+} \phi(n) = 0$ , we obtain the continuity of  $\phi$  on  $[0, \infty)$ . Moreover,  $\phi$  is strictly convex on  $(0, \infty)$  since  $\phi''(n) = 1/n > 0$ . By the fundamental theorem of convex analysis, for any  $n_1, n_2 \in [0, \infty)$  with  $n_1 \neq n_2$  and  $\lambda \in (0, 1)$ , the following inequality

$$\phi(\lambda n_1 + (1 - \lambda)n_2) < \lambda\phi(n_1) + (1 - \lambda)\phi(n_2) \quad (6.3)$$

holds. Integrating (6.3) over  $\Omega$  and employing the linearity of integrals yields

$$\mathcal{F}_1(\lambda n_1 + (1 - \lambda)n_2) < \lambda\mathcal{F}_1(n_1) + (1 - \lambda)\mathcal{F}_1(n_2),$$

establishing that  $\mathcal{F}_1(n)$  is strictly convex for  $n \geq 0$ .

For  $\mathcal{F}_2(c, \nabla c)$ , which depends on both  $c$  and  $\nabla c$ , to confirm its strict convexity, we need to verify the convexity of the bivariate function  $f(u, \mathbf{v}) = \frac{|\mathbf{v}|^2}{u}$ , where  $u = c > 0$  and  $\mathbf{v} = \nabla c$ . Specifically, define  $f : \mathbb{R}^+ \times \mathbb{R}^d \rightarrow \mathbb{R}$  as  $f(u, \mathbf{v}) = \frac{\sum_{i=1}^d v_i^2}{u}$ . Its Hessian matrix  $\mathbf{H}_f$  is given by

$$\mathbf{H}_f = \frac{2}{u^3} \begin{pmatrix} |\mathbf{v}|^2 & -uv_1 & \dots & -uv_d \\ -uv_1 & u^2 & \dots & 0 \\ \vdots & \vdots & \ddots & \vdots \\ -uv_d & 0 & \dots & u^2 \end{pmatrix}.$$

For any vector  $\mathbf{z} = (a, b_1, \dots, b_d)^T \in \mathbb{R}^{d+1}$ , we have

$$\mathbf{z}^T \mathbf{H}_f \mathbf{z} = \frac{2}{u^3} (a^2 |\mathbf{v}|^2 - 2a u \mathbf{v} \cdot \mathbf{b} + u^2 |\mathbf{b}|^2) = \frac{2}{u^3} |a\mathbf{v} - u\mathbf{b}|^2 \geq 0, \quad (6.4)$$

indicating that the Hessian matrix  $\mathbf{H}_f$  is positive semi-definite, which implies that  $\mathcal{F}_2(c, \nabla c)$  is jointly convex.

Combining the above analyses, we conclude that the functional  $\mathcal{F}(t)$  is jointly convex on the admissible set. Moreover, the function  $\mathcal{F}(t)$  enjoys the following significant property.

**Lemma 6.1 (Variational inequality).** *Let  $\mathcal{F}(t)$  be the convex functional defined in (6.2). Then for all  $t > 0$ ,*

$${}_0^C \mathfrak{D}_t^\alpha \mathcal{F}(t) \leq \int_{\Omega} \frac{\delta \mathcal{F}}{\delta n} {}_0^C \mathfrak{D}_t^\alpha n \, d\mathbf{x} + \int_{\Omega} \frac{\delta \mathcal{F}}{\delta c} {}_0^C \mathfrak{D}_t^\alpha c \, d\mathbf{x}, \quad (6.5)$$

where  $\frac{\delta \mathcal{F}}{\delta n}$  and  $\frac{\delta \mathcal{F}}{\delta c}$  denote the variational derivatives of  $\mathcal{F}$  with respect to  $n$  and  $c$ , respectively.

**Proof.** By the linearity of the Caputo fractional derivative  ${}_0^C \mathfrak{D}_t^\alpha$ , it follows that

$${}_0^C \mathfrak{D}_t^\alpha \mathcal{F}(t) = {}_0^C \mathfrak{D}_t^\alpha \mathcal{F}_1(t) + {}_0^C \mathfrak{D}_t^\alpha \mathcal{F}_2(t).$$

To obtain the result of (6.5), we estimate each term separately.

For  $\mathcal{F}_1$ , by employing the extended fractional convex inequality (Lemma 2.12 in Ref. 62) and invoking the strict convexity of  $\mathcal{F}_1(t)$ , we obtain, for all  $t > 0$ ,

$${}_0^C \mathfrak{D}_t^\alpha \int_{\Omega} n \log\left(\frac{n}{\bar{n}}\right) \, d\mathbf{x} \leq \int_{\Omega} \left(\log\left(\frac{n}{\bar{n}}\right) + 1\right) {}_0^C \mathfrak{D}_t^\alpha n \, d\mathbf{x} = \int_{\Omega} \frac{\delta \mathcal{F}_1}{\delta n} {}_0^C \mathfrak{D}_t^\alpha n \, d\mathbf{x}, \quad (6.6)$$

with  $\frac{\delta \mathcal{F}_1}{\delta n} = \log\left(\frac{n}{\bar{n}}\right) + 1 = \frac{\delta \mathcal{F}}{\delta n}$ . The final equality follows from the homogeneous Neumann boundary condition ( $\mathbf{J} \cdot \nu = 0$ , which indicates that there is no matter entering or leaving the boundary). By Gauss's divergence theorem, we have  $\int_{\Omega} {}_0^C \mathfrak{D}_t^\alpha n \, d\mathbf{x} = - \int_{\Omega} \nabla \cdot \mathbf{J} \, d\mathbf{x} = - \int_{\partial\Omega} \mathbf{J} \cdot \nu \, d\sigma =$

0, with the flux  $\mathbf{J}$  defined as  $\mathbf{J} := -\mathcal{D}\nabla n + \mathcal{D}\chi_c \frac{n}{c} \nabla c$ . This is also another characterization of the law of conservation of mass.

For  $\mathcal{F}_2$ , the presence of spatial gradients prevents a direct application of convex inequality. To preserve the proof structure and address this issue, we first introduce the Bregman's distance (see, e.g., Ref. 19) to manage the jointly convex function  $\mathcal{F}_2(c, \nabla c)$ . Define  $f(t) = f(c(t), \nabla c(t)) := |\nabla c|^2/c$ . At any time  $t$ , for past moments  $s$  and a fixed point  $\mathbf{x} \in \Omega \subset \mathbb{R}^d$ , by virtue of the joint convexity of  $f(c, \nabla c)$  (see (6.4)), the following exact identity holds

$$\begin{aligned} f(c(s), \nabla c(s)) &= f(c(t), \nabla c(t)) + \frac{\partial f}{\partial c}(t)[c(s) - c(t)] \\ &\quad + \frac{\partial f}{\partial(\nabla c)}(t) \cdot [\nabla c(s) - \nabla c(t)] + \mathfrak{B}(s, t), \end{aligned} \quad (6.7)$$

where  $\mathfrak{B}(s, t) \geq 0$  (for  $s \in [0, t]$ ) represents the Bregman distance associated with  $f$  when  $f$  is jointly convex. Note that  $\mathfrak{B}(s, t) = 0$  if and only if  $(c(s), \nabla c(s)) = (c(t), \nabla c(t))$ .

Using the equivalent representation of the Caputo derivative (see, e.g., Ref. 62)

$${}_0^C \mathfrak{D}_t^\alpha f(t) = \frac{f(t) - f(0)}{\Gamma(1-\alpha)t^\alpha} + \frac{\alpha}{\Gamma(1-\alpha)} \int_0^t \frac{f(t) - f(s)}{(t-s)^{\alpha+1}} ds,$$

and substituting the expression for  $f(t) - f(s)$  derived from (6.7) into the pointwise derivative, we obtain

$$\begin{aligned} {}_0^C \mathfrak{D}_t^\alpha f(t) &= \underbrace{\frac{\partial f(t)}{\partial c} \left[ \frac{c(t) - c(0)}{\Gamma(1-\alpha)t^\alpha} + \frac{\alpha}{\Gamma(1-\alpha)} \int_0^t \frac{c(t) - c(s)}{(t-s)^{\alpha+1}} ds \right]}_{\frac{\partial f}{\partial c} \cdot {}_0^C \mathfrak{D}_t^\alpha c} \\ &\quad + \underbrace{\sum_{i=1}^d \frac{\partial f(t)}{\partial(\partial_{x_i} c)} \left[ \frac{\partial_{x_i} c(t) - \partial_{x_i} c(0)}{\Gamma(1-\alpha)t^\alpha} + \frac{\alpha}{\Gamma(1-\alpha)} \int_0^t \frac{\partial_{x_i} c(t) - \partial_{x_i} c(s)}{(t-s)^{\alpha+1}} ds \right]}_{\frac{\partial f}{\partial \nabla c} \cdot {}_0^C \mathfrak{D}_t^\alpha \nabla c} \\ &\quad - \underbrace{\left[ \frac{\mathfrak{B}(0, t)}{\Gamma(1-\alpha)t^\alpha} + \frac{\alpha}{\Gamma(1-\alpha)} \int_0^t \frac{\mathfrak{B}(s, t)}{(t-s)^{\alpha+1}} ds \right]}_{\mathcal{R}(t) \geq 0} \\ &= \frac{\partial f}{\partial c} {}_0^C \mathfrak{D}_t^\alpha c + \frac{\partial f}{\partial \nabla c} \cdot {}_0^C \mathfrak{D}_t^\alpha \nabla c - \mathcal{R}(\mathbf{x}, t). \end{aligned} \quad (6.8)$$

Since the kernel  $(t-s)^{-\alpha}$  is independent of the spatial variable  $\mathbf{x}$ , by Leibniz's integral rule and  $c$  is  $C^1$  in  $\mathbf{x}$ , the gradient operator commutes with the time fractional derivative operator, i.e.,  ${}_0^C \mathfrak{D}_t^\alpha \nabla c = \nabla {}_0^C \mathfrak{D}_t^\alpha c$ . Integrating both side of (6.8) over  $\Omega$  yields

$${}_0^C \mathfrak{D}_t^\alpha \mathcal{F}_2 = \theta \int_\Omega \frac{\partial f}{\partial c} {}_0^C \mathfrak{D}_t^\alpha c \, d\mathbf{x} + \theta \int_\Omega \frac{\partial f}{\partial \nabla c} \cdot \nabla ({}_0^C \mathfrak{D}_t^\alpha c) \, d\mathbf{x} - \theta \int_\Omega \mathcal{R}(\mathbf{x}, t) \, d\mathbf{x}.$$

Applying Green's formula (integration by parts) with the homogeneous Neumann condition, we get

$${}_0^C \mathfrak{D}_t^\alpha \mathcal{F}_2 = \int_\Omega \left[ \theta \left( -\frac{|\nabla c|^2}{c^2} - 2\nabla \cdot \frac{\nabla c}{c} \right) \right] {}_0^C \mathfrak{D}_t^\alpha c \, d\mathbf{x} - \theta \int_\Omega \mathcal{R}(\mathbf{x}, t) \, d\mathbf{x}.$$

Recalling that the variational derivative is given by  $\frac{\delta \mathcal{F}_2}{\delta c} = \theta \left( \frac{\partial f}{\partial c} - \nabla \cdot \frac{\partial f}{\partial \nabla c} \right) = \theta \left( -\frac{|\nabla c|^2}{c^2} - 2\nabla \cdot \frac{\nabla c}{c} \right) = \frac{\delta \mathcal{F}_2}{\delta c}$ , and noting the non-negativity of the remainder term  $\int_\Omega \mathcal{R}(\mathbf{x}, t) \, d\mathbf{x} \geq 0$ , it follows that

$${}_0^C \mathfrak{D}_t^\alpha \mathcal{F}_2 \leq \int_\Omega \frac{\delta \mathcal{F}_2}{\delta c} {}_0^C \mathfrak{D}_t^\alpha c \, d\mathbf{x}, \quad t > 0. \quad (6.9)$$

Combining (6.6) and (6.9) yields the desired inequality (6.5). This completes the proof of the lemma.  $\square$

Crucially, Lemma 6.1 establishes a variational inequality (6.5) that bridges the fractional energy law and the system's long-term decay. This result is indispensable for proving the convergence of the Lyapunov functional and represents one of the central technical innovations of this work.

**Lemma 6.2.** *Let  $\Omega \subset \mathbb{R}^d$  ( $d \geq 2$ ) be a bounded domain with smooth boundary, and  $(n, c)$  be a solution of System (1.1). For the convex functional  $\mathcal{F}(t)$  defined in (6.2), if  $0 < \chi < 1/2$ , then it holds that  ${}^C_0\mathcal{D}_t^\alpha \mathcal{F}(t) < 0$  for all  $t > 0$ . Furthermore, there is a positive constant  $\lambda > 0$  such that the dissipation estimate*

$${}^C_0\mathcal{D}_t^\alpha \mathcal{F}(t) \leq -\lambda \mathcal{F}(t), \quad t > 0, \quad (6.10)$$

holds, which implies

$$\mathcal{F}(t) \leq \mathcal{F}(0)E_\alpha(-\lambda t^\alpha) \leq \mathcal{F}(0) < \infty, \quad t > 0. \quad (6.11)$$

**Proof.** For brevity, we denote the variational derivatives by  $\mu_n := \frac{\delta \mathcal{F}}{\delta n}$  and  $\mu_c := \frac{\delta \mathcal{F}}{\delta c}$ . By invoking Lemma 6.1 and substituting the dynamics from System (1.1) into the variational inequality (6.5), followed by integration by parts, results in

$${}^C_0\mathcal{D}_t^\alpha \mathcal{F} \leq \langle \mu_n, {}^C_0\mathcal{D}_t^\alpha n \rangle + \langle \mu_c, {}^C_0\mathcal{D}_t^\alpha c \rangle := \mathcal{I}_n(t) + \mathcal{I}_c(t). \quad (6.12)$$

A direct computation yields

$$\begin{aligned} \mathcal{I}_n(t) &:= \int_{\Omega} \left( \log\left(\frac{n}{\bar{n}}\right) + 1 \right) {}^C_0\mathcal{D}_t^\alpha n \, dx \\ &= \int_{\Omega} \log\left(\frac{n}{\bar{n}}\right) \left[ \mathcal{D}\Delta n - \mathcal{D}\chi \nabla \cdot \left( \frac{n}{c} \nabla c \right) \right] dx \quad \left( \because \int_{\Omega} {}^C_0\mathcal{D}_t^\alpha n \, dx = 0 \right) \\ &= -\mathcal{D} \int_{\Omega} \nabla \log n \cdot \nabla n \, dx + \mathcal{D}\chi \int_{\Omega} \nabla \log n \cdot \frac{n}{c} \nabla c \, dx \\ &= -4\mathcal{D} \int_{\Omega} |\nabla \sqrt{n}|^2 \, dx + 2\mathcal{D}\chi \int_{\Omega} \frac{\sqrt{n}}{c} \nabla \sqrt{n} \cdot \nabla c \, dx. \end{aligned}$$

Similarly,

$$\begin{aligned} \mathcal{I}_c(t) &:= \int_{\Omega} \theta \left( -2\frac{\Delta c}{c} + \frac{|\nabla c|^2}{c^2} \right) [\mathcal{D}\Delta c - \gamma c + n] \, dx \\ &= -2\theta \mathcal{D} \int_{\Omega} \frac{(\Delta c)^2}{c} \, dx + \theta \mathcal{D} \int_{\Omega} \frac{|\nabla c|^2 \Delta c}{c^2} \, dx - \gamma \theta \int_{\Omega} \frac{|\nabla c|^2}{c} \, dx \\ &\quad + 4\theta \int_{\Omega} \frac{\sqrt{n} \nabla \sqrt{n} \cdot \nabla c}{c} \, dx - \theta \int_{\Omega} \frac{n |\nabla c|^2}{c^2} \, dx. \end{aligned}$$

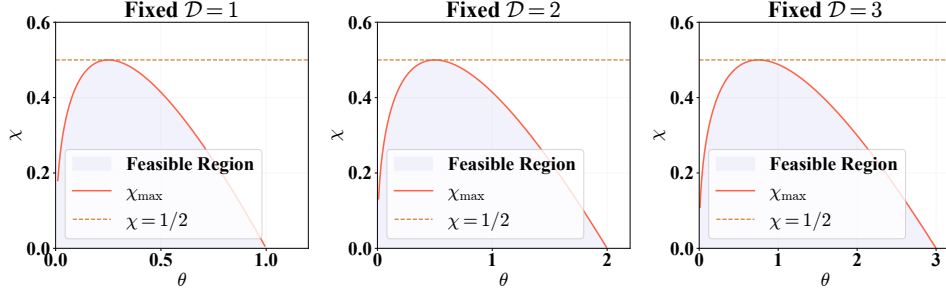


Fig. 5: (Color online) Numerical illustration of the feasible region determined by Problem (6.14) under various fixed  $\mathcal{D}$ .

Combining  $\mathcal{I}_n$  and  $\mathcal{I}_c$ , we get

$$\begin{aligned}
 \mathcal{I}(t) &= \underbrace{-4\mathcal{D} \int_{\Omega} |\nabla \sqrt{n}|^2 dx + 2(\mathcal{D}\chi + 2\theta) \int_{\Omega} \frac{\sqrt{n} \nabla \sqrt{n} \cdot \nabla c}{c} dx - \theta \int_{\Omega} \frac{n |\nabla c|^2}{c^2} dx}_{:= \mathcal{J}_1} \\
 &\quad \underbrace{-2\theta \mathcal{D} \int_{\Omega} \frac{(\Delta c)^2}{c} dx + \theta \mathcal{D} \int_{\Omega} \frac{|\nabla c|^2 \Delta c}{c^2} dx - \gamma \theta \int_{\Omega} \frac{|\nabla c|^2}{c} dx}_{:= \mathcal{J}_2} \\
 &=: \mathcal{J}_1 + \mathcal{J}_2 - \gamma \theta \int_{\Omega} \frac{|\nabla c|^2}{c} dx.
 \end{aligned} \tag{6.13}$$

Defining  $\mathbf{u}(\mathbf{x}, t) := \nabla \sqrt{n}$  and  $\mathbf{v}(\mathbf{x}, t) := \frac{\sqrt{n} \nabla c}{c}$ , then the term  $\mathcal{J}_1$  can be rewritten as

$$\mathcal{J}_1 = \int_{\Omega} \left[ -4\mathcal{D} |\mathbf{u}|^2 + 2(\mathcal{D}\chi + 2\theta) \mathbf{u} \cdot \mathbf{v} - \theta |\mathbf{v}|^2 \right] dx.$$

The integrand is the quadratic form

$$\mathcal{Q}(\mathbf{u}, \mathbf{v}) := \begin{pmatrix} \mathbf{u} \\ \mathbf{v} \end{pmatrix}^T \mathbf{A} \begin{pmatrix} \mathbf{u} \\ \mathbf{v} \end{pmatrix}, \quad \text{with } \mathbf{A} := \begin{pmatrix} -4\mathcal{D} & \mathcal{D}\chi + 2\theta \\ \mathcal{D}\chi + 2\theta & -\theta \end{pmatrix}.$$

By Sylvester's criterion (for  $-\mathbf{A}$  positive definite), its negative definite necessary and sufficient condition is that the determinant  $\det(\mathbf{A}) > 0$  (and the first-order principal form  $-4\mathcal{D} < 0$  obviously true), i.e.,

$$4\mathcal{D}\theta - (\mathcal{D}\chi + 2\theta)^2 > 0 \iff 4\theta^2 - 4\mathcal{D}(1 - \chi)\theta + \mathcal{D}^2\chi^2 < 0. \tag{6.14}$$

When  $0 < \chi < 1/2$ , the discriminant of the above quadratic inequality is  $\Delta = 16\mathcal{D}^2(1 - 2\chi) > 0$ , and the solution set of this inequality is exactly  $\theta \in (\theta_-, \theta_+)$  with  $\theta_{\pm} = \frac{\mathcal{D}}{2}(1 - \chi \pm \sqrt{1 - 2\chi})$ . The reason for setting  $0 < \chi < 1/2$  is clearly observed from Fig. 5. Choosing  $\theta$  in this interval, the quadratic form is strongly negative definite, thus, there exists a constant  $\mu_0 > 0$ , such that

$$\mathcal{J}_1 \leq -\mu_0 \int_{\Omega} \left( |\nabla \sqrt{n}|^2 + \frac{n |\nabla c|^2}{c^2} \right) dx. \tag{6.15}$$

For  $\mathcal{J}_2$ , since  $\Omega$  is convex and leveraging the lower bound  $c \geq C_{\mathbb{N}} > 0$  from Lemma 4.5, we apply the pointwise identity  $\frac{1}{2}\Delta|\nabla c|^2 = |\nabla^2 c|^2 + \nabla c \cdot \nabla(\Delta c)$  (cf. the proof of Lemma 3.1 in Ref. 132) and the fact that  $\partial\nu|\nabla c|^2 \leq 0$  (see Lemma 3.1 in Ref. 79) to obtain

$$\begin{aligned} \mathcal{J}_2 &= -2\theta\mathcal{D} \int_{\Omega} \frac{(\Delta c)^2}{c} d\mathbf{x} + \theta\mathcal{D} \int_{\Omega} \frac{|\nabla c|^2 \Delta c}{c^2} d\mathbf{x} \\ &= -2\theta\mathcal{D} \int_{\Omega} c |\nabla^2 \log c|^2 d\mathbf{x} + \theta\mathcal{D} \int_{\partial\Omega} \frac{1}{c} \frac{\partial|\nabla c|^2}{\partial\nu} dS \leq 0. \end{aligned} \quad (6.16)$$

This finding is further supported by Ref. 24, specifically Lemma 3.1. Substituting the estimates (6.15) and (6.16) into (6.12) or (6.13), and invoking the lower bound of  $c$ , we arrive at the total energy dissipation:

$${}^C\mathfrak{D}_t^\alpha \mathcal{F}(t) \leq -\mu_0 \int_{\Omega} |\nabla\sqrt{n}|^2 d\mathbf{x} - \gamma\theta \int_{\Omega} \frac{|\nabla c|^2}{c} d\mathbf{x} < 0, \quad t > 0. \quad (6.17)$$

This confirms that the functional  $\mathcal{F}(t)$  is non-increasing along the trajectories of the system.

To rigorously establish the dissipation estimate (6.10), we utilize the Logarithmic Sobolev Inequality (LSI)<sup>45</sup>. Since  $\Omega \subset \mathbb{R}^d$  is a bounded domain with smooth boundary,  $\bar{\Omega}$  can be regarded as a compact smooth Riemannian manifold with boundary, endowed with the Euclidean metric. In this geometric setting, the Ricci curvature is zero, and the convexity of  $\partial\Omega$  ensures that the second fundamental form of the boundary is non-negative. Following the framework of Deuschel and Stroock Ref. 34, Chung and Yau Ref. 26, the Neumann Laplace operator on such a manifold satisfies the logarithmic Sobolev inequality (LSI). Specifically, we define the normalized probability measure  $d\mu = d\mathbf{x}/|\Omega|$  and the corresponding density  $f = n/\bar{n}$ , where  $\bar{n} = \tilde{M}/|\Omega|$  is the spatial average under mass conservation. Employing the identity  $|\nabla\sqrt{f}|^2 = \frac{1}{4} \frac{|\nabla f|^2}{f}$ , on the set  $\{f > 0\}$ , the LSI is given by

$$\int_{\Omega} f \log f d\mu \leq \frac{1}{2\rho} \int_{\Omega} \frac{|\nabla f|^2}{f} d\mu,$$

with  $\rho \geq \min\left\{\frac{\lambda_1}{8e}, \frac{1}{d \cdot D(\Omega)^2}\right\} > 0$ , and where  $D(\Omega)$  denotes the diameter of  $\Omega$ ,  $\lambda_1$  is the first eigenvalue of the Laplacian, and  $e$  denotes the Euler constant. To map this to our physical variables, we observe that

$$\int_{\Omega} \frac{n}{\bar{n}} \log\left(\frac{n}{\bar{n}}\right) \frac{d\mathbf{x}}{|\Omega|} = \frac{1}{\tilde{M}} \int_{\Omega} n \ln\left(\frac{n}{\bar{n}}\right) d\mathbf{x} = \frac{\mathcal{F}_1(t)}{\tilde{M}},$$

and

$$\int_{\Omega} \frac{|\nabla(n/\bar{n})|^2}{n/\bar{n}} \frac{d\mathbf{x}}{|\Omega|} = \frac{1}{\bar{n}|\Omega|} \int_{\Omega} \frac{|\nabla n|^2}{n} d\mathbf{x} = \frac{4}{\tilde{M}} \int_{\Omega} |\nabla\sqrt{n}|^2 d\mathbf{x}.$$

Substituting these back into LSI and eliminating the mass  $\tilde{M}$ , we obtain the functional bound

$$\mathcal{F}_1(t) \leq \frac{2}{\rho} \int_{\Omega} |\nabla\sqrt{n}|^2 d\mathbf{x}, \quad t > 0.$$

Hence, the first dissipation term in the energy law satisfies

$$\mu_0 \int_{\Omega} |\nabla\sqrt{n}|^2 d\mathbf{x} \geq \tilde{\lambda} \mathcal{F}_1(t), \quad t > 0 \quad (6.18)$$

where the decay rate  $\tilde{\lambda} := \mu_0\rho/2 > 0$  is determined by the geometric spectral gap of  $\Omega$ .

For the second component  $\mathcal{F}_2(t) = \theta \int_{\Omega} \frac{|\nabla c|^2}{c} dx$ , the linear degradation term directly yields

$$\gamma \theta \int_{\Omega} \frac{|\nabla c|^2}{c} dx = \gamma \mathcal{F}_2(t). \quad (6.19)$$

Inserting (6.18) and (6.19) into the energy evolution equation (6.17), we arrive at

$${}_0^C \mathcal{D}_t^\alpha \mathcal{F}(t) \leq -\tilde{\lambda} \mathcal{F}_1(t) - \gamma(\theta \mathcal{F}_2(t)), \quad t > 0. \quad (6.20)$$

By setting  $\lambda := \min\{\tilde{\lambda}, \gamma\} > 0$ , the inequality simplifies to

$${}_0^C \mathcal{D}_t^\alpha \mathcal{F}(t) \leq -\lambda(\mathcal{F}_1(t) + \theta \mathcal{F}_2(t)) = -\lambda \mathcal{F}(t), \quad t > 0. \quad (6.21)$$

By Lemma 3.2, we conclude that

$$\mathcal{F}(t) \leq \mathcal{F}(0) E_\alpha(-\lambda t^\alpha), \quad t > 0, \quad (6.22)$$

where  $E_\alpha(\cdot)$  is the Mittag-Leffler function. This result characterizes the algebraic decay of the system toward its equilibrium state, completing the proof.  $\square$

**Lemma 6.3 (Nonlocal Lyapunov dissipation).** *Let  $\Omega \subset \mathbb{R}^d$  ( $d \geq 2$ ) be a bounded domain with smooth boundary. Suppose  $(n, c)$  is the mild global solution of Problem (1.1) with  $\gamma > 0$ ,  $0 < \chi < 1/2$ , and  $\alpha \in (0, 1)$ . Let  $\mathcal{E}[(n, c)](t)$  be the Lyapunov functional defined in (6.1), with associated energy  $\mathcal{F}(t)$  given by (6.2). Then for some  $\lambda > 0$ ,*

$$\mathcal{F}(t) + \frac{\lambda}{\Gamma(\alpha)} \mathcal{E}[(n, c)](t) \leq \mathcal{F}(0), \quad t > 0. \quad (6.23)$$

As a consequence, the solution satisfies the uniform bounds

$$\mathcal{F}(t) \leq \mathcal{F}(0), \quad \text{and} \quad \mathcal{E}[(n, c)](t) \leq \frac{\Gamma(\alpha)}{\lambda} \mathcal{F}(0), \quad t > 0.$$

**Proof.** Applying the Riemann-Liouville fractional integral  ${}_0 I_t^\alpha$  to the dissipation inequality (6.10) established in Lemma 6.2, we obtain

$${}_0 I_t^\alpha ({}_0^C \mathcal{D}_t^\alpha \mathcal{F}(t)) \leq -\lambda {}_0 I_t^\alpha (\mathcal{F}(t)).$$

By Invoking the fundamental theorem of fractional calculus for Caputo derivatives, which states that for  $0 < \alpha < 1$ ,  ${}_0 I_t^\alpha ({}_0^C \mathcal{D}_t^\alpha f(t)) = f(t) - f(0)$  (cf. Ref. 104), we deduce that

$$\mathcal{F}(t) - \mathcal{F}(0) \leq -\lambda {}_0 I_t^\alpha \mathcal{F}(t), \quad t > 0.$$

According to (6.1), since  ${}_0 I_t^\alpha \mathcal{F}(t) = \frac{1}{\Gamma(\alpha)} \mathcal{E}[(n, c)](t)$ , we obtain

$$\mathcal{F}(t) + \frac{\lambda}{\Gamma(\alpha)} \mathcal{E}(t) \leq \mathcal{F}(0), \quad t > 0,$$

which is exactly (6.23). By virtue of the non-negativity of  $\mathcal{E}[(n, c)](t)$  immediately gives  $\mathcal{F}(t) \leq \mathcal{F}(0)$ . Moreover, since  $\mathcal{F}(t)$  is also non-negative, rearranging (6.23) directly implies

$$\mathcal{E}[(n, c)](t) \leq \frac{\Gamma(\alpha)}{\lambda} \mathcal{F}(0), \quad \forall t > 0.$$

This completes the proof.  $\square$

## 6.2. Global well-posedness

According to Theorem 5.2, the well-posedness of local mild solutions is known. To extend globally, it suffices to show that the working norm remains uniformly bounded on the time interval  $[0, \infty)$ .

**Lemma 6.4.** *Let  $d = 2$ ,  $\gamma > 0$ , and let  $\Omega \subset \mathbb{R}^2$  be a bounded domain with smooth boundary. Suppose  $0 < \chi < \frac{1}{2}$ , and let  $(n, c)$  be a global mild solution of System (1.1) on  $[0, \infty)$ . Then, for every finite  $q > 2$ , there exists a constant  $C = C(\|n_0\|_{L^\infty}, \|c_0\|_{W^{1,\infty}}, q, \Omega) > 0$  such that*

$$\sup_{t \geq 0} (\|n(\cdot, t)\|_{L^\infty} + \|c(\cdot, t)\|_{W^{1,q}}) \leq C.$$

Here the dependence of  $C$  on the fixed parameters  $\alpha, \mathcal{D}, \gamma, \chi$  and  $C_*$  (lower bound of  $c$ ) is suppressed.

**Proof.** We prove the estimate on an arbitrary finite interval  $[0, T]$ , with constants independent of  $T$ . Since  $T > 0$  is arbitrary, the desired uniform-in-time estimate follows by letting  $T \rightarrow \infty$ . To this end, we proceed by breaking the proof into the following sequence of implications, with the outline presented in Fig. 6.

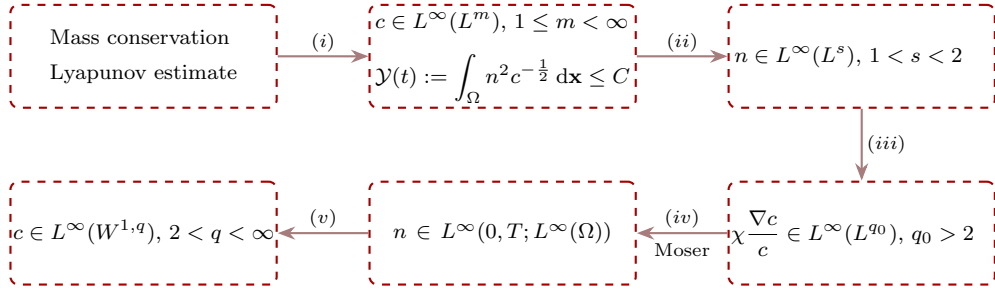


Fig. 6: Schematic diagram of the bootstrap argument used to prove uniform boundedness of  $(n, c)$ .

- **Step (i):**  $L^m$ -bound for  $c$ ,  $1 \leq m < \infty$ .

We start from the a priori estimates already obtained above. By virtue of the dissipation property established in Lemma 6.2, for some  $\lambda > 0$ , we have

$$\mathcal{F}(t) \leq \mathcal{F}(0) E_\alpha(-\lambda t^\alpha) \leq \mathcal{F}(0) < \infty, \quad t > 0. \quad (6.24)$$

Recalling the definition of  $\mathcal{F}(t)$  in (6.2), the uniform bound on  $\mathcal{F}(t)$  directly implies that the relative entropy term  $\int_\Omega n \log(n/\bar{n}) dx$  is bounded from (6.24), where  $\bar{n} = \frac{1}{|\Omega|} \int_\Omega n dx$ . By utilizing the properties of the logarithm, and combining it with the mass conservation  $\|n(\mathbf{x}, t)\|_{L^1} = \|n_0\|_{L^1} \equiv \tilde{M}$  from Lemma 4.3, we can decompose the integral as

$$\int_\Omega n \log\left(\frac{n}{\bar{n}}\right) dx = \int_\Omega n \log n dx - \tilde{M} \log \bar{n} \leq C, \quad 0 < t < T. \quad (6.25)$$

Similarly, as both terms in  $\mathcal{F}$  are nonnegative, this gives in particular

$$\int_\Omega \frac{|\nabla c|^2}{c} dx \leq C, \quad 0 < t < T. \quad (6.26)$$

We next extract from (4.12) a uniform  $L^1$ -bound for  $c$ . To this end, set  $C_c(t) := \int_{\Omega} c(\mathbf{x}, t) d\mathbf{x}$ . Then (4.12) can be written in the compact form

$$C_c(t) + \gamma {}_0I_t^\alpha C_c(t) = C_c(0) + \tilde{M} {}_0I_t^\alpha 1(t), \quad (6.27)$$

where  ${}_0I_t^\alpha$  denotes the Riemann-Liouville fractional integral. Indeed,  ${}_0I_t^\alpha 1(t) = \frac{t^\alpha}{\Gamma(1+\alpha)}$ . Equivalently, (6.27) can be rearranged as

$$C_c(t) - C_c(0) = {}_0I_t^\alpha (\tilde{M} - \gamma C_c)(t).$$

This is precisely the Volterra integral formulation of the scalar Caputo equation

$${}^C\mathfrak{D}_t^\alpha C_c(t) + \gamma C_c(t) = \tilde{M}, \quad C_c(0) = \int_{\Omega} c_0(\mathbf{x}) d\mathbf{x}.$$

Thus the spatial total mass of  $c$  is governed by a one-dimensional fractional relaxation equation with a constant source term  $\tilde{M}$ .

For completeness, we derive the explicit representation. Taking the Laplace transform of (6.27), and using  $\mathcal{L}\{{}_0I_t^\alpha f\}(z) = z^{-\alpha} \mathcal{L}\{f\}(z)$  (cf. Ref. 104), we obtain

$$\widehat{C}_c(z) + \gamma z^{-\alpha} \widehat{C}_c(z) = C_c(0) z^{-1} + \tilde{M} z^{-\alpha-1}.$$

Equivalently,

$$\widehat{C}_c(z) = \frac{C_c(0) z^{\alpha-1}}{z^\alpha + \gamma} + \frac{\tilde{M} z^{-1}}{z^\alpha + \gamma}. \quad (6.28)$$

By employing the standard Laplace transform identity for the Mittag-Leffler function, namely  $\mathcal{L}\{t^{\beta-1} E_{\alpha, \beta}(-\gamma t^\alpha)\}(z) = \frac{z^{\alpha-\beta}}{z^\alpha + \gamma}$  for any  $\beta > 0$ , we infer from (6.28) that

$$C_c(t) = C_c(0) E_\alpha(-\gamma t^\alpha) + \tilde{M} t^\alpha E_{\alpha, \alpha+1}(-\gamma t^\alpha). \quad (6.29)$$

The second term in (6.29) is uniformly bounded. Indeed, by the series definition of the Mittag-Leffler functions,

$$\begin{aligned} \gamma t^\alpha E_{\alpha, \alpha+1}(-\gamma t^\alpha) &= \gamma t^\alpha \sum_{j=0}^{\infty} \frac{(-\gamma t^\alpha)^j}{\Gamma(\alpha j + \alpha + 1)} = \sum_{k=1}^{\infty} \frac{(-1)^{k-1} (\gamma t^\alpha)^k}{\Gamma(\alpha k + 1)} \\ &= 1 - \sum_{k=0}^{\infty} \frac{(-\gamma t^\alpha)^k}{\Gamma(\alpha k + 1)} = 1 - E_\alpha(-\gamma t^\alpha). \end{aligned}$$

Therefore,

$$C_c(t) = C_c(0) E_\alpha(-\gamma t^\alpha) + \frac{\tilde{M}}{\gamma} (1 - E_\alpha(-\gamma t^\alpha)). \quad (6.30)$$

Since  $0 < \alpha < 1$ , the function  $E_\alpha(-\gamma t^\alpha)$  is completely monotone on  $t > 0$ , and in particular  $0 \leq E_\alpha(-\gamma t^\alpha) \leq 1$  for  $t \geq 0$  (cf. Refs. 62, 42). Hence (6.30) gives

$$0 \leq C_c(t) \leq C_c(0) + \frac{\tilde{M}}{\gamma}, \quad t > 0.$$

Since  $c > 0$ , we have  $\|c(\cdot, t)\|_{L^1(\Omega)} = C_c(t)$ . Consequently,

$$\sup_{0 < t < T} \|c(\cdot, t)\|_{L^1(\Omega)} \leq C_c(0) + \frac{\tilde{M}}{\gamma} \leq C. \quad (6.31)$$

The estimate in (6.26) gives

$$\|\nabla\sqrt{c}\|_{L^2}^2 = \frac{1}{4} \int_{\Omega} \frac{|\nabla c|^2}{c} \, d\mathbf{x} \leq C.$$

Together with (6.31), this yields

$$\sup_{0 < t < T} \|\sqrt{c}(\cdot, t)\|_{H^1(\Omega)} \leq C.$$

Since  $d = 2$ , the Sobolev embedding  $H^1(\Omega) \hookrightarrow L^r(\Omega)$  holds for every finite  $r \geq 1$ . Hence, for every finite  $m \geq 1$ ,

$$\sup_{0 < t < T} \|c(\cdot, t)\|_{L^m(\Omega)} \leq C_m. \quad (6.32)$$

- **Step (ii):**  $L^s$ -bound for  $n$  with  $s \in (1, 2)$ .

We now introduce the auxiliary weighted functional  $\mathcal{Y}(t) := \int_{\Omega} n^2 c^{-\frac{1}{2}} \, d\mathbf{x}$ . This quantity serves as an intermediate bootstrap functional, upgrading the entropy-level information to an  $L^s$ -bound for  $n$  with some exponent  $s > 1$ .

Consider the density  $\Phi(n, c) := n^2 c^{-\frac{1}{2}}$ . A direct computation gives  $\Phi_{nn} = 2c^{-\frac{1}{2}}$ ,  $\Phi_{cc} = \frac{3}{4}n^2 c^{-\frac{5}{2}}$ , and  $\Phi_{nc} = -nc^{-\frac{3}{2}}$ . Moreover,

$$\Phi_{nn}\Phi_{cc} - \Phi_{nc}^2 = \frac{1}{2}n^2 c^{-3} \geq 0.$$

Thus  $\Phi$  is convex on  $\mathbb{R} \times (0, \infty)$ . Applying the Caputo variational inequality in Lemma 6.1, or equivalently the same convexity argument used in its proof, gives

$${}_0^C \mathfrak{D}_t^\alpha \mathcal{Y}(t) \leq \int_{\Omega} \left( 2nc^{-\frac{1}{2}} {}_0^C \mathfrak{D}_t^\alpha n - \frac{1}{2}n^2 c^{-\frac{3}{2}} {}_0^C \mathfrak{D}_t^\alpha c \right) \, d\mathbf{x}. \quad (6.33)$$

Substituting System (1.1) into (6.33) and integrating by parts, we get

$$\begin{aligned} {}_0^C \mathfrak{D}_t^\alpha \mathcal{Y}(t) \leq & \mathcal{D} \left[ -2 \int_{\Omega} c^{-\frac{1}{2}} |\nabla n|^2 \, d\mathbf{x} + (2 + 2\chi) \int_{\Omega} nc^{-\frac{3}{2}} \nabla n \cdot \nabla c \, d\mathbf{x} \right. \\ & \left. - \left( \frac{3}{4} + \chi \right) \int_{\Omega} n^2 c^{-\frac{5}{2}} |\nabla c|^2 \, d\mathbf{x} \right] + \frac{\gamma}{2} \int_{\Omega} n^2 c^{-\frac{1}{2}} \, d\mathbf{x} - \frac{1}{2} \int_{\Omega} n^3 c^{-\frac{3}{2}} \, d\mathbf{x}. \end{aligned} \quad (6.34)$$

Let  $A := c^{-\frac{1}{4}} |\nabla n|$  and  $B := nc^{-\frac{5}{4}} |\nabla c|$ . Then  $nc^{-\frac{3}{2}} |\nabla n| |\nabla c| = AB$ . By Young's inequality,

$$(2 + 2\chi)AB \leq 2A^2 + \frac{(2 + 2\chi)^2}{8} B^2.$$

Therefore the gradient contribution in (6.34) is bounded from above by

$$-\mathcal{D} \left( \left( \frac{3}{4} + \chi \right) - \frac{(2 + 2\chi)^2}{8} \right) \int_{\Omega} n^2 c^{-\frac{5}{2}} |\nabla c|^2 \, d\mathbf{x}.$$

Since  $\left( \frac{3}{4} + \chi \right) - \frac{(2 + 2\chi)^2}{8} = \frac{1}{4} - \frac{\chi^2}{2} > 0$  for  $0 < \chi < \frac{1}{2}$ , this contribution is non-positive. Hence

$${}_0^C \mathfrak{D}_t^\alpha \mathcal{Y}(t) \leq \frac{\gamma}{2} \mathcal{Y}(t) - \frac{1}{2} \int_{\Omega} n^3 c^{-\frac{3}{2}} \, d\mathbf{x}. \quad (6.35)$$

It remains to relate the last integral to  $\mathcal{Y}(t)$ . Since  $\mathcal{Y}(t) = \int_{\Omega} (n^3 c^{-3/2})^{2/3} c^{1/2} \, d\mathbf{x}$ , Hölder's inequality and (6.32) with  $m = 3/2$  imply

$$\mathcal{Y}(t) \leq \left( \int_{\Omega} n^3 c^{-\frac{3}{2}} \, d\mathbf{x} \right)^{2/3} \left( \int_{\Omega} c^{\frac{3}{2}} \, d\mathbf{x} \right)^{1/3} \leq C \left( \int_{\Omega} n^3 c^{-\frac{3}{2}} \, d\mathbf{x} \right)^{2/3}.$$

Consequently,

$$\int_{\Omega} n^3 c^{-\frac{3}{2}} \, d\mathbf{x} \geq C\mathcal{Y}(t)^{3/2}. \quad (6.36)$$

Combining (6.35) and (6.36), we obtain

$${}_0^C \mathcal{D}_t^\alpha \mathcal{Y}(t) \leq a\mathcal{Y}(t) - b\mathcal{Y}(t)^{3/2}$$

for some  $a, b > 0$ . The scalar comparison principle Lemma [Appendix A.3](#) yields

$$\sup_{0 < t < T} \mathcal{Y}(t) \leq C. \quad (6.37)$$

Let  $s \in (1, 2)$ . Since  $n^s = (n^2 c^{-1/2})^{s/2} c^{s/4}$ , Hölder's inequality gives

$$\int_{\Omega} n^s \, d\mathbf{x} \leq \mathcal{Y}(t)^{\frac{s}{2}} \left( \int_{\Omega} c^{\frac{s}{2(2-s)}} \, d\mathbf{x} \right)^{(2-s)/2}.$$

Using (6.32) and (6.37), we infer

$$\sup_{0 < t < T} \|n(\cdot, t)\|_{L^s(\Omega)} \leq C_s, \quad 1 < s < 2. \quad (6.38)$$

- **Step (iii):** The estimate for  $\mathbf{V} := \chi \frac{\nabla c}{c}$ .

We now improve the spatial regularity of  $c$ . By employing the mild formulation, as written with the operators defined in (4.3), and applying  $\mathcal{A}^{1/2}$  to it, we obtain

$$\mathcal{A}^{1/2} c(t) = \mathcal{A}^{1/2} E_\alpha(-t^\alpha \mathcal{A}_\gamma) c_0 + \int_0^t (t-\tau)^{\alpha-1} \mathcal{A}^{1/2} E_{\alpha,\alpha}(-(t-\tau)^\alpha \mathcal{A}_\gamma) n(\tau) \, d\tau. \quad (6.39)$$

The initial term is bounded in  $L^{q_0}(\Omega)$  for every finite  $q_0 > 1$ , because  $c_0 \in W^{1,\infty}(\Omega)$  and the Mittag-Leffler family is bounded on the corresponding fractional domain.

Fix  $s \in (1, 2)$  as in (6.38). Choose  $q_0 > 2$ , sufficiently close to 2, such that  $\mu := \frac{1}{s} - \frac{1}{q_0} < \frac{1}{2}$ . This is possible because  $s > 1$ . By the refined estimate from Ref. [16](#), Lemma 2.7 and Remark 2.8 (ii), we note that for  $1 \leq p \leq q \leq \infty$  satisfying  $\frac{1}{p} - \frac{1}{q} < \frac{1}{d}$ , the following inequality holds

$$\|\mathcal{A}^{1/2} E_{\alpha,\alpha}(-t^\alpha \mathcal{A}_\gamma) n\|_{L^q} \leq C \times \begin{cases} t^{-\frac{\alpha}{2} - \frac{\alpha d}{2}(\frac{1}{p} - \frac{1}{q})} \|n(\mathbf{x}, t)\|_{L^p}, & \text{for } 0 < t < 1, \\ t^{-2\alpha + \frac{\alpha}{2} + \frac{\alpha d}{2}(\frac{1}{p} - \frac{1}{q})} \|n(\mathbf{x}, t)\|_{L^p}, & \text{for } t > 1, \end{cases} \quad (6.40)$$

Consequently, we obtain

$$\|\mathcal{A}^{1/2} E_{\alpha,\alpha}(-\tau^\alpha \mathcal{A}_\gamma) f\|_{L^{q_0}} \leq C \begin{cases} \tau^{-\frac{\alpha}{2} - \alpha\mu} \|f\|_{L^s}, & 0 < \tau < 1, \\ \tau^{-2\alpha + \frac{\alpha}{2} + \alpha\mu} \|f\|_{L^s}, & \tau > 1. \end{cases}$$

After multiplication by the convolution factor  $\tau^{\alpha-1}$ , the kernels become  $\tau^{-1+\alpha(\frac{1}{2}-\mu)}$  for  $0 < \tau < 1$ , and  $\tau^{-1-\alpha(\frac{1}{2}-\mu)}$  for  $\tau > 1$ . Both are integrable because  $\mu < \frac{1}{2}$ . Hence, using (6.38) in (6.39), we obtain

$$\sup_{0 < t < T} \|\mathcal{A}^{1/2} c(\cdot, t)\|_{L^{q_0}} \leq C. \quad (6.41)$$

By the graph norm equivalence for the Neumann Laplacian,  $\|\nabla c\|_{L^{q_0}} \leq C\|\mathcal{A}^{1/2}c\|_{L^{q_0}}$ , up to the harmless constant mode. Therefore  $\sup_{0 < t < T} \|\nabla c(\cdot, t)\|_{L^{q_0}} \leq C$ . Using the previously established lower bound  $c \geq C_* > 0$ , we obtain

$$\sup_{0 < t < T} \|\mathbf{V}(\cdot, t)\|_{L^{q_0}} \leq C, \quad \mathbf{V} := \chi \frac{\nabla c}{c}. \quad (6.42)$$

- **Step** (iv):  $L^\infty$ -bootstrap for  $n$  via Moser iteration.

The first equation in System (1.1) can be rewritten as  ${}_0^C \mathfrak{D}_t^\alpha n = \mathcal{D}\Delta n - \mathcal{D}\nabla \cdot (n\mathbf{V})$ . For  $r \geq 1$ , set  $Y_r(t) := \|n(\cdot, t)\|_{L^r}^r = \int_\Omega n^r dx$ . Let  $p \geq 2$  and put  $w = n^{p/2}$ . Testing the equation for  $n$  by  $pn^{p-1}$ , using the fractional convex inequality for  $z \mapsto z^p$ , and integrating by parts, we obtain

$${}_0^C \mathfrak{D}_t^\alpha Y_p + \frac{4\mathcal{D}(p-1)}{p} \|\nabla w\|_{L^2}^2 \leq 2\mathcal{D}(p-1) \int_\Omega w |\mathbf{V}| |\nabla w| dx.$$

Young's inequality yields

$${}_0^C \mathfrak{D}_t^\alpha Y_p + C_1 \|\nabla w\|_{L^2}^2 \leq C_2 p^2 \int_\Omega w^2 |\mathbf{V}|^2 dx, \quad (6.43)$$

where  $C_1, C_2 > 0$  are independent of  $p \geq 2$ . By Hölder's inequality and (6.42),

$$\int_\Omega w^2 |\mathbf{V}|^2 dx \leq C \|w\|_{L^{\frac{2q_0}{q_0-2}}}^2. \quad (6.44)$$

Since  $d = 2$ , the Gagliardo–Nirenberg inequality gives

$$\|w\|_{L^{\frac{2q_0}{q_0-2}}} \leq C \|\nabla w\|_{L^2}^\vartheta \|w\|_{L^1}^{1-\vartheta} + C \|w\|_{L^1}, \quad (6.45)$$

where  $\vartheta = 1 - \frac{q_0-2}{2q_0} = \frac{q_0+2}{2q_0} \in (0, 1)$ . Since  $\|w\|_{L^1} = \int_\Omega n^{p/2} dx = Y_{p/2}(t)$ , we infer from (6.45) that

$$\|w\|_{L^{\frac{2q_0}{q_0-2}}}^2 \leq C \|\nabla w\|_{L^2}^{2\vartheta} Y_{p/2}(t)^{2(1-\vartheta)} + C Y_{p/2}(t)^2. \quad (6.46)$$

Combining (6.43), (6.44), and (6.46), we get

$$C_2 p^2 \int_\Omega w^2 |\mathbf{V}|^2 dx \leq C p^2 \|\nabla w\|_{L^2}^{2\vartheta} Y_{p/2}(t)^{2(1-\vartheta)} + C p^2 Y_{p/2}(t)^2.$$

By Young's inequality, for every  $\varepsilon > 0$ ,

$$C p^2 \|\nabla w\|_{L^2}^{2\vartheta} Y_{p/2}(t)^{2(1-\vartheta)} \leq \varepsilon \|\nabla w\|_{L^2}^2 + C_\varepsilon p^{\frac{2}{1-\vartheta}} Y_{p/2}(t)^2.$$

Thus, after enlarging the exponent if necessary, there exists  $\beta := \max\left\{2, \frac{2}{1-\vartheta}\right\} > 0$  such that

$$C_2 p^2 \int_\Omega w^2 |\mathbf{V}|^2 dx \leq \varepsilon \|\nabla w\|_{L^2}^2 + C p^\beta Y_{p/2}(t)^2.$$

Choosing  $\varepsilon > 0$  sufficiently small, we obtain

$${}_0^C \mathfrak{D}_t^\alpha Y_p + \kappa \|\nabla w\|_{L^2}^2 \leq C p^\beta Y_{p/2}(t)^2. \quad (6.47)$$

We also use the two-dimensional Gagliardo–Nirenberg inequality

$$\|w\|_{L^2} \leq C \|\nabla w\|_{L^2}^{1/2} \|w\|_{L^1}^{1/2} + C \|w\|_{L^1}.$$

After squaring and applying Young's inequality, for any fixed  $\delta > 0$ ,

$$Y_p(t) = \|w\|_{L^2}^2 \leq \delta \|\nabla w\|_{L^2}^2 + C_\delta Y_{p/2}(t)^2.$$

Equivalently,

$$\|\nabla w\|_{L^2}^2 \geq \delta^{-1} Y_p(t) - C_\delta \delta^{-1} Y_{p/2}(t)^2. \quad (6.48)$$

Combining (6.47) and (6.48), and then fixing  $\delta > 0$ , we arrive at

$${}_0^C \mathfrak{D}_t^\alpha Y_p + \eta Y_p \leq C p^\beta Y_{p/2}(t)^2, \quad p \geq 2, \quad (6.49)$$

where  $\eta > 0$  and  $C > 0$  are independent of  $p$ .

We now perform the Moser iteration. Let  $p_k := s2^k$  and  $A_k := \sup_{0 < t < T} \|n(\cdot, t)\|_{L^{p_k}(\Omega)}$ . By (6.38),  $A_0 < \infty$ . Since  $p_k = s2^k \geq 2s > 2$  for  $k \geq 1$ , we apply (6.49) with  $p = p_k$ . The scalar fractional variation-of-constants formula gives

$$Y_{p_k}(t) \leq Y_{p_k}(0) E_\alpha(-\eta t^\alpha) + C p_k^\beta \int_0^t (t-\tau)^{\alpha-1} E_{\alpha,\alpha}(-\eta(t-\tau)^\alpha) Y_{p_{k-1}}(\tau)^2 d\tau.$$

Using  $0 \leq E_\alpha(-\eta t^\alpha) \leq 1$  and  $\int_0^\infty \tau^{\alpha-1} E_{\alpha,\alpha}(-\eta \tau^\alpha) d\tau = \frac{1}{\eta}$ , we infer

$$\sup_{0 < t < T} Y_{p_k}(t) \leq Y_{p_k}(0) + C p_k^\beta \sup_{0 < t < T} Y_{p_{k-1}}(t)^2.$$

Since  $p_k = 2p_{k-1}$ ,  $A_k^{p_k} \leq Y_{p_k}(0) + C p_k^\beta A_{k-1}^{p_k}$ . Because  $n_0 \in L^\infty(\Omega)$ , there exists  $C_0 \geq 1$  such that  $Y_{p_k}(0) = \|n_0\|_{L^{p_k}}^{p_k} \leq C_0^{p_k}$ . Therefore

$$A_k^{p_k} \leq C_0^{p_k} + C (s2^k)^\beta A_{k-1}^{p_k}.$$

Set  $\tilde{A}_k := \max\{A_k, A_0, C_0, 1\}$ . Then

$$\tilde{A}_k^{p_k} \leq C (1 + 2^{k\beta}) \tilde{A}_{k-1}^{p_k}.$$

Taking the  $p_k = s2^k$ -th root gives

$$\tilde{A}_k \leq (C(1 + 2^{k\beta}))^{1/(s2^k)} \tilde{A}_{k-1}.$$

Thus

$$\tilde{A}_k \leq \tilde{A}_0 \prod_{j=1}^k (C(1 + 2^{j\beta}))^{1/(s2^j)}.$$

Since  $\sum_{j=1}^\infty \frac{\log(C(1+2^{j\beta}))}{s2^j} < \infty$ , the product is finite. Hence  $\sup_{k \geq 0} A_k < \infty$ . Let  $M_* := \sup_{k \geq 0} A_k$ . For fixed  $t \in (0, T)$ , one has  $\|n(\cdot, t)\|_{L^{p_k}} \leq M_*$ ,  $k = 0, 1, 2, \dots$ . If there existed  $\lambda > M_*$  such that  $|\{x \in \Omega : n(x, t) > \lambda\}| > 0$ , then

$$\lambda |\{n(\cdot, t) > \lambda\}|^{1/p_k} \leq \|n(\cdot, t)\|_{L^{p_k}} \leq M_*$$

for all  $k$ . Letting  $k \rightarrow \infty$  gives  $\lambda \leq M_*$ , a contradiction. Therefore

$$\sup_{0 < t < T} \|n(\cdot, t)\|_{L^\infty} \leq C. \quad (6.50)$$

- **Step (v):**  $W^{1,q}$ -regularity estimate for  $c$ .

It remains to estimate  $c$  in  $W^{1,q}(\Omega)$  for arbitrary finite  $q > 2$ . By (6.50),  $\sup_{0 < t < T} \|n(\cdot, t)\|_{L^q} \leq C$ . Applying again the mild representation of  $c$  and the refined estimate (6.40), now with  $p = q$ , we obtain

$$\left\| \mathcal{A}^{1/2} E_{\alpha,\alpha}(-\tau^\alpha \mathcal{A}_\gamma) f \right\|_{L^q} \leq C \begin{cases} \tau^{-\frac{\alpha}{2}} \|f\|_{L^q}, & 0 < \tau < 1, \\ \tau^{-\frac{3\alpha}{2}} \|f\|_{L^q}, & \tau > 1. \end{cases}$$

After multiplication by  $\tau^{\alpha-1}$ , the kernels become  $\tau^{-1+\frac{\alpha}{2}}$  for  $0 < \tau < 1$ , and  $\tau^{-1-\frac{\alpha}{2}}$ ,  $\tau > 1$ . Both are integrable. Hence  $\sup_{0 < t < T} \|\mathcal{A}^{1/2}c(\cdot, t)\|_{L^q} \leq C$ . Together with (6.32) and the graph norm equivalence for the Neumann Laplacian, this gives

$$\sup_{0 < t < T} \|c(\cdot, t)\|_{W^{1,q}} \leq C.$$

Combining this estimate with (6.50), we conclude that

$$\sup_{0 < t < T} (\|n(\cdot, t)\|_{L^\infty} + \|c(\cdot, t)\|_{W^{1,q}}) \leq C.$$

The constant is independent of  $T$ . Since  $T > 0$  was arbitrary, letting  $T \rightarrow \infty$  proves

$$\sup_{t \geq 0} (\|n(\cdot, t)\|_{L^\infty} + \|c(\cdot, t)\|_{W^{1,q}}) \leq C.$$

The proof is complete.  $\square$

**Remark 6.2.** The proof above is essentially two-dimensional. The main reason is that the estimate  $\mathcal{Y}(t) := \int_{\Omega} n^2 c^{-\frac{1}{2}} \mathbf{d}\mathbf{x} \leq C$  only provides an initial improvement of the integrability of  $n$ . In dimension three, the same strategy may still be adapted: indeed, one can choose  $s \in (\frac{3}{2}, \frac{12}{7})$  and then choose  $q_0 > 3$  such that  $\frac{1}{s} - \frac{1}{q_0} < \frac{1}{3}$ . This would allow the refined smoothing estimate for the  $c$ -equation to yield the subcritical drift estimate  $\mathbf{V} := \chi \frac{\nabla c}{c} \in L^\infty(0, T; L^{q_0}(\Omega))$ ,  $q_0 > 3$ , which is the condition needed to close the Moser iteration in three dimensions. For dimensions  $d \geq 4$ , however, the present bootstrap mechanism no longer closes. More precisely, the weighted estimate for  $\mathcal{Y}(t)$  does not provide an exponent  $s > d/2$ . Consequently, one cannot obtain, by this argument, a subcritical drift bound of the form  $\mathbf{V} \in L^\infty(0, T; L^{q_0}(\Omega))$ ,  $q_0 > d$ . This subcritical drift estimate is precisely the ingredient required in the Moser iteration for the drift-diffusion equation satisfied by  $n$ . Thus the present proof should be regarded as a two-dimensional argument; a possible three-dimensional extension would require a separate treatment of the exponents, whereas dimensions  $d \geq 4$  cannot be covered by this bootstrap scheme. Whether global bounded solutions continue to exist for arbitrary dimensions  $d \geq 4$  remains an interesting open problem.

**Remark 6.3.** By virtue of the uniform bounds for  $n$  and  $c$  established in Lemma 6.4 for all  $t > 0$ , and following the arguments in Lemmas 5.3 and 5.4, the regularity results derived in those lemmas remain valid for  $t \in [\tau, \infty)$  with an arbitrarily small  $\tau > 0$ .

**Proof of Theorem 3.2.** The proof of this theorem is established by combining the theoretical results derived in the preceding sections. Specifically, the uniform upper bound obtained in Lemma 6.4 ensures the existence of a positive constant  $M$ , independent of  $t$ , such that

$$\sup_{t > 0} (\|n(\mathbf{x}, t)\|_{L^\infty} + \|c(\mathbf{x}, t)\|_{W^{1,p}}) \leq M, \quad p > d. \quad (6.51)$$

This establishes the bound mentioned in (3.10). Furthermore, by coupling the mass conservation from Lemma 4.3 and the local well-posedness from Theorem 5.2 with the non-blowup criterion in (6.51), a standard continuation argument guarantees that the system admits a unique global mild solution. Concurrently, leveraging the uniform boundedness from Lemma 6.4, the mass conservation property established in Lemma 4.3 and applying regularity proof techniques analogous

to those in Lemmas 5.3 and 5.4, the regularity properties in (3.9) are readily verified. We omit the detailed steps for brevity, thereby completing the proof.  $\square$

**Proof of Theorem 3.1.** The proof follows by combining the mass conservation property established in Lemma 4.3 with the global well-posedness provided in Theorem 3.2.  $\square$

## 7. Simulations with Non-Negativity/Positivity-Preserving PINNs

In this section, we perform numerical simulations using the popular Physics-Informed Neural Networks (PINNs) to visualize the solution behavior of System (1.1) and to validate the theoretical results established above.

### 7.1. Methodology: DNN architecture and implementations

This subsection describes the numerical method used to solve the system (1.1). The problem is highly nonlinear and strongly coupled, with a time-nonlocal structure. To handle these difficulties, a time-marching PINNs algorithm is employed. A distinguishing feature of the algorithm is that it preserves the non-negativity of  $n(x, y, t)$  and the strict positivity of  $c(x, y, t)$ , which are properties established earlier in Lemmas 4.4 and 4.6.

Let  $\Omega \subset \mathbb{R}^d$  ( $d = 2$ ) be a bounded domain with smooth boundary. For  $(x, y) \in \Omega$ , the following variable transformations are introduced. These are motivated by Refs. 57, 83, 126.

$$\begin{cases} n(\cdot, t) = \rho(\cdot, t)^2 \geq 0, & \text{for } \rho(\cdot, t) : \Omega \times \mathbb{R}_+ \rightarrow \mathbb{R}; \\ c(\cdot, t) = \exp(v(\cdot, t)) > 0, & \text{for } v(\cdot, t) : \Omega \times \mathbb{R}_+ \rightarrow \mathbb{R}. \end{cases} \quad (7.1)$$

Substituting the transformation (7.1) into the original problem (1.1) leads to the following reformulated system in terms of  $(\rho(\cdot, t), v(\cdot, t))$ :

$$\begin{cases} {}_0^C \mathfrak{D}_t^\alpha (\rho^2(\cdot, t)) = \mathcal{D}\Delta(\rho^2(\cdot, t)) - \mathcal{D}\chi \nabla \cdot (\rho^2(\cdot, t) \nabla v(\cdot, t)), & \Omega \times (0, T], \\ {}_0^C \mathfrak{D}_t^\alpha (e^{v(\cdot, t)}) = \mathcal{D}\Delta(e^{v(\cdot, t)}) - \gamma e^{v(\cdot, t)} + \rho^2(\cdot, t), & \Omega \times (0, T], \\ \rho(\cdot, 0) = \sqrt{n_0(x)}, \quad v(\cdot, 0) = \ln(c_0(\cdot)), & \Omega \times \{0\}, \\ \nabla \rho(\cdot, t) \cdot \nu = 0, \quad \nabla v(\cdot, t) \cdot \nu = 0, & \partial\Omega \times (0, T]. \end{cases} \quad (7.2)$$

Here,  $\nu$  denotes the outward normal vector. This formulation has two useful features. It guarantees the non-negativity of  $n(\cdot, t)$  and the strict positivity of  $c(\cdot, t)$  by construction. It also replaces the logarithmic gradient term  $\nabla c(\cdot, t)/c(\cdot, t)$  with the simpler linear gradient  $\nabla v(\cdot, t)$ , which is numerically more favorable.

To solve System (7.2) numerically, a Deep Neural Network (DNN) framework is employed. The algorithm preserves the non-negativity and positivity of the solution variables.

The numerical procedure begins with the defining of the solution domain  $\Omega$ . Collocation points are sampled from the interior and the boundary, denoted respectively by  $\xi_\ell^n$  ( $\ell = 1, 2, \dots, M_{in}$ ) and  $\xi_j^{bc}$  ( $j = 1, 2, \dots, M_{bc}$ ), respectively. These spatial coordinates are subsequently fed into the network's input layer. Accordingly, the detailed implementation steps are described as follows.

- **Step (i):** Time semi-discretization. The  $L_1$  scheme is employed for the temporal semi-discretization of the coupled system (7.2).

The  $L_1$  scheme is a widely approach for discretizing the Caputo fractional derivative in time<sup>8,63</sup>. To implement the scheme, we first partition the time interval  $[0, T]$  uniformly into  $N$

subintervals of length  $\tau = T/N$ , giving the grid points  $t_j = j\tau$  for  $j = 0, 1, \dots, N$ . The core principle of the  $L_1$  scheme lies in approximating the integrand of the Caputo derivative via piecewise linear interpolation over the grid points  $t_j$ . The discrete approximation of the Caputo derivative at  $t = t_j$  is given by<sup>41,119</sup>

$${}^C_0\mathcal{D}_t^\alpha f(t_j) \approx \frac{\tau^{-\alpha}}{\Gamma(2-\alpha)} \left( a_0 f^j - \sum_{k=1}^{j-1} (a_{j-k-1} - a_{j-k}) f^k - a_{j-1} f^0 \right), \quad (7.3)$$

where  $f^j := f(t_j)$ ,  $\alpha \in (0, 1)$ , and the coefficients are defined as  $a_k := (k+1)^{1-\alpha} - k^{1-\alpha}$  for  $k = 0, 1, \dots, j-1$ . In particular,  $a_0 = 1$ , and the sequence  $a_k$  is positive and monotonically decreasing.

The  $L_1$  scheme (7.3) is unconditionally stable for discretizing the Caputo derivative and attains a global convergence rate of  $O(\tau^{2-\alpha})$  on uniform grids<sup>41,63</sup>. As  $\alpha \rightarrow 1$ , it reduces to the classical first-order backward Euler method. The non-local property of the time non-local derivatives is explicitly reflected in the summation term, which involves all previous time levels  $f^k$ . This differs from integer-order derivatives, which depend only on local information.

Let  $\rho^j = \rho(\cdot, t_j)$  and  $v^j = v(\cdot, t_j)$  denote the semi-discrete solutions at time  $t_j$ . Accordingly,  $n^j = (\rho^j)^2$  and  $c^j = \exp(v^j)$ . Applying the  $L_1$  scheme (7.3) to System (7.2) at  $t = t_j$  for  $j \in \{0, 1, 2, \dots, N\}$  yields the following semi-discrete system

$$\begin{cases} \frac{\tau^{-\alpha}}{\Gamma(2-\alpha)} \left[ (\rho^j)^2 - \sum_{k=1}^{j-1} (a_{j-k-1} - a_{j-k}) (\rho^k)^2 - a_{j-1} (\rho^0)^2 \right] \\ \quad = \mathcal{D}\Delta(\rho^j)^2 - \mathcal{D}\chi\nabla \cdot ((\rho^j)^2 \nabla v^j), \\ \frac{\tau^{-\alpha}}{\Gamma(2-\alpha)} \left[ \exp(v^j) - \sum_{k=1}^{j-1} (a_{j-k-1} - a_{j-k}) \exp(v^k) - a_{j-1} \exp(v^0) \right] \\ \quad = \mathcal{D}\Delta(\exp(v^j)) - \gamma \exp(v^j) + (\rho^j)^2, \\ \rho^0 = \sqrt{n_0}, \quad v^0 = \ln(c_0), \quad \nabla \rho^j \cdot \nu = 0, \quad \nabla v^j \cdot \nu = 0. \end{cases} \quad (7.4)$$

To streamline the notation, we rewrite the semi-discrete system (7.4) in the following operator form

$$\begin{cases} \mathcal{P}_\rho[\rho^j, v^j] = 0, & \mathcal{P}_v[\rho^j, v^j] = 0, \\ \Xi[\rho^0, v^0] = 0, & \tilde{\mathcal{B}}[\rho^j, v^j] = 0. \end{cases} \quad (7.5)$$

Here,  $\mathcal{P}_\rho$  and  $\mathcal{P}_v$  represent the discrete differential operators corresponding to the PDEs for  $\rho^j$  and  $v^j$ ;  $\tilde{\mathcal{B}}$  encapsulates the boundary conditions, and  $\Xi$  collects the initial conditions. All are formulated abstractly based on the semi-discrete system (7.4).

With the semi-discrete scheme (7.4), we employ the PINNs to solve the resulting system (7.4), leading to a mesh-free, positivity-preserving, multi-objective optimization-based time-marching PINNs algorithm. For an overall picture of the framework, we refer the reader to Fig. 7. The detailed algorithmic procedure is presented as follows.

- **Step (ii):** Solution representation via Deep Neural Networks (DNNs).

At each time step  $t_j$ , the unknown functions  $\rho(\cdot, t_j)$  and  $v(\cdot, t_j)$  are approximated by two independent feedforward neural networks, denoted by  $\mathcal{N}_{\theta_j}$  and  $\mathcal{N}_{\phi_j}$ , respectively. Unlike recurrent neural networks, feedforward neural networks are characterized by an acyclic connectivity pattern, where information flows strictly in one direction from the input to the output.

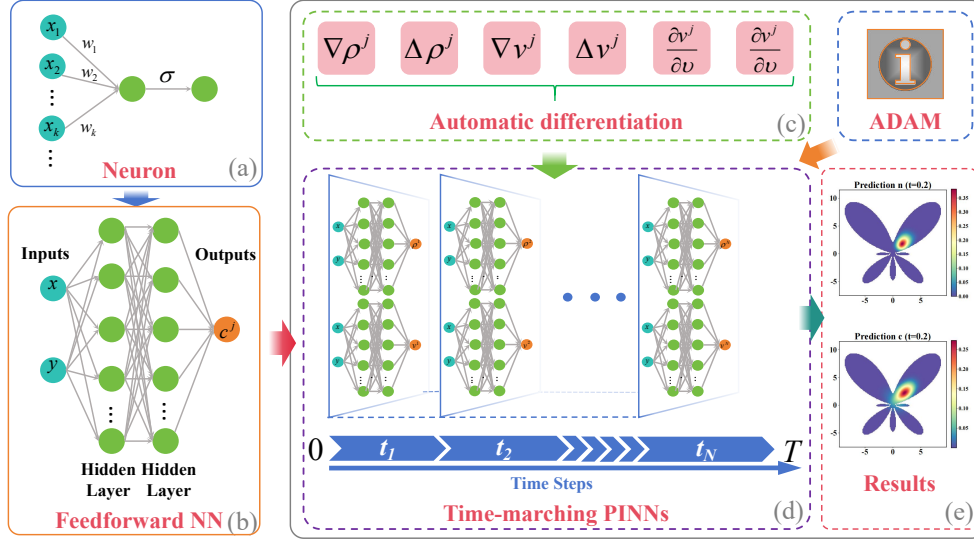


Fig. 7: Schematic workflow of the multi-objective positivity/non-negativity-preserving time-marching PINNs. The panels illustrate: (a) a single neuron model; (b) the multi-layer perceptron (MLP) architecture; (c) the automatic differentiation mechanism; (d) the overall time-marching PINN framework; and (e) snapshots of typical numerical results.

As illustrated in Fig. 7, the network consists of  $L$  sequential layers. Formally, let  $\mathbf{x}^{(i)}$  denote the output vector of the  $i$ -th layer. The transition from one layer to the next is given by Ref. 17:

$$\mathbf{x}^{(i+1)} = \sigma \left( \mathbf{W}^{(i)} \mathbf{x}^{(i)} + \mathbf{b}^{(i)} \right), \quad i = 0, 1, \dots, L-1, \quad (7.6)$$

where  $\sigma$  is a non-linear activation function,  $\mathbf{W}^{(i)}$  is the learnable weight matrix, and  $\mathbf{b}^{(i)}$  is the bias vector. Specifically, the dimensions of these components are as follows:

- For the input layer ( $i = 0$ ):  $\mathbf{x}^{(0)} = \mathbf{x} \in \Omega \subset \mathbb{R}^d$ , where  $d$  being the spatial dimension. The weight matrix  $\mathbf{W}^{(0)} \in \mathbb{R}^{m \times d}$  and  $\mathbf{b}^{(0)} \in \mathbb{R}^m$ , with  $m$  being the fixed number of neurons in each hidden layer.
- For hidden layers ( $1 \leq i \leq L-2$ ):  $\mathbf{x}^{(i)} \in \mathbb{R}^m$ , with  $\mathbf{W}^{(i)} \in \mathbb{R}^{m \times m}$  and  $\mathbf{b}^{(i)} \in \mathbb{R}^m$ .
- For the output layer ( $i = L-1$ ): the final output  $\mathbf{x}^{(L)} \in \mathbb{R}^1$  (representing  $\rho^j$  or  $v^j$ ) is produced with  $\mathbf{W}^{(L-1)} \in \mathbb{R}^{1 \times m}$  and  $\mathbf{b}^{(L-1)} \in \mathbb{R}$ .

This architecture is commonly known as a multi-layer perceptron (MLP). The hidden layers are typically fully connected, meaning each neuron in one layer connects to every neuron in the next<sup>17</sup>. This dense connectivity enables the network to approximate the complex nonlinear mappings required by the time-nonlocal system.

In this framework, the neural networks take as input the collocation points  $\xi_\ell^n \in \Omega$  ( $\ell = 1, 2, \dots, M_m$ ) and  $\xi_j^{bc} \in \partial\Omega$  ( $j = 1, 2, \dots, M_{bc}$ ), and output the corresponding field values  $\rho^j$  and  $v^j$  at each time step  $t_j$ , as illustrated in Fig. 7 (b). Mathematically, the neural network approximations are expressed as<sup>107</sup>

$$\rho(\mathbf{x}, t_j) \approx \rho_{\theta_j}^j(\mathbf{x}) := \mathcal{N}_{\theta_j} = \zeta_{\theta_j}^{(L-1)} \circ \sigma \circ \zeta_{\theta_j}^{(L-2)} \circ \sigma \circ \dots \circ \zeta_{\theta_j}^{(0)}(\mathbf{x}), \quad (7.7)$$

$$v(\mathbf{x}, t_j) \approx v_{\phi_j}^j(\mathbf{x}) := \mathcal{N}_{\phi_j} = \zeta_{\phi_j}^{(L-1)} \circ \sigma \circ \zeta_{\phi_j}^{(L-2)} \circ \sigma \circ \dots \circ \zeta_{\phi_j}^{(0)}(\mathbf{x}), \quad (7.8)$$

where  $\sigma$  is the activation function, applied element-wise to the output of each hidden layer to introduce the necessary non-linearity to the network. For PINNs,  $\sigma$  is required to be at least  $C^2$ -continuous, so that second-order spatial derivatives such as the Laplacian  $\Delta$  are well-defined. Here we use the Sigmoid Linear Unit function, defined as  $\sigma(\cdot) = \text{SiLU}(\cdot)$ , given by  $\text{SiLU}(x) = x \cdot \frac{1}{1+e^{-x}}$ . This function is infinitely differentiable and helps mitigate the vanishing gradient problem during backpropagation, making it a common choice for solving PDEs. The affine transformation at each layer  $i$  is given as

$$\zeta_{\theta_j}^{(i)}(\mathbf{x}) = \mathbf{W}_{\theta_j}^{(i)} \mathbf{x} + \mathbf{b}_{\theta_j}^{(i)}, \quad \zeta_{\phi_j}^{(i)}(\mathbf{x}) = \mathbf{W}_{\phi_j}^{(i)} \mathbf{x} + \mathbf{b}_{\phi_j}^{(i)}, \quad i = 0, 1, \dots, L-1. \quad (7.9)$$

For a hidden layer width  $m$  and spatial dimension  $d$ , the weight matrices satisfy  $\mathbf{W}^{(0)} \in \mathbb{R}^{m \times d}$ ,  $\mathbf{W}^{(i)} \in \mathbb{R}^{m \times m}$  for  $1 < i < L-2$ , and  $\mathbf{W}^{(L-1)} \in \mathbb{R}^{1 \times m}$ . To maintain accuracy, we use the same network architecture (depth  $L$  and width  $m$ ) across all time steps.

Since the semi-discrete system (7.4) has a time-stepping structure, the solution is computed sequentially at each time step  $t_j$  for  $j = 1, 2, \dots, N$ , starting from the initial state at  $j = 0$ . We adopt a time-marching strategy based on PINNs<sup>107</sup>, in which a separate neural network is constructed at each time level  $t_j$  to approximate  $\rho^j(\mathbf{x})$  and  $v^j(\mathbf{x})$ . As depicted in Fig. 7 (d), this step-by-step procedure ensures that the historical values required by the  $L_1$  scheme are already fixed when solving for the current time level.

- **Step (iii):** Spatial derivative computation.

In the time-marching PINNs implementation, all required spatial derivatives, including  $\nabla \rho^j$ ,  $\Delta \rho^j$ ,  $\nabla v^j$ ,  $\Delta v^j$ , and the normal derivatives  $\frac{\partial \rho^j}{\partial \nu}$  and  $\frac{\partial v^j}{\partial \nu}$  for  $j \in \{0, 1, 2, \dots, N\}$ , are computed via the automatic differentiation (AD)<sup>12</sup>, which is natively supported in modern deep learning frameworks. This approach avoids manual derivation or numerical discretization of spatial operators, and helps maintain high accuracy in enforcing the physical constraints in (7.4).

- **Step (iv):** Construction of the loss functions.

To train the neural networks at each time step  $t_j$ , a composite loss function is constructed. It consists of the residuals from the semi-discrete PDE system, boundary conditions, and initial conditions.

Specifically, at each  $t_j$ , we define the loss function as the weighted sum

$$\begin{aligned} \mathcal{L}oss(\theta_j, \phi_j; t_j) &= \lambda_{PDE} \mathcal{L}oss_{RS}(\theta_j, \phi_j; t_j) + \lambda_{BC} \mathcal{L}oss_{BC}(\theta_j, \phi_j; t_j) \\ &\quad + \lambda_{IC} \mathcal{L}oss_{IC}(\theta_0, \phi_0; t_0), \end{aligned} \quad (7.10)$$

where  $\phi_j = \{\mathbf{W}_{\phi_j}^{(i)}, \mathbf{b}_{\phi_j}^{(i)}\}$  and  $\theta_j = \{\mathbf{W}_{\theta_j}^{(i)}, \mathbf{b}_{\theta_j}^{(i)}\}$  ( $j = 1, 2, \dots, N$  and  $i = 0, 1, \dots, L-1$ ) are the trainable parameters of the networks at time level  $t_j$ . The weights  $\lambda_{PDE}$ ,  $\lambda_{BC}$  and  $\lambda_{IC}$  are penalty parameters that balance the contributions of the PDE residuals, boundary conditions, and initial conditions, respectively.

The total loss  $\mathcal{L}oss(\theta_j, \phi_j; t_j)$  is evaluated using collocation points sampled inside the domain  $\Omega$  and on the boundary  $\partial\Omega$ , with  $M_m$  interior points and  $M_{bc}$  boundary points. The individual loss components are defined below.

- Residuals of the semi-discrete PDE system within the domain.

The interior loss at  $t_j$  is defined as the sum of the residuals of the PDEs for the *Myxobacteria* density and the chemoattractant concentration

$$\mathcal{Loss}_{RS}(\theta_j, \phi_j; t_j) = \mathcal{Loss}_{RS}^\rho(\theta_j, \phi_j; t_j) + \mathcal{Loss}_{RS}^v(\theta_j, \phi_j; t_j), \quad j = 1, 2, \dots, N, \quad (7.11)$$

where the individual residuals are computed as the Mean Squared Error (MSE) over the interior collocation points  $\xi_\ell^{in} \in \Omega$ :

$$\begin{cases} \mathcal{Loss}_{RS}^\rho(\theta_j, \phi_j; t_j) = \frac{1}{M_{in}} \sum_{\ell=1}^{M_{in}} (\mathcal{P}_\rho[\mathcal{N}_{\theta_j} \odot \mathcal{N}_{\phi_j}](\xi_\ell^{in}))^2, & \xi_\ell^{in} \in \Omega, \ell = 1, \dots, M_{in}, \\ \mathcal{Loss}_{RS}^v(\theta_j, \phi_j; t_j) = \frac{1}{M_{in}} \sum_{\ell=1}^{M_{in}} (\mathcal{P}_v[\mathcal{N}_{\theta_j} \odot \mathcal{N}_{\phi_j}](\xi_\ell^{in}))^2, & \xi_\ell^{in} \in \Omega, \ell = 1, \dots, M_{in}. \end{cases}$$

Here the symbol “ $\odot$ ” indicates the mutual coupling between the two neural networks, which arises from the coupling between the PDEs in the system.

- Boundary condition loss.

The Neumann boundary conditions on  $\partial\Omega$  are enforced through the boundary loss

$$\mathcal{Loss}_{BC}(\theta_j, \phi_j; t_j) = \mathcal{Loss}_{BC}^\rho(\theta_j; t_j) + \mathcal{Loss}_{BC}^v(\phi_j; t_j), \quad j = 1, 2, \dots, N, \quad (7.12)$$

where the residuals are evaluated at boundary collocation points  $\xi_k^{bc} \in \partial\Omega$  as

$$\begin{cases} \mathcal{Loss}_{BC}^\rho(\theta_j; t_j) = \frac{1}{M_{bc}} \sum_{j=1}^{M_{bc}} (\tilde{\mathcal{B}}[\mathcal{N}_{\theta_j}](\xi_j^{bc}))^2, & \xi_j^{bc} \in \partial\Omega, j = 1, \dots, M_{bc}, \\ \mathcal{Loss}_{BC}^v(\phi_j; t_j) = \frac{1}{M_{bc}} \sum_{j=1}^{M_{bc}} (\tilde{\mathcal{B}}[\mathcal{N}_{\phi_j}](\xi_j^{bc}))^2, & \xi_j^{bc} \in \partial\Omega, j = 1, \dots, M_{bc}. \end{cases}$$

- Initial condition loss.

To ensure consistency with the initial data  $\rho^0$  and  $v^0$ , the initial loss is defined as

$$\mathcal{Loss}_{IC}(\theta_j, \phi_j; t_0) = \mathcal{Loss}_{IC}^\rho(\theta_j; t_0) + \mathcal{Loss}_{IC}^v(\phi_j; t_0), \quad j = 1, 2, \dots, N, \quad (7.13)$$

with residuals

$$\begin{cases} \mathcal{Loss}_{IC}^\rho(\theta_j; t_0) = \frac{1}{M_{in}} \sum_{\ell=1}^{M_{in}} (\Xi[\mathcal{N}_{\theta_j}](\xi_\ell^{in}) - \rho^0(\xi_\ell^{in}))^2, & \xi_\ell^{in} \in \Omega, \ell = 1, \dots, M_{in}, \\ \mathcal{Loss}_{IC}^v(\phi_j; t_0) = \frac{1}{M_{in}} \sum_{\ell=1}^{M_{in}} (\Xi[\mathcal{N}_{\phi_j}](\xi_\ell^{in}) - v^0(\xi_\ell^{in}))^2, & \xi_\ell^{in} \in \Omega, \ell = 1, \dots, M_{in}. \end{cases}$$

**Step V:** Sequential time-stepping optimization with parameter transfer.

At each time level  $t_j$ , the optimal network parameters  $\theta_j^*$  and  $\phi_j^*$  are obtained by solving the minimization problem

$$(\theta_j^*, \phi_j^*) = \arg \min_{(\theta_j, \phi_j)} \mathcal{Loss}(\theta_j, \phi_j; t_j). \quad (7.14)$$

This is carried out using the ADAM optimizer<sup>1</sup>, a stochastic gradient-based method widely used in deep learning.

The semi-discrete systems are solved sequentially in a time-marching manner. For each step  $j \in \{1, 2, \dots, N\}$ , the network parameters are initialized with the optimized values from the previous time level, i.e.,  $\theta_{j-1}^*$  and  $\phi_{j-1}^*$  (with the initial condition used for  $j = 1$ ). This parameter transfer strategy exploits the temporal continuity of the solution, providing a good initial guess that facilitates efficient and stable convergence. After the loss is minimized iteratively via ADAM, the resulting approximations  $\rho^j$  and  $v^j$  are stored as historical data for the subsequent steps.

In this time-marching PINNs framework, error accumulation is mitigated by training independent networks at each time step. The parameters from previous steps serve only as a warm start; they are fully re-optimized through the physics-constrained loss. This strategy confines approximation errors to individual time levels, while still benefiting from the stability of the  $L_1$  discretization and the expressive power of deep neural networks.

## 7.2. Simulations: 2D case with known source terms

To validate the numerical performance of the proposed algorithm, we consider a two-dimensional circular domain  $\Omega = \{(x, y) : x^2 + y^2 \leq R^2\}$  with radius  $R > 0$ . Defining the auxiliary spatial function  $\phi = (r^2 - R^2)^2$  where  $r^2 = x^2 + y^2$ . We employ the method of manufactured solutions by adding source terms  $f(x, y, t)$  and  $g(x, y, t)$  to the governing equations for  $\rho$  and  $v$  in (7.2), respectively:

$$\begin{aligned} f(x, y, t) &= e^{-\phi} \left\{ \Gamma(\alpha + 1) - (1 + t^\alpha) \left( \mathcal{D} - \frac{\mathcal{D}\chi}{3} \right) \left( 16r^2(r^2 - R^2)^2 - 16r^2 + 8R^2 \right) \right\}, \\ g(x, y, t) &= e^{-\phi/3} \Gamma(\alpha + 1) - \mathcal{D}(1 + t^\alpha) e^{-\phi/3} \left( \frac{16}{9} r^2 (r^2 - R^2)^2 - \frac{16}{3} r^2 + \frac{8}{3} R^2 \right) \\ &\quad + \gamma e^{-\phi/3} (1 + t^\alpha) - e^{-\phi} (1 + t^\alpha). \end{aligned}$$

This construction yields exact solutions with weak temporal regularity ( $c^\alpha(0, T)$ ,  $0 < \alpha < 1$ ), given by

$$\begin{cases} n(x, y, t) = \rho(x, y, t)^2 = e^{-\phi} (1 + t^\alpha), \\ c(x, y, t) = \exp(v(x, y, t)) = e^{-\phi/3} (1 + t^\alpha). \end{cases} \quad (7.15)$$

These exact solutions are consistent with the prescribed initial and boundary conditions.

For the numerical experiments, the parameters are set as  $R = 1$ ,  $\mathcal{D} = 1.0$ ,  $\chi = 0.25$  (with  $\chi \in (0, 1/2)$ ), and  $\gamma = 1.0$ . The time interval  $[0, T]$  with  $T = 0.5$  is uniformly divided into  $N = 20.0$  steps. We use  $M_m = 1000.0$  interior collocation points and  $M_{bc} = 1000.0$  boundary points. The neural network has 3 hidden layers, each with 64 neurons. At each time step, the model is trained for 2500 iterations with a decreasing learning rate  $lr = 1e - 3$ . The loss weights are set to  $\lambda_{PDE} = 1.0$ ,  $\lambda_{BC} = 100.0$ , and  $\lambda_{IC} = 100.0$ . To evaluate the accuracy of the algorithm, we define the relative  $L^2$  error

$$\text{Relative } L^2 \text{ Error} = \frac{\|u_{predic} - u_{exact}\|_{L^2(\Omega)}}{\|u_{exact}\|_{L^2(\Omega)}}, \quad u \in \{n, c\}, \quad (7.16)$$

for both solution components.

The numerical results on the unit disk are presented in Figures 8, 9, 10, 11, 12, and 13. These experiments demonstrate that a compact feedforward neural network is capable of approximating the solutions with satisfactory accuracy. Three main observations can be highlighted:

- **Good accuracy:** The predicted solutions agree well with the exact ones, with absolute errors generally within 2% and the relative  $L^2$  error remaining stable across all time

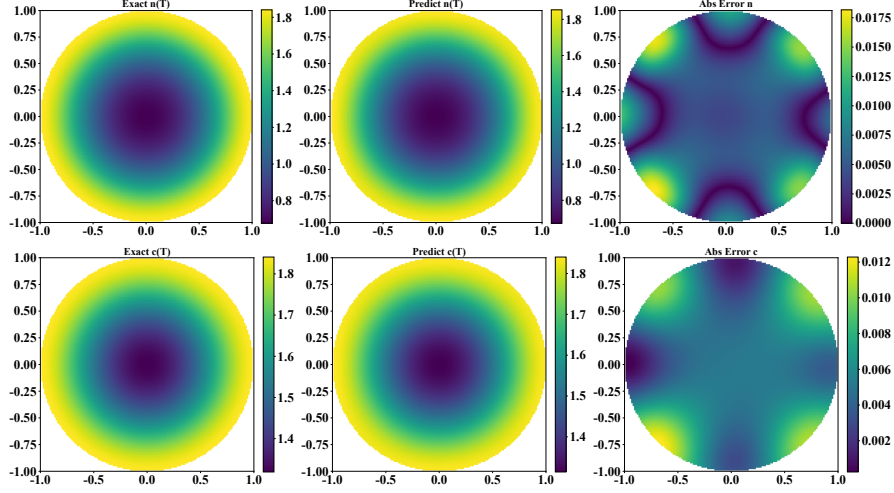


Fig. 8: (Color online) Visual comparison between the reference and approximate solutions for  $\alpha = 0.25$  at the final time  $T = 0.5$ .

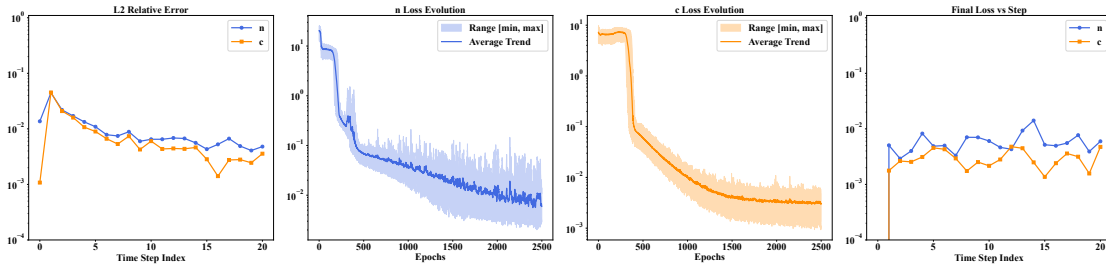


Fig. 9: (Color online) Numerical performance of the positivity-preserving time-marching PINN for  $\alpha = 0.25$  at final time  $T = 0.5$ . The panels show, from left to right: the relative  $L^2$  error, the the loss evolution for  $n(x, y, t)$  and  $c(x, y, t)$  at each epoch, and the evolution of the total loss against the number of time steps.

steps. This confirms that the proposed PINNs framework can effectively capture the solution behavior even with relatively limited network capacity.

- **Stable Training:** The training processes for both  $n(x, y, t)$  and  $c(x, y, t)$  are smooth, with the loss functions decreasing steadily toward convergence. The independent network architecture and parameter transfer strategy appear to contribute positively to training stability, without introducing noticeable oscillations or overshooting.
- **Robustness:** The algorithm performs consistently well across different values of the fractional order  $\alpha$ , indicating that the time-marching scheme, combined with the  $L_1$  discretization, is adaptable to various degrees of nonlocal memory effects.

Overall, these results indicate that the proposed method is reliable and computationally efficient, and offers sufficient accuracy for the present test cases.

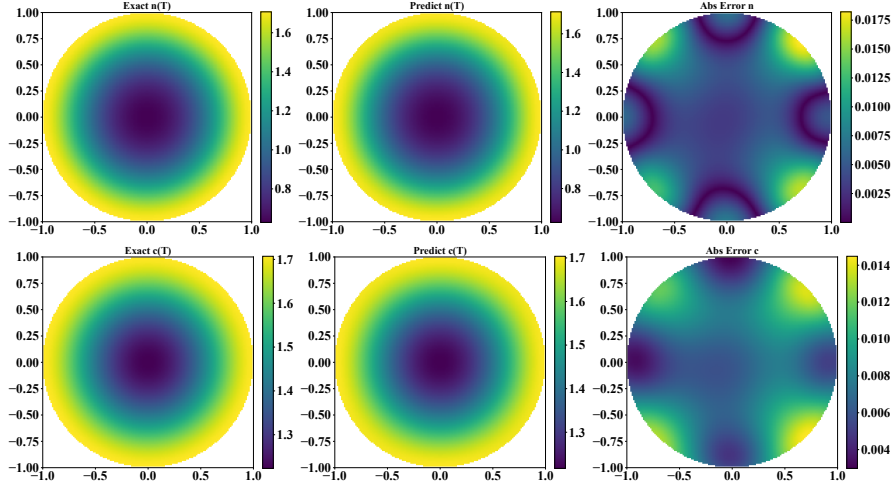


Fig. 10: (Color online) Visual comparison of the reference solution and the approximate solution for  $\alpha = 0.50$  at the final time  $T = 0.5$ .

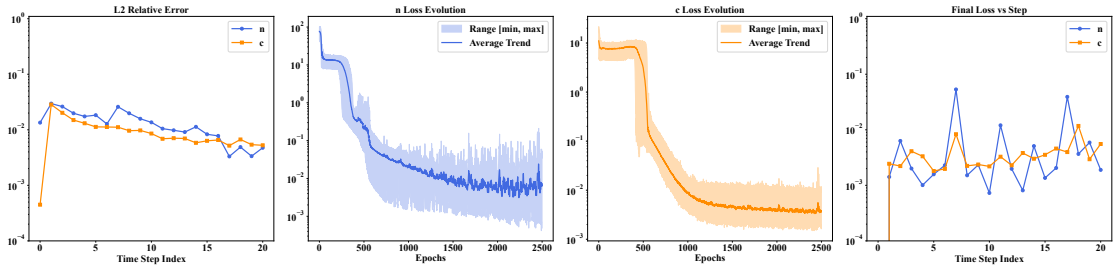


Fig. 11: (Color online) The numerical performance of the non-negativity/positivity-preserving time-marching PINNs algorithm when  $\alpha = 0.50$  and  $T = 0.5$ . From left to right, the relative  $L^2$  error, the training loss for  $n$  and  $c$  at each time step, and the final loss versus time steps.

### 7.3. Simulations: 2D case with Gaussian initial data

To evaluate the numerical performance of the proposed time-marching PINNs on complex geometries, we consider a two-dimensional bounded domain  $\Omega \subset \mathbb{R}^2$ , often referred to as the “butterfly” domain. Its boundary is parameterized in polar coordinates  $(r, \phi)$  by

$$\partial\Omega := \left\{ (r, \phi) \mid r(\phi) = 3 \times \left| e^{\sin(\phi)} - 2 \cos(4\phi) + \sin^5\left(\frac{2\phi - \pi}{24}\right) \right|, \phi \in [0, 2\pi] \right\}. \quad (7.17)$$

This highly irregular and non-convex region is chosen intentionally to illustrate the flexibility of deep neural networks in handling complex spatial domains. Unlike traditional grid-based methods, the present approach does not require mesh generation, which becomes particularly advantageous for such intricate geometries.

To ensure mathematical consistency between the initial data and the homogeneous Neumann boundary conditions, a quadratic masking factor  $\Psi(x, y)$  is introduced. The initial distributions

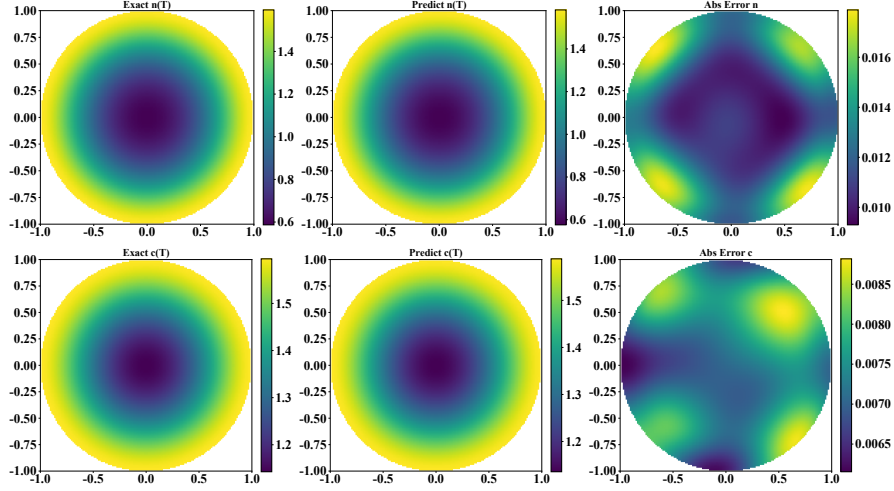


Fig. 12: (Color online) Visual comparison of the reference solution and the approximate solution for  $\alpha = 0.75$  at the final time  $T = 0.5$ .

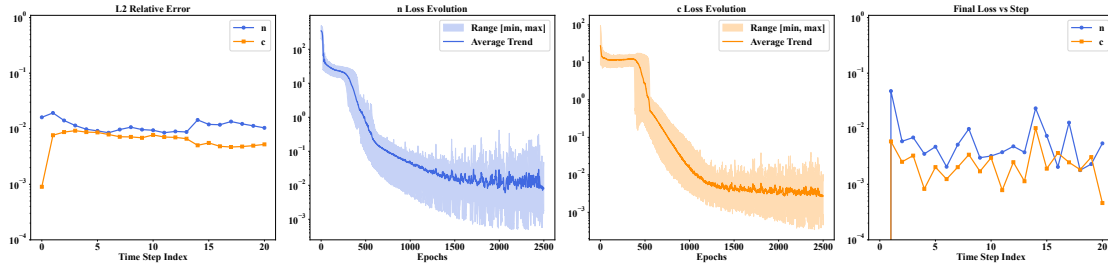


Fig. 13: (Color online) The numerical performance of the non-negativity/positivity-preserving time-marching PINNs algorithm when  $\alpha = 0.75$  and  $T = 0.5$ . From left to right, the figures illustrate the  $L^2$  relative error, the total loss trends of  $n$  and  $c$  at each time step, and the final loss versus time steps.

$n(x, y, t)$  and  $c(x, y, t)$  are defined as

$$\begin{cases} n(x, y, 0) = \pi |\cos(\pi x) \cos(\pi y)| \exp(-0.75 [(x-2)^2 + (y-2)^2]) \cdot \Psi(x, y), \\ c(x, y, 0) = \pi |\cos(\pi x) \cos(\pi y)| \exp(-0.25 [(x-2)^2 + (y-2)^2]) \cdot \Psi(x, y). \end{cases} \quad (7.18)$$

The compatibility factor  $\Psi(x, y)$  is given by

$$\Psi(x, y) := (1 - \sigma^2(x, y))^2, \quad \sigma(x, y) := \frac{\sqrt{x^2 + y^2}}{r(\text{atan2}(y, x))}, \quad (7.19)$$

where  $r(\phi)$  is the radial distance at angle  $\phi$ , as defined in (7.17), and  $\phi = \text{atan2}(y, x)$  is the four-quadrant inverse tangent (available in PyTorch code `torch.atan2(y, x)`).

By construction, the factor  $\Psi(x, y)$  vanishes quadratically at the boundary, where  $\sigma = 1$ . This ensures two key properties:

- Boundary value vanishing:  $\Psi(1) = 0$ , so both  $n(x, y, t)$  and  $c(x, y, t)$  vanish on  $\partial\Omega$ .

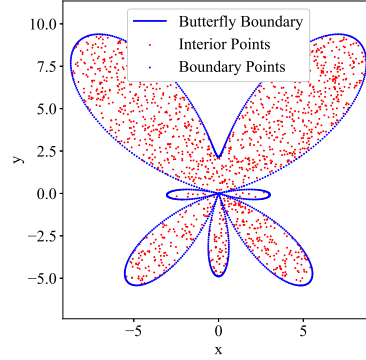


Fig. 14: (Color online) Numerical visualization of the 2D butterfly-shaped computational domain, showing the distribution of interior collocation points and boundary sampling points.

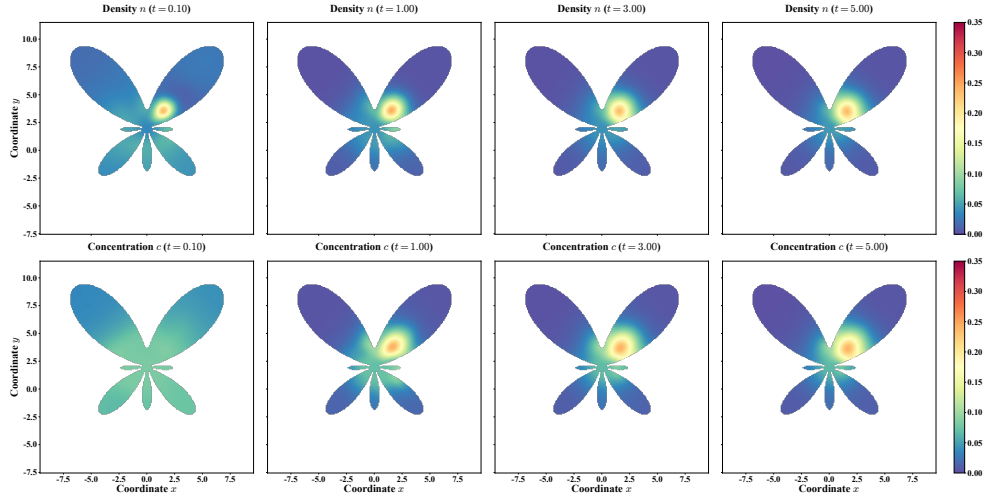


Fig. 15: (Color online) Evolution of solutions on the butterfly-shaped domain computed by the time-marching PINNs for  $\alpha = 0.25$ . The simulation parameters are  $N = 50$ ,  $T = 5$ ,  $\mathcal{D} = 1$ ,  $\chi = 0.25$ ,  $\gamma = 1$ . The neural network consists of five hidden layers with 100 neurons each, employs SiLU( $\cdot$ ) activation functions, and is trained for 1500 iterations per time step with a decreasing learning rate of  $1e - 3$ .

- Gradient vanishing:  $\frac{\partial \Psi}{\partial \sigma} \Big|_{\sigma=1} = 0$ , which guarantees that the normal derivatives  $\frac{\partial n(x,y,t)}{\partial \nu}$  and  $\frac{\partial c(x,y,t)}{\partial \nu}$  are zero regardless of the boundary curvature.

This construction provides a robust foundation for the convergence of the time-marching PINNs framework on irregular domains.

This numerical experiment aims to visualize the dynamical evolution of the system on a complex geometry, specifically the butterfly-shaped domain (7.17)), and to provide numerical evidence supporting global existence. The network architecture and parameter settings are kept

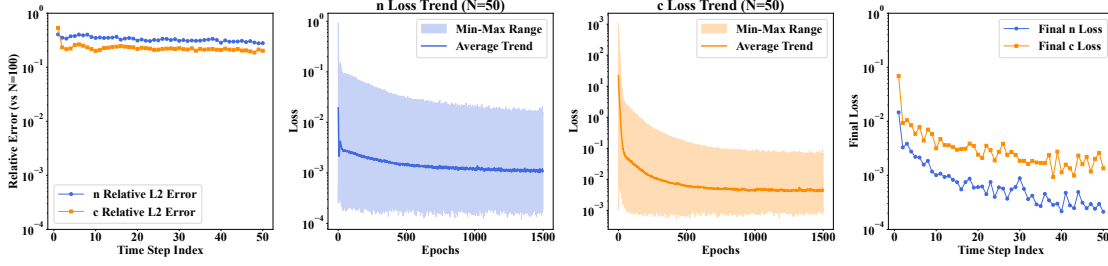


Fig. 16: (Color online) The numerical performance of the non-negativity/positivity-preserving time-marching PINNs algorithm with  $\alpha = 0.25$ . From left to right, the figures illustrate the  $L^2$  relative error, the total Loss trends of  $n$  and  $c$  at each time step, and the final loss versus time steps.

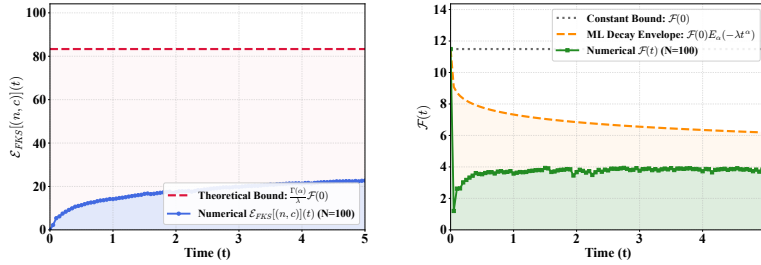


Fig. 17: (Color online) The theoretical and numerical results of the energy functions with  $\alpha = 0.25$ . From left to right, the figures illustrate the evolution of the novel Lyapunov function, defined by (6.1), and the jointly convex function  $\mathcal{F}(t)$  (defined in (6.2)) over time  $t$ .

consistent with those in Subsection 7.2 to ensure compatibility and robustness.

Since no analytical solution is available, a high-fidelity reference solution ( $n_{\text{Ref}, N=100}$ ,  $c_{\text{Ref}, N=100}$ ) is generated using the proposed time-marching PINNs algorithm with  $N = 100$  time steps, 1500 iterations per step, and 3 hidden layers each with 64 neurons. To evaluate the accuracy of the algorithm, the relative  $L^2$  error is defined as

$$\text{Relative } L^2 \text{ Error} = \frac{\|u_{\text{predic}} - u_{\text{Ref}, N=100}\|_{L^2(\Omega)}}{\|u_{\text{Ref}, N=100}\|_{L^2(\Omega)}}, \quad u \in \{n, c\}. \quad (7.20)$$

The numerical results are presented in Figures 15 – 23. Several observations can be drawn:

- The evolution of  $(n, c)$  shown in Figures 15, 18 and 21) reveals that different values of  $\alpha$  lead to different diffusion rates. In particular, a larger  $\alpha$  corresponds to faster spreading. This is consistent with the modeling assumptions: since a larger  $\alpha$  implies shorter waiting times, it results in higher mobility, which accelerates the dispersion of both myxobacteria and slime.
- The numerical performance illustrated in Figures 16, 19, and 22 demonstrates the stable training dynamics of our proposed deep learning algorithm. These results highlight the robustness of the DNN framework, especially for problems defined on non-trivial domains. While there is still room for quantitative improvement in the relative  $L^2$  error,

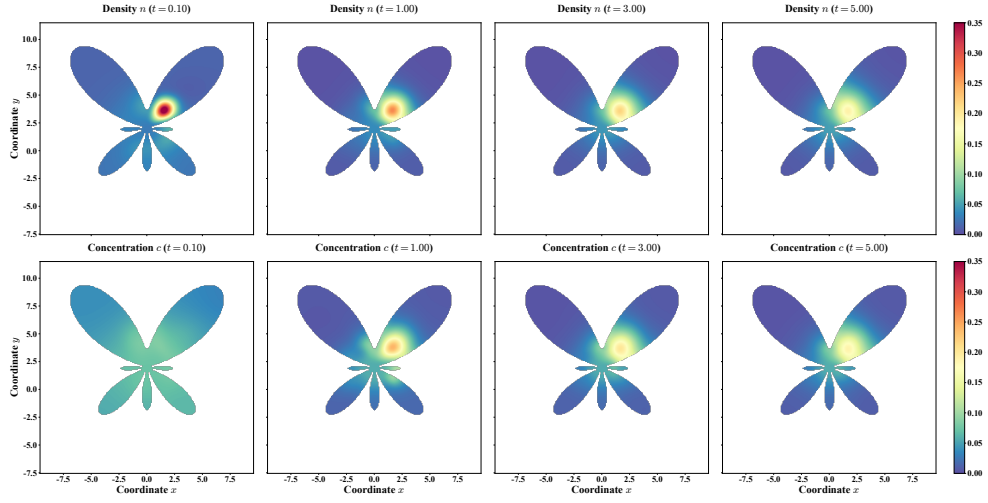


Fig. 18: (Color online) Spatiotemporal evolution of the solutions on a bounded butterfly domain with  $\alpha = 0.50$  and  $N = 50$ . All other parameters remain consistent with those in Fig. 15.

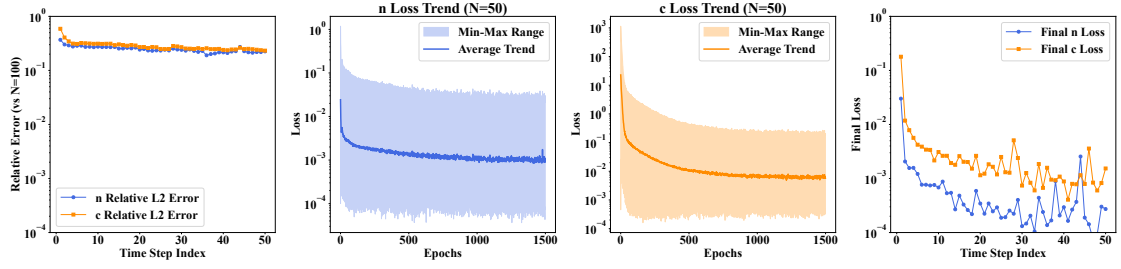


Fig. 19: (Color online) Numerical performance of the non-negativity/positivity-preserving time-marching PINNs algorithm for  $\alpha = 0.50$ . All other parameters are consistent with those in Fig. 16.

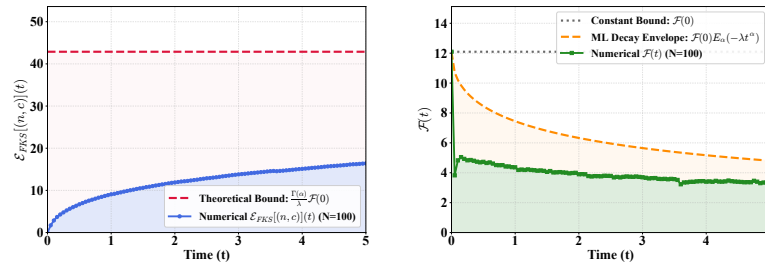


Fig. 20: (Color online) The theoretical and numerical results of the energy functions with  $\alpha = 0.5$ . From left to right, the figures illustrate the evolution of the novel Lyapunov function, defined by (6.1), and the jointly convex function  $\mathcal{F}(t)$  (defined in (6.2)) over time  $t$ .

the current accuracy is sufficient for capturing the essential dynamics and meets the practical needs of the simulation.

- Figures 17, 20, and 23 provide numerical verification of the new energy functionals defined in (see (6.1) and (6.2)). The observed behavior is in good agreement with the theoretical results in Lemmas 6.2 and 6.3. Specifically, the Lyapunov functional  $\mathcal{E}$  remains uniformly bounded, confirming the estimate  $\mathcal{E}[(n, c)](t) \leq \frac{\Gamma(\alpha)}{\lambda} \mathcal{F}(0)$  for  $t > 0$ . Meanwhile, the convex functional  $\mathcal{F}(t)$  exhibits the expected dissipation property, satisfying  $\mathcal{F}(t) \leq \mathcal{F}(0)E_\alpha(-\lambda t^\alpha)$  for  $t > 0$ .

In summary, the proposed method reproduces the expected diffusion behavior and respects the theoretical energy constraints on irregular geometries. The flexibility of the architecture also suggests that it can be extended to more complex coupled systems, offering a promising numerical tool for such problems.

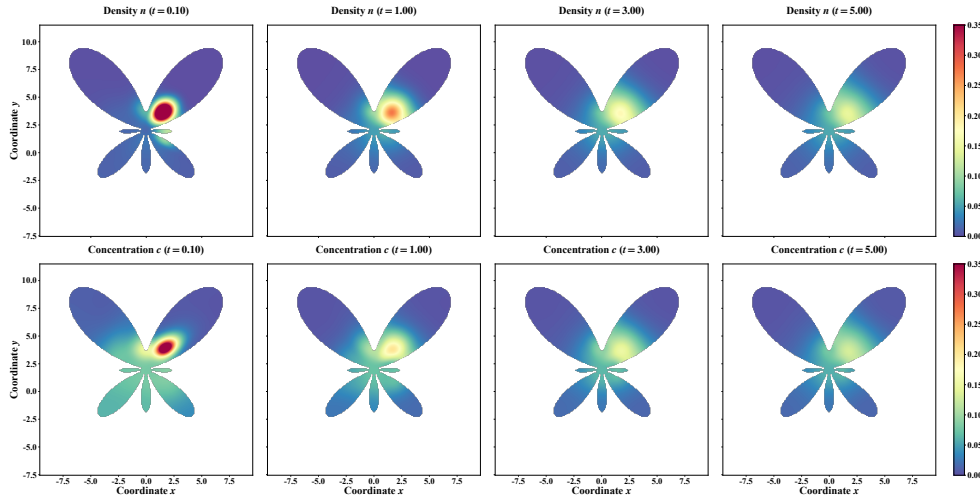


Fig. 21: (Color online) The dynamical evolutions of solutions on the bounded butterfly domain with  $\alpha = 0.75$ . All other parameters are set the same as Fig. 15.

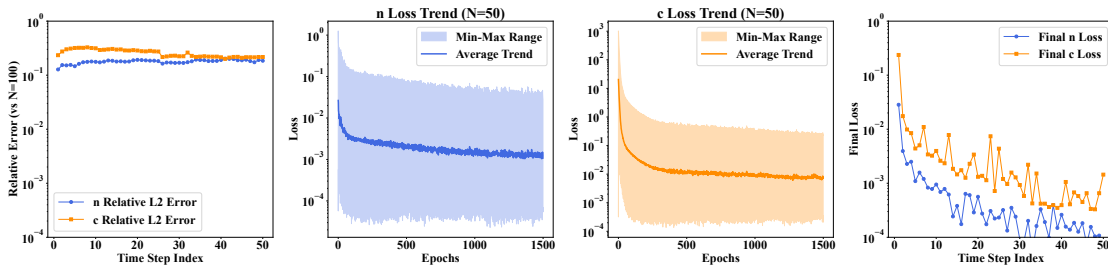


Fig. 22: (Color online) The numerical performance of the non-negativity/positivity-preserving time-marching PINNs algorithm with  $\alpha = 0.75$ . All other parameters are set the same as Fig. 16.

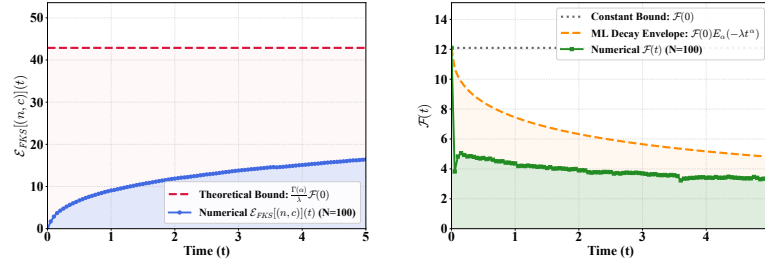


Fig. 23: (Color online) The theoretical and numerical results of the energy functions with  $\alpha = 0.75$ . From left to right, the figures illustrate the evolution of the novel Lyapunov function, defined by (6.1), and the jointly convex function  $\mathcal{F}(t)$  (defined in (6.2)) over time  $t$ .

## 8. Concluding Remarks

In this paper, we establish a comprehensive framework to accurately characterize the global dynamic behavior of chemotactic gliding-diffusion and aggregation in myxobacteria. To this end, we synergistically integrate stochastic modeling, rigorous mathematical analysis, and deep learning-based simulations. We first established a robust physical foundation by constructing a lattice-based discrete agent model at the microscopic scale to capture actual kinetic behavior on rough soil surfaces, with our assumptions validated through comparative experimental data. Bridging biological insights with stochastic modeling, we rigorously derived the macroscopic model (1.1) from a subordinated Langevin equation, ensuring both physical and mathematical consistency. On the theoretical side, we establish a definitive solution theory by incorporating an analytical framework based on a novel Lyapunov function, innovative fractional convexity inequality, and generalized Sobolev spaces. This analytical framework successfully overcomes the inherent difficulties of time-nonlocal operators and establishes global well-posedness, mass conservation, and novel regularity results. To address numerical challenges, we design a multi-objective, positivity/non-negativity-preserving time-marching PINNs algorithm with independent network architectures and temporal semi-discretization. The method demonstrates exceptional robustness and high generalizability across a broad class of KS-type systems. Numerical benchmarks on complex geometries, most notably the ‘butterfly-shaped’ domain, not only verify the accuracy of our scheme but also provide empirical validation of the global existence and long-term stability of the solutions.

In conclusion, this research offers insights into these complex processes by synergistically combining multiscale modeling, rigorous mathematical analysis, and computational methods, and thus provides a promising framework for future investigations of biological dynamics on rough surfaces and irregular geometries.

As an initial exploratory effort, this study opens several promising avenues for future research:

- **Experimentally**, engaging in collaborating with microbiologists to integrate empirical data will further strengthen the model’s reliability and predictive capacity.
- **Mathematically**, several directions are particularly worth pursuing. A natural next step is to investigate global existence and possible blow-up in higher-dimensional domains ( $d \geq 4$ ), and to establish sharper conditions on the chemotactic sensitivity coefficient  $\chi$  that guarantee global boundedness. Other promising extensions include coupling the

system with fluid dynamics to model more realistic environments (e.g., Refs. 32, 88, 121), incorporating source terms to describe cell proliferation and death (e.g., Ref. 52), or considering the combined influence of both (e.g., Refs. 30, 29). It should be noted that when source terms are present, mass conservation is lost, which introduces substantial additional difficulties in the analysis.

- **Numerically**, while the proposed deep neural network approach is effective, the non-local operators currently incur high computational costs. Future efforts will focus on optimizing network architecture to reduce overhead without sacrificing physical fidelity.
- **Broad applications**, extending the current two-dimensional framework to three-dimensional complex geometries or multi-species interacting networks stands as a natural and impactful next step.

## Appendix A. Auxiliary Results and Lemmas

In this appendix, we collect several auxiliary lemmas and supporting results, together with their proofs, that are used repeatedly in the main text.

### A.1. Continuum Limit of the Transition Probabilities

In the absence of environmental heterogeneity, the particle performs an unbiased nearest-neighbor random walk with transition probabilities  $p_r = p_l = 1/2$ . This corresponds to isotropic local exploration without any directional preference. Biologically, when the surrounding slime field or chemoattractant distribution is spatially homogeneous, the cells do not possess sufficient directional information and therefore move randomly.

Chemotactic sensing is modeled as a weak perturbation of aforementioned symmetric motion rather than a deterministic steering mechanism. In other words, the environmental signal does not generate additional transition probability, but instead redistributes the directional preference between rightward and leftward motion. Following the standard framework of weakly biased random walks (see, e.g., 51, 116), we write the transition probabilities as symmetric perturbations around the unbiased state

$$p_r = \frac{1}{2} + \varepsilon B(x, t), \quad p_l = \frac{1}{2} - \varepsilon B(x, t), \quad \varepsilon > 0, \quad (\text{A.1})$$

where  $B(x, t)$  describes the local directional bias induced by the surrounding signal field, while  $\varepsilon$  measures the strength of this bias and thus serves as the chemotactic sensitivity coefficient. This structure automatically preserves probability normalization,  $p_r + p_l = 1$ , guarantees that the unbiased state is recovered whenever the local environment is spatially symmetric, namely when  $B(x, t) = 0$ .

In the context of Myxobacterial aggregation, cells compare the signal intensities sensed within their local neighborhood before selecting a preferred moving direction (see (2.4)). Motivated by this mechanism, we define the directional bias through the normalized local contrast

$$B(x, t) = \frac{v(x + \delta_x, t) - v(x - \delta_x, t)}{v(x - \delta_x, t) + v(x + \delta_x, t)}, \quad (\text{A.2})$$

where  $v(x, t) > 0$  denotes the local slime concentration or chemoattractant field. Here, the numerator measures the directional asymmetry of the perceived signal, while the denominator represents the overall background intensity within the sensing range. Consequently, the cellular

response depends on the relative environmental contrast rather than the absolute concentration level, which is consistent with the experimentally observed adaptive sensing behavior in many biological aggregation processes.

According to (A.2), the model possesses the following natural biological interpretations:

- If  $v(x + \delta_x, t) > v(x - \delta_x, t)$ , then  $B(x, t) > 0$ , meaning that the right-hand side contains a stronger slime signal, and the Myxobacteria are therefore more likely to glide toward the right;
- If  $v(x + \delta_x, t) < v(x - \delta_x, t)$ , then  $B(x, t) < 0$ , indicating a stronger signal on the left-hand side, and the cells preferentially move leftward;
- If  $v(x + \delta_x, t) = v(x - \delta_x, t)$ , then  $B(x, t) = 0$ , and the system naturally returns to the unbiased random walk  $p_r = p_l = 1/2$ .

By gathering (A.1) and (A.2) and setting  $\varepsilon = \frac{\chi}{4}$ , the transition probabilities can be rewritten as

$$\begin{cases} p_r(x, t) = \frac{1}{2} + \frac{\chi}{4} \frac{v(x + \delta_x, t) - v(x - \delta_x, t)}{v(x - \delta_x, t) + v(x + \delta_x, t)}, \\ p_l(x, t) = \frac{1}{2} - \frac{\chi}{4} \frac{v(x + \delta_x, t) - v(x - \delta_x, t)}{v(x - \delta_x, t) + v(x + \delta_x, t)}. \end{cases} \quad (\text{A.3})$$

where  $\chi > 0$  is the chemotactic sensitivity coefficient characterizing the strength of directional response to environmental heterogeneity. By construction,  $p_r(x, t) + p_l(x, t) = 1$ . Let the random displacement during a single transition be denoted by  $\xi \in \{+\delta_x, -\delta_x\}$ . Then the first two Kramers–Moyal coefficients (see, e.g., Ref. 109) are given by

$$\begin{cases} m_1(x, t) := \mathbb{E}[\xi | x, t] = \delta_x (p_r(x, t) - p_l(x, t)), \\ m_2(x, t) := \mathbb{E}[\xi^2 | x, t] = (\delta_x)^2 (p_r(x, t) + p_l(x, t)) = (\delta_x)^2. \end{cases}$$

Hence, the asymmetric component  $p_r - p_l$  generates the effective directional drift, while the symmetric component  $p_r + p_l$  determines the diffusive spreading.

Assuming that  $v$  is sufficiently smooth, Taylor expansion around  $x$  gives

$$v(x \pm \delta_x, t) = v(x, t) \pm \delta_x \partial_x v(x, t) + \mathcal{O}(\delta_x^2).$$

Substituting these expansions into (A.3), we obtain

$$\begin{aligned} p_r - p_l &= \frac{\chi}{2} \frac{v(x + \delta_x, t) - v(x - \delta_x, t)}{v(x + \delta_x, t) + v(x - \delta_x, t)} = \frac{\chi}{2} \frac{2\delta_x \partial_x v(x) + \mathcal{O}(\delta_x^3)}{2v(x) + \mathcal{O}(\delta_x^2)} \\ &= \frac{\chi}{2} \delta_x \partial_x \ln v(x) + \mathcal{O}(\delta_x^3). \end{aligned}$$

Therefore,

$$m_1(x, t) = \frac{\chi}{2} \delta_x^2 \partial_x \ln v(x, t) + \mathcal{O}(\delta_x^4), \quad m_2(x, t) = (\delta_x)^2.$$

Under the anomalous diffusive scaling  $\delta_x^2 \sim \tau^\alpha$  with  $\alpha \in (0, 1)$ , the effective drift and diffusion coefficients are formally identified as<sup>109</sup>

$$D^{(1)}(x, t) = \lim_{\tau \rightarrow 0} \frac{m_1(x, t)}{\tau^\alpha}, \quad D^{(2)}(x, t) = \lim_{\tau \rightarrow 0} \frac{m_2(x, t)}{2\tau^\alpha}.$$

Introducing the generalized diffusion coefficient  $\mathcal{D} = \frac{\delta_x^2}{2\tau^\alpha}$ , we obtain

$$D^{(1)}(x, t) = \chi \mathcal{D} \partial_x \ln v(x, t), \quad D^{(2)}(x, t) = \mathcal{D}.$$

According to the standard Kramers-Moyal formalism for continuous diffusion limits (see, e.g., Ch. 4 in Ref. 109), truncation at second order yields the Fokker-Planck equation

$$\frac{\partial P(x, t)}{\partial t} = -\frac{\partial}{\partial x}(D^{(1)}(x, t)P(x, t)) + \frac{\partial^2}{\partial x^2}(D^{(2)}(x, t)P(x, t)), \quad (\text{A.4})$$

which is statistically equivalent to the Itô Langevin equation

$$\dot{x}(t) = D^{(1)}(x, t) + \sqrt{2D^{(2)}(x, t)}\dot{W}(t). \quad (\text{A.5})$$

Substituting the expressions for  $D^{(1)}$  and  $D^{(2)}$  into (A.5), we arrive at

$$\dot{x}(t) = \chi \mathcal{D} \partial_x \ln v(x, t) + \sqrt{2\mathcal{D}}\dot{W}(t).$$

Therefore, the continuum limit of the weakly biased random walk naturally generates a macroscopic drift directed along the logarithmic gradient of the slime field, which quantitatively describes the tendency of Myxobacteria to aggregate toward regions with stronger environmental signals.

## A.2. Key Supporting Lemmas

**Lemma Appendix A.1.** For  $\alpha \in (0, 1)$ , and  $f(t) \in AC(\bar{D})$ , there holds

$${}_0^C \mathcal{D}_t^\alpha |f(t)| \leq \text{sgn}(f(t)) \cdot {}_0^C \mathcal{D}_t^\alpha f(t), \quad (\text{A.6})$$

where  $\text{sgn}(\cdot)$  denotes the standard sign function, and  $AC(\cdot)$  the class of absolutely continuous functions.

**Proof.** For the sign function  $\text{sgn}(\cdot)$  the sub-gradient property states that  $|b| - |a| \geq \text{sgn}(a)(b - a)$  for all  $a, b \in \mathbb{R}$ . Taking  $a = f(t)$  and  $b = f(0)$  yields

$$\frac{|f(t)| - |f(0)|}{\Gamma(1 - \alpha)t^\alpha} \leq \frac{1}{\Gamma(1 - \alpha)} \text{sgn}(f(t)) \frac{f(t) - f(0)}{t^\alpha}, \quad \forall t > 0. \quad (\text{A.7})$$

and similarly,

$$\frac{|f(t)| - |f(s)|}{\Gamma(1 - \alpha)(t - s)^{\alpha+1}} \leq \frac{1}{\Gamma(1 - \alpha)} \text{sgn}(f(t)) \frac{f(t) - f(s)}{(t - s)^{\alpha+1}}, \quad \forall s \in [0, t] \subset D. \quad (\text{A.8})$$

For  $\alpha \in (0, 1)$ , Lemma 2.10 in Ref. 62 gives the following representation of the Caputo fractional derivative for  $|f(t)|$ ,

$${}_0^C \mathcal{D}_t^\alpha |f(t)| = \frac{1}{\Gamma(1 - \alpha)} \left( \frac{|f(t)| - |f(0)|}{t^\alpha} + \alpha \int_0^t \frac{|f(t)| - |f(s)|}{(t - s)^{\alpha+1}} ds \right). \quad (\text{A.9})$$

Substituting inequalities (A.7) and (A.8) into (A.9) and carrying out straightforward sign manipulation leads to

$${}_0^C \mathcal{D}_t^\alpha |f(t)| \leq \text{sgn}(f(t)) \cdot \frac{1}{\Gamma(1 - \alpha)} \left( \frac{f(t) - f(0)}{t^\alpha} + \alpha \int_0^t \frac{f(t) - f(s)}{(t - s)^{\alpha+1}} ds \right).$$

The expression inside the brackets coincides with the definition of  ${}_0^C \mathcal{D}_t^\alpha f(t)$ . Therefore, the point-wise inequality (A.6) is established.  $\square$

**Lemma Appendix A.2.** *Let  $\Omega \subset \mathbb{R}^d$  ( $d \geq 2$ ) be a bounded domain with smooth boundary, and let  $\mathcal{A} = -\Delta$  denote the Neumann Laplacian on  $L^p(\Omega)$  with  $1 < p < \infty$ . Define  $\mathcal{P}_\alpha(t) = t^{\alpha-1}E_{\alpha,\alpha}(-t^\alpha\mathcal{A})$ . Then, for all  $t > 0$ , there exist a constant  $C > 0$  such that*

$$\left\| \mathcal{A}_\gamma^\sigma \mathcal{P}_\alpha^\gamma(t) \right\|_{L^p \rightarrow L^p} \leq C t^{\alpha(1-\sigma)-m-1}, \quad \sigma \in \{0, 1/2, 1\}. \quad (\text{A.10})$$

Furthermore, for  $\gamma > 0$  define  $\mathcal{A}_\gamma := \mathcal{A} + \gamma I$  and  $\mathcal{P}_\alpha^\gamma(t) = t^{\alpha-1}E_{\alpha,\alpha}(-t^\alpha\mathcal{A}_\gamma)$ . Then, for  $t > 0$ , there exist additional constant  $C > 0$  such that

$$\left\| \partial_t^m \mathcal{A}_\gamma^\sigma \mathcal{P}_\alpha^\gamma(t) \right\|_{L^p \rightarrow L^p} \leq C t^{\alpha(1-\sigma)-m-1}(1+t^\alpha)^{-1}, \quad (\text{A.11})$$

where  $m = 0, 1$  and  $\sigma \in \{0, 1/2, 1\}$ .

**Proof.** We first prove the estimates for  $\mathcal{P}_\alpha(t)$ . By the Hankel contour representation of the Mittag-Leffler function (see, e.g., Ref. 104),  $E_{\alpha,\alpha}(\tau) = \frac{1}{2\pi i} \int_\Gamma \frac{e^\zeta}{\zeta^{\alpha-\tau}} d\zeta$ , where  $\Gamma$  is a sectorial contour contained in  $\Sigma_\theta := \{z \in \mathbb{C} : |\arg(z)| < \theta, z \neq 0\}$  with  $\theta \in (\pi/2, \pi)$ . Since the Neumann Laplacian  $\mathcal{A} = -\Delta$  on  $L^p(\Omega)$  is sectorial, this representation extends to  $\mathcal{A}$ . By substituting  $\tau = -t^\alpha\mathcal{A}$ , performing the variable transformation  $\zeta = zt$ , and combining these with the result  $\mathcal{L}\{t^{\alpha-1}E_{\alpha,\alpha}(-\lambda t^\alpha)\} = \frac{1}{z^{\alpha+\lambda}}$ , we obtain

$$\mathcal{P}_\alpha(t) = \frac{1}{2\pi i} \int_\Gamma e^{zt} (z^\alpha + \mathcal{A})^{-1} dz.$$

Since  $\mathcal{A}$  is sectorial, there exists  $\theta \in (\pi/2, \pi)$  such that  $\|(z + \mathcal{A})^{-1}\|_{L^p \rightarrow L^p} \leq \frac{C}{|z|}$  for all  $z \notin \Sigma_\theta$ . We choose  $\Gamma$  to be the sectorial contour  $\Gamma = \{z \in \mathbb{C} : |\arg(z)| = \theta, r = |z| \geq 1/t\} \cup \{z \in \mathbb{C} : r = |z| = 1/t, |\arg(z)| \leq \theta\}$  oriented counter-clockwise. For  $z \in \Gamma \subset \Sigma_\theta$ , the term  $z^\alpha$  also lies in a sector avoiding the negative real axis, and thus the resolvent bound yields  $\|(z^\alpha + \mathcal{A})^{-1}\|_{L^p \rightarrow L^p} \leq C|z|^{-\alpha}$ . Moreover,  $\Re(z) \leq -c|z|$  on the branches of  $\Gamma$ , leading to  $|e^{zt}| \leq e^{-ct|z|}$ . Following standard estimates by the Laplace transform method (see, e.g., Refs. 62, 86, 89, 90), for  $\sigma = 0$  and  $\sigma = 1$  the estimate in (A.10) can be directly proved analogously to the proof of Theorem 6.4 in Ref. 62. Furthermore, for  $1 < p < \infty$ , by the interpolation inequality (moment inequality) of sectorial operators (see e.g., Proposition 6.6.4 in Ref. 49), we have  $\|\mathcal{A}^{1/2}u\|_{L^p} \leq C\|u\|_{L^p}^{1/2}\|\mathcal{A}u\|_{L^p}^{1/2}$ . Applying this, we derive

$$\|\mathcal{P}_\alpha(t)\|_{L^p \rightarrow W^{1,p}} \leq C (t^{\alpha-1})^{1/2} (t^{-1})^{1/2} \leq C t^{\alpha/2-1}.$$

This completes the estimate of (A.10).

We now proceed to prove (A.11). For  $m \in \{0, 1\}$  and  $\sigma \in \{0, \frac{1}{2}, 1\}$ , the Hankel contour representation yields

$$\partial_t^m \mathcal{A}_\gamma^\sigma \mathcal{P}_\alpha^\gamma(t) = \frac{1}{2\pi i} \int_\Gamma e^{zt} z^m \mathcal{A}_\gamma^\sigma (z^\alpha + \mathcal{A}_\gamma)^{-1} dz,$$

where  $\Gamma$  is a standard sectorial contour, as denoted previously. We first consider the cases  $\sigma = 0$  and  $\sigma = 1$ . Since  $\mathcal{A}_\gamma$  is sectorial and  $\sigma(\mathcal{A}_\gamma) \subset [\gamma, \infty)$ , the resolvent estimate  $\|(z^\alpha + \mathcal{A}_\gamma)^{-1}\|_{L^p \rightarrow L^p} \leq C(|z|^\alpha + \gamma)^{-1}$  holds uniformly for all  $z \in \Gamma$ . Moreover, the contour  $\Gamma$  can be chosen such that  $\Re(z) \leq -c|z|$  for  $z \in \Gamma$ , and hence  $|e^{zt}| \leq e^{-ct|z|}$ . For  $\sigma = 0$ , the resolvent estimate directly gives  $\|\mathcal{A}_\gamma^0(z^\alpha + \mathcal{A}_\gamma)^{-1}\|_{L^p \rightarrow L^p} \leq C(|z|^\alpha + \gamma)^{-1}$ . For  $\sigma = 1$ , using the identity  $\mathcal{A}_\gamma(z^\alpha + \mathcal{A}_\gamma)^{-1} = I - z^\alpha(z^\alpha + \mathcal{A}_\gamma)^{-1}$ , and observing that  $\int_\Gamma e^{zt} z^m dz = 0$  by Cauchy's theorem, we obtain

$$\partial_t^m \mathcal{A}_\gamma \mathcal{P}_\alpha^\gamma(t) = -\frac{1}{2\pi i} \int_\Gamma e^{zt} z^{m+\alpha} (z^\alpha + \mathcal{A}_\gamma)^{-1} dz.$$

Therefore, both cases  $\sigma = 0$  and  $\sigma = 1$ , the integrand admits the unified bound  $|e^{zt}||z|^{m+\alpha\sigma}(|z|^\alpha + \gamma)^{-1}$ . Consequently,

$$\|\partial_t^m \mathcal{A}_\gamma^\sigma \mathcal{P}_\alpha^\gamma(t)\|_{L^p \rightarrow L^p} \leq C \int_{1/t}^\infty e^{tr \cos(\theta)} \frac{r^{m+\alpha\sigma}}{r^\alpha + \gamma} dr + \int_{-\theta}^\theta e^{t\Re(z)} \frac{|z|^{m+\alpha\sigma}}{|z|^\alpha + \gamma} |dz| := I_1 + I_2,$$

where  $I_1$  corresponds to the integration over the branches and  $I_2$  corresponds to the circular arc.

For the circular arc, we have  $|z| = 1/t$  and  $|dz| = \frac{1}{t} d\varphi$ . Furthermore,  $\Re(z) \leq |z| \cos \theta$ , so  $|e^{zt}| \leq e^{\cos \theta} \leq C$ . Thus, we have

$$I_2 = \int_{-\theta}^\theta |e^{zt}| \frac{|z|^{m+\alpha\sigma}}{|z|^\alpha + \gamma} |dz| \leq C \int_{-\theta}^\theta \frac{t^{-(m+\alpha\sigma)}}{t^{-\alpha} + \gamma} \frac{1}{t} d\varphi \leq Ct^{-m-\alpha\sigma-1} \frac{1}{t^{-\alpha} + \gamma}.$$

Since  $\frac{1}{t^{-\alpha} + \gamma} = \frac{t^\alpha}{1 + \gamma t^\alpha} \leq Ct^\alpha(1 + t^\alpha)^{-1}$ , we obtain

$$I_2 \leq Ct^{\alpha(1-\sigma)-m-1}(1 + t^\alpha)^{-1}.$$

For the branches, we have  $\Re(z) \leq -c|z|$  which implies  $|e^{zt}| \leq e^{-ctr}$ . Thus, making the substitution  $s = tr$ , we obtain

$$I_1 \leq Ct^{\alpha(1-\sigma)-m-1} \int_1^\infty e^{-cs} \frac{s^{m+\alpha\sigma}}{s^\alpha + \gamma t^\alpha} ds.$$

To estimate the integral, we distinguish two cases.

- For  $0 < t \leq 1$ : Since  $s^\alpha + \gamma t^\alpha \geq s^\alpha$ , it follows that

$$\int_1^\infty e^{-cs} \frac{s^{m+\alpha\sigma}}{s^\alpha + \gamma t^\alpha} ds \leq \int_1^\infty e^{-cs} s^{m+\alpha(\sigma-1)} ds \leq C.$$

The last inequality holds for  $m + \alpha(\sigma - 1) \geq -\alpha > -1$ , ensuring the above Gamma-type integral converges and yielding  $\int_0^\infty e^{-cs} \frac{s^{m+\alpha\sigma}}{s^\alpha + \gamma t^\alpha} ds \leq C$ .

- For  $t > 1$ : We have  $s^\alpha + \gamma t^\alpha \geq \gamma t^\alpha$ , which gives

$$\int_1^\infty e^{-cs} \frac{s^{m+\alpha\sigma}}{s^\alpha + \gamma t^\alpha} ds \leq \frac{1}{\gamma t^\alpha} \int_1^\infty e^{-cs} s^{m+\alpha\sigma} ds \leq Ct^{-\alpha}.$$

Combining the above estimates, we conclude that  $\int_1^\infty e^{-cs} \frac{s^{m+\alpha\sigma}}{s^\alpha + \gamma t^\alpha} ds \leq C(1 + t^\alpha)^{-1}$ . Hence, for  $\sigma \in \{0, 1\}$ , the following holds

$$\|\partial_t^m \mathcal{A}_\gamma^\sigma \mathcal{P}_\alpha^\gamma(t)\|_{L^p \rightarrow L^p} \leq Ct^{\alpha(1-\sigma)-m-1}(1 + t^\alpha)^{-1}.$$

It remains to consider the case  $\sigma = \frac{1}{2}$ . By the moment inequality for sectorial operators,  $\|\mathcal{A}_\gamma^{1/2} u\|_{L^p} \leq C \|u\|_{L^p}^{1/2} \|\mathcal{A}_\gamma u\|_{L^p}^{1/2}$ , we obtain

$$\begin{aligned} \|\partial_t^m \mathcal{A}_\gamma^{1/2} \mathcal{P}_\alpha^\gamma(t)\|_{L^p \rightarrow L^p} &= \|\mathcal{A}_\gamma^{1/2} (\partial_t^m \mathcal{P}_\alpha^\gamma(t))\|_{L^p \rightarrow L^p} \\ &\leq C \|\partial_t^m \mathcal{P}_\alpha^\gamma(t)\|_{L^p \rightarrow L^p}^{1/2} \|\mathcal{A}_\gamma \partial_t^m \mathcal{P}_\alpha^\gamma(t)\|_{L^p \rightarrow L^p}^{1/2}. \end{aligned}$$

Substituting the estimates already established for  $\sigma = 0$  and  $\sigma = 1$ , we arrive at

$$\begin{aligned} \|\partial_t^m \mathcal{A}_\gamma^{1/2} \mathcal{P}_\alpha^\gamma(t)\|_{L^p \rightarrow L^p} &\leq C \left( t^{\alpha-m-1} (1 + t^\alpha)^{-1} \right)^{1/2} \left( t^{-m-1} (1 + t^\alpha)^{-1} \right)^{1/2} \\ &= Ct^{\alpha/2-m-1} (1 + t^\alpha)^{-1}. \end{aligned}$$

Consequently, for all  $m \in \{0, 1\}$  and  $\sigma \in \{0, \frac{1}{2}, 1\}$ ,

$$\|\partial_t^m \mathcal{A}_\gamma^\sigma \mathcal{P}_\alpha^\gamma(t)\|_{L^p \rightarrow L^p} \leq Ct^{\alpha(1-\sigma)-m-1}(1 + t^\alpha)^{-1}.$$

This completes the proof.  $\square$

**Lemma Appendix A.3 (A scalar comparison principle).** *Let  $\alpha \in (0, 1)$ ,  $a, b > 0$ , and  $\theta > 0$ . Suppose that  $Y \geq 0$  is sufficiently regular so that*

$${}_0^C D_t^\alpha Y(t) = \frac{Y(t) - Y(0)}{\Gamma(1 - \alpha)t^\alpha} + \frac{\alpha}{\Gamma(1 - \alpha)} \int_0^t \frac{Y(t) - Y(s)}{(t - s)^{\alpha+1}} ds, \quad t > 0.$$

*Assume moreover that  ${}_0^C D_t^\alpha Y(t) \leq aY(t) - bY(t)^{1+\theta}$  for  $t > 0$ . Then*

$$\sup_{t \geq 0} Y(t) \leq \max \left\{ Y(0), \left( \frac{a}{b} \right)^{1/\theta} \right\}.$$

**Proof.** Set  $K := \max \left\{ Y(0), \left( \frac{a}{b} \right)^{1/\theta} \right\}$ . We prove that  $Y(t) \leq K$  for all  $t \geq 0$ . Suppose otherwise. Then there exist  $T > 0$  and  $\tilde{t} \in [0, T]$  such that

$$Y(\tilde{t}) = \max_{0 \leq t \leq T} Y(t) > K.$$

Since  $Y(0) \leq K$ , we have  $\tilde{t} > 0$ . Moreover,  $Y(\tilde{t}) \geq Y(s)$ ,  $0 \leq s \leq \tilde{t}$ . Therefore, by the above representation formula,

$${}_0^C D_t^\alpha Y(\tilde{t}) = \frac{Y(\tilde{t}) - Y(0)}{\Gamma(1 - \alpha)\tilde{t}^\alpha} + \frac{\alpha}{\Gamma(1 - \alpha)} \int_0^{\tilde{t}} \frac{Y(\tilde{t}) - Y(s)}{(\tilde{t} - s)^{\alpha+1}} ds \geq 0.$$

On the other hand,

$$Y(\tilde{t}) > \left( \frac{a}{b} \right)^{1/\theta}$$

implies

$$aY(\tilde{t}) - bY(\tilde{t})^{1+\theta} = Y(\tilde{t}) (a - bY(\tilde{t})^\theta) < 0,$$

which contradicts the assumed differential inequality. Hence  $Y(t) \leq K$  for all  $t \geq 0$ .  $\square$

## Declarations

### *Conflict of interest*

The authors declared that they have no conflict of interest.

## Acknowledgments

The first author would like to express sincere gratitude to Prof. Tiejun Li for his insightful guidance on AI4SC. Fugui Ma is supported by the Peking University Boya Postdoctoral Fellowship. Lei Wu is supported by NSF under grant DMS-2405161.

## References

1. K. D. B. J. Adam, A method for stochastic optimization, *arXiv:1412.6980*.
2. R. A. Adams and J. J. F. Fournier, *Sobolev Spaces*, volume 140 (Elsevier/Academic Press, Amsterdam, 2003), second edition.
3. J. Adler, Chemotaxis in bacteria: Motile Escherichia coli migrate in bands that are influenced by oxygen and organic nutrients., *Science* **153** (1966) 708–716.

4. M. Aida, K. Osaki, T. Tsujikawa, A. Yagi and M. Mimura, Chemotaxis and growth system with singular sensitivity function, *Nonlinear Anal.-Real World Appl.* **6** (2005) 323–336.
5. M. Al-Refai and Y. Luchko, Comparison principles for solutions to the fractional differential inequalities with the general fractional derivatives and their applications, *J. Differential Equations* **319** (2022) 312–324.
6. A. A. Alikhanov, A priori estimates for solutions of boundary value problems for equations of fractional order, *Differ. Uravn.* **46** (2010) 658–664.
7. H. Amann, *Linear and quasilinear parabolic problems. Vol. II*, volume 106 of *Monographs in Mathematics* (Birkhäuser/Springer, Cham, 2019), function spaces.
8. C. N. Angstmann, A. M. Erickson, B. I. Henry, A. V. McGann, J. M. Murray and J. A. Nichols, A general framework for fractional order compartment models, *SIAM Rev.* **63** (2021) 375–392.
9. D. Applebaum, *Lévy Processes And Stochastic Calculus*, volume 116 (Cambridge University Press, Cambridge, 2009), second edition.
10. G. Arumugam and J. Tyagi, Keller-Segel chemotaxis models: A review, *Acta Appl. Math.* **171** (2021) 6, 82.
11. P. Auscher and P. Tchamitchian, Square roots of elliptic second order divergence operators on strongly Lipschitz domains:  $L^p$  theory, *Math. Ann.* **320** (2001) 577–623.
12. A. G. Baydin, B. A. Pearlmutter, A. A. Radul and J. M. Siskind, Automatic differentiation in machine learning: A survey, *J. Mach. Learn. Res.* **18** (2018) 1–43.
13. N. Bellomo, N. Outada, J. Soler, Y. Tao and M. Winkler, Chemotaxis and cross-diffusion models in complex environments: Models and analytic problems toward a multiscale vision, *Math. Models Methods Appl. Sci.* **32** (2022) 713–792.
14. H. C. Berg and D. A. Brown, Chemotaxis in *Escherichia coli* analysed by three-dimensional tracking, *Nature* **239** (1972) 500–504.
15. M. Bezerra, C. Cuevas, C. Silva and H. Soto, On the fractional doubly parabolic Keller-Segel system modelling chemotaxis, *Sci. China Math.* **65** (2022) 1827–1874.
16. M. Bezerra, C. Cuevas and A. Viana, Local and global solutions for a subdiffusive parabolic-parabolic Keller-Segel system, *Z. Angew. Math. Phys.* **75** (2024) Paper No. 172, 30.
17. C. M. Bishop and H. Bishop, *Deep Learning: Foundations and Concepts* (Springer, Cham, 2024).
18. J. Bouvard, C. Douarche, P. Mergaert, H. Auradou and F. Moisy, Direct measurement of the aerotactic response in a bacterial suspension, *Phys. Rev. E* **106** (2022) 034404.
19. L. M. Brègman, A relaxation method of finding a common point of convex sets and its application to the solution of problems in convex programming, *U.S.S.R. Comput. Math. Math. Phys.* **7** (1967) 200–217.
20. H. Brezis, *Functional Analysis, Sobolev Spaces And Partial Differential Equations*, Universitext (Springer, New York, 2011).
21. E. O. Budrene and H. C. Berg, Dynamics of formation of symmetrical patterns by chemotactic bacteria, *Nature* **376** (1995) 49–53.
22. V. I. Burenkov and E. B. Davies, Spectral stability of the Neumann Laplacian, *J. Differential Equations* **186** (2002) 485–508.
23. L. Chen, F. Kong and Q. Wang, Stationary ring and concentric-ring solutions of the Keller-Segel model with quadratic diffusion, *SIAM J. Math. Anal.* **52** (2020) 4565–4615.
24. L. Chen, F. Kong and Q. Wang, Global and exponential attractor of the repulsive Keller-Segel model with logarithmic sensitivity, *European J. Appl. Math.* **32** (2021) 599–617.
25. A. Chertock and A. Kurganov, A second-order positivity preserving central-upwind scheme for chemotaxis and haptotaxis models, *Numer. Math.* **111** (2008) 169–205.
26. F. R. Chung and S.-T. Yau, Logarithmic harnack inequalities, *Math. Res. Lett.* **3** (1996) 793–812.
27. M. Costa, C. Cuevas, C. Silva and H. Soto, Well-posedness and blow-up of the fractional Keller-Segel model on domains, *Math. Nachr.* **296** (2023) 5569–5592.
28. J. Cremer, T. Honda, Y. Tang, J. Wong-Ng, M. Vergassola and T. Hwa, Chemotaxis as a navigation strategy to boost range expansion, *Nature* **575** (2019) 658–663.
29. F. Dai and B. Liu, How far do indirect signal production mechanisms influence regularity in the three-dimensional Keller-Segel-Navier-Stokes system?, *Math. Models Methods Appl. Sci.* **33** (2023) 2823–2877.

30. F. Dai and T. Xiang, Boundedness and asymptotic stabilization in a two-dimensional Keller-Segel-Navier-Stokes system with sub-logistic source, *Math. Models Methods Appl. Sci.* **32** (2022) 2237–2294.
31. W. Dawid, Biology and global distribution of myxobacteria in soils, *FEMS Microbiol. Rev.* **24** (2000) 403–427.
32. P. de Anna, A. A. Pahlavan, Y. Yawata, R. Stocker and R. Juanes, Chemotaxis under flow disorder shapes microbial dispersion in porous media, *Nat. Phys.* **17** (2020) 68–73.
33. W. Deng, R. Hou, W. Wang and P. Xu, *Modeling Anomalous Diffusion—From Statistics To Mathematics* (World Scientific Publishing Co. Pte. Ltd., Hackensack, NJ, 2020).
34. J.-D. Deuschel and D. W. Stroock, Hypercontractivity and spectral gap of symmetric diffusions with applications to the stochastic Ising models, *J. Funct. Anal.* **92** (1990) 30–48.
35. Y. Epshteyn and A. Kurganov, New interior penalty discontinuous Galerkin methods for the Keller-Segel chemotaxis model, *SIAM J. Numer. Anal.* **47** (2008) 386–408.
36. Y. Epshteyn and Q. Xia, Efficient numerical algorithms based on difference potentials for chemotaxis systems in 3D, *J. Sci. Comput.* **80** (2019) 26–59.
37. G. Estrada-Rodriguez, H. Gimperlein and K. J. Painter, Fractional Patlak-Keller-Segel equations for chemotactic superdiffusion, *SIAM J. Appl. Math.* **78** (2018) 1155–1173.
38. X. Fang, L. Qiao, F. Zhang and F. Sun, Explore deep network for a class of fractional partial differential equations, *Chaos Solitons Fractals* **172** (2023) 113528.
39. F. Filbet, A finite volume scheme for the Patlak-Keller-Segel chemotaxis model, *Numer. Math.* **104** (2006) 457–488.
40. D. Fujiwara, Concrete characterization of the domains of fractional powers of some elliptic differential operators of the second order, *Proc. Japan Acad.* **43** (1967) 82–86.
41. G.-h. Gao, Z.-z. Sun and H.-w. Zhang, A new fractional numerical differentiation formula to approximate the Caputo fractional derivative and its applications, *J. Comput. Phys.* **259** (2014) 33–50.
42. R. Gorenflo, A. A. Kilbas, F. Mainardi and S. Rogosin, *Mittag-Leffler functions, related topics and applications*, Springer Monographs in Mathematics (Springer, Berlin, [2020] ©2020), second edition [of 3244285].
43. G. Gripenberg, S.-O. Londen and O. Staffans, *Volterra Integral and Functional Equations*, volume 34 of *Encyclopedia Of Mathematics And Its Applications* (Cambridge University Press, Cambridge, 1990).
44. P. Grisvard, *Elliptic Problems In Nonsmooth Domains*, volume 69 of *Classics in Applied Mathematics* (SIAM, Philadelphia, PA, 2011), reprint of the 1985 original [MR0775683], With a foreword by Susanne C. Brenner.
45. L. Gross, Logarithmic Sobolev inequalities, *American Journal of Mathematics* **97** (1975) 1061–1083.
46. L. Guo, X. H. Li and Y. Yang, Energy dissipative local discontinuous Galerkin methods for Keller-Segel chemotaxis model, *J. Sci. Comput.* **78** (2019) 1387–1404.
47. L. Guo, H. Wu, X. Yu and T. Zhou, Monte Carlo fPINNs: deep learning method for forward and inverse problems involving high dimensional fractional partial differential equations, *Comput. Methods Appl. Mech. Engrg.* **400** (2022) 115523.
48. P. Gyrya and L. Saloff-Coste, Neumann and Dirichlet heat kernels in inner uniform domains, *Astérisque* (2011) viii+144.
49. M. Haase, *The Functional Calculus for Sectorial Operators*, volume 169 of *Operator Theory: Advances and Applications* (Birkhäuser Verlag, Basel, 2006).
50. B. I. Henry, T. A. M. Langlands and P. Straka, Fractional Fokker-Planck equations for subdiffusion with space- and time-dependent forces, *Phy. Rev. Lett.* **105** (2010) 170602.
51. T. Hillen and K. J. Painter, A user’s guide to PDE models for chemotaxis, *J. Math. Biol.* **58** (2009) 183–217.
52. T. Hillen, K. J. Painter and M. Winkler, Convergence of a cancer invasion model to a logistic chemotaxis model, *Math. Models Methods Appl. Sci.* **23** (2013) 165–198.
53. F. Höfling and T. Franosch, Anomalous transport in the crowded world of biological cells, *Rep. Progr. Phys.* **76** (2013) 046602.

54. Q. Hou, C.-J. Liu, Y.-G. Wang and Z. Wang, Stability of boundary layers for a viscous hyperbolic system arising from chemotaxis: One-dimensional case, *SIAM J. Math. Anal.* **50** (2018) 3058–3091.
55. J. Hu and X. Zhang, Positivity-preserving and energy-dissipative finite difference schemes for the Fokker-Planck and Keller-Segel equations, *IMA J. Numer. Anal.* **43** (2023) 1450–1484.
56. X. Huang, O. Goubet and J. Shen, Numerical analysis of a semi-implicit Euler scheme for the Keller-Segel model, *ESAIM Math. Model. Numer. Anal.* **60** (2026) 517–540.
57. X. Huang and J. Shen, Bound/positivity preserving SAV schemes for the Patlak-Keller-Segel-Navier-Stokes system, *J. Comput. Phys.* **480** (2023) 112034.
58. S. T. Islam and T. Mignot, The mysterious nature of bacterial surface (gliding) motility: A focal adhesion-based mechanism in *Myxococcus xanthus*, *Semin. Cell Dev. Biol.* **46** (2015) 143–154.
59. R. Jain, N.-H. Le, L. Bertaux and et al., Fatty acid metabolism and the oxidative stress response support bacterial predation, *Proc. Natl. Acad. Sci. USA.* **122** (2025) e2420875122.
60. R. Jiang and F. Lin, Riesz transform on exterior Lipschitz domains and applications, *Adv. Math.* **453** (2024) Paper No. 109852, 48.
61. Z. Jiang and L. Wang, Mild solutions to the Cauchy problem for time-space fractional Keller-Segel-Navier-Stokes system, *Fract. Calc. Appl. Anal.* **28** (2025) 1503–1538.
62. B. Jin, *Fractional Differential Equations: An Approach Via Fractional Derivatives*, volume 206 of *Applied Mathematical Sciences* (Springer, Cham, 2021).
63. B. Jin, R. Lazarov and Z. Zhou, An analysis of the L1 scheme for the subdiffusion equation with nonsmooth data, *IMA J. Numer. Anal.* **36** (2016) 197–221.
64. H.-Y. Jin and Z.-A. Wang, Critical mass on the Keller-Segel system with signal-dependent motility, *Proc. Amer. Math. Soc.* **148** (2020) 4855–4873.
65. D. Kaiser, Coupling cell movement to multicellular development in myxobacteria, *Nat. Rev. Microbiol.* **1** (2003) 45–54.
66. G. E. Karniadakis, I. G. Kevrekidis, L. Lu, P. Perdikaris, S. Wang and L. Yang, Physics-informed machine learning, *Nat. Rev. Phys.* **3** (2021) 422–440.
67. T. Kato, Schrödinger operators with singular potentials, *Israel J. Math.* **13** (1972) 135–148 (1973).
68. N. I. Kavallaris and P. Souplet, Grow-up rate and refined asymptotics for a two-dimensional Patlak-Keller-Segel model in a disk, *SIAM J. Math. Anal.* **40** (2008/09) 1852–1881.
69. D. B. Kearns, A field guide to bacterial swarming motility, *Nat. Rev. Microbiol.* **8** (2010) 634–644.
70. J. M. Keegstra, F. Carrara and R. Stocker, The ecological roles of bacterial chemotaxis, *Nat. Rev. Microbiol.* **20** (2022) 491–504.
71. E. F. Keller and L. A. Segel, Initiation of slime mold aggregation viewed as an instability, *J. Theoret. Biol.* **26** (1970) 399–415.
72. E. F. Keller and L. A. Segel, Traveling bands of chemotactic bacteria: A theoretical analysis, *J. Theor. Biol.* **30** (1971) 235–248.
73. A. A. Kilbas, H. M. Srivastava and J. J. Trujillo, *Theory And Applications Of Fractional Differential Equations*, volume 204 (Elsevier Science B.V., Amsterdam, 2006).
74. M. A. Kiskowski, Y. Jiang and M. S. Alber, Role of streams in myxobacteria aggregate formation, *Phys. Biol.* **1** (2004) 173–183.
75. J. Klafter and I. M. Sokolov, *First Steps in Random Walks: From Tools to Applications* (Oxford University Press, Oxford, 2015).
76. H. Köhlwien, *Polyangium fuscum (Myxobacteriales). Cystenkeimung und Schwarmentwicklung* (Encyclopaedia Cinematographica, E1582, G. Wolf, ed., Institut für den Wissenschaftlichen Film, Göttingen,, 1971).
77. H. Köhlwien, H. Reichenbach, H. Heunert and H. Kuczka, *Schwarmentwicklung und Morphogenese bei Myxobakterien—Archangium, Myxococcus, Chondrococcus, Chondromyces* (Encyclopaedia Cinematographica, C893, G. Wolf, ed., Institut für den Wissenschaftlichen Film, Göttingen,, 1968).
78. T. A. M. Langlands and B. I. Henry, Fractional chemotaxis diffusion equations, *Phys. Rev. E* **81** (2010) 051102, 12.
79. J. Lankeit, A new approach toward boundedness in a two-dimensional parabolic chemotaxis system with singular sensitivity, *Math. Methods Appl. Sci.* **39** (2016) 394–404.
80. J. Lankeit and M. Winkler, A generalized solution concept for the Keller-Segel system with logarithmic sensitivity: Global solvability for large nonradial data, *NoDea-Nonlinear Differ. Equ. Appl.*

- 24** (2017) 49.
81. J. Li, T. Li and Z.-A. Wang, Stability of traveling waves of the Keller-Segel system with logarithmic sensitivity, *Math. Models Methods Appl. Sci.* **24** (2014) 2819–2849.
  82. N. Lindemulder, E. Lorist, F. B. Roodenburg and M. C. Veraar, Functional calculus on weighted Sobolev spaces for the Laplacian on rough domains, *J. Differential Equations* **454** (2026) Paper No. 113884, 71.
  83. J.-G. Liu, L. Wang and Z. Zhou, Positivity-preserving and asymptotic preserving method for 2D Keller-Segel equations, *Math. Comp.* **87** (2018) 1165–1189.
  84. N. Livne, M. Koler and A. Vaknin, Collective condensation and auto-aggregation of *Escherichia coli* in uniform acidic environments, *Commun. Biol.* **7** (2024) 1028.
  85. N. Livne, A. Vaknin and O. Agam, Pattern formation in *E. coli* through negative chemotaxis: Instability, condensation, and merging, *Phys. Rev. Res.* **7** (2025) 023095.
  86. F. Ma, Scaling crossover of the generalized Jeffreys-type law, *arXiv:2510.07930*.
  87. F. Ma, W. Tian and W. Deng, Corrigendum to “Mathematical modeling and analysis for the chemotactic diffusion in porous media with incompressible Navier-Stokes equations over bounded domain” [J. Differ. Equ. 436 (2025) 113305], *J. Differential Equations* **443** (2025) 113656.
  88. F. Ma, W. Tian and W. Deng, Mathematical modeling and analysis for the chemotactic diffusion in porous media with incompressible Navier-Stokes equations over bounded domain, *J. Differential Equations* **436** (2025) 113305.
  89. F. Ma, L. Zhao, W. Deng and Y. Wang, Analyses of the contour integral method for time fractional normal-subdiffusion transport equation, *J. Sci. Comput.* **97** (2023) 45.
  90. F. Ma, L. Zhao, Y. Wang and W. Deng, The contour integral method for Feynman-Kac equation with two internal states, *Comput. Math. Appl.* **151** (2023) 80–100.
  91. M. Magdziarz, A. Weron and J. Klafter, Equivalence of the fractional Fokker-Planck and subordinated Langevin equations: the case of a time-dependent force, *Phys. Rev. Lett.* **101** (2008) 210601.
  92. M. Magdziarz, A. Weron and K. Weron, Fractional Fokker-Planck dynamics: Stochastic representation and computer simulation, *Phys. Rev. E* **75** (2007) 016708.
  93. T. N. Malla, L. Aldama, V. Leon and et al., Observation of early events in the photoactivation of Myxobacterial phytochrome using time-resolved serial femtosecond crystallography, *Commun. Chem.* **8** (2025) 183.
  94. E. M. F. Mauriello, T. Mignot, Z. Yang and D. R. Zusman, Gliding motility revisited: How do the myxobacteria move without flagella?, *Microbiol. Mol. Biol. R.* **74** (2010) 229–249.
  95. M. J. McBride, P. Hartzell and D. R. Zusman, *Myxobacteria II* (ASM Press, Washington DC, 1993).
  96. L. D. McClenny and U. M. Braga-Neto, Self-adaptive physics-informed neural networks, *J. Comput. Phys.* **474** (2023) 111722.
  97. M. M. Meerschaert and P. Straka, Inverse stable subordinators, *Math. Model. Nat. Phenom.* **8** (2013) 1–16.
  98. O. Mendez and M. Mitrea, Complex powers of the Neumann Laplacian in Lipschitz domains, *Math. Nachr.* **223** (2001) 77–88.
  99. M. Meyer, L. Schimansky-Geier and P. Romanczuk, Active Brownian agents with concentration-dependent chemotactic sensitivity, *Phys. Rev. E* **89** (2014) 022711.
  100. N. Mittal, E. O. Budrene, M. P. Brenner and A. van Oudenaarden, Motility of *Escherichia coli* cells in clusters formed by chemotactic aggregation, *Proc. Natl. Acad. Sci. USA.* **100** (2003) 13259–13263.
  101. B. Nan, J. Chen, J. C. Neu, R. M. Berry, G. Oster and D. R. Zusman, Myxobacteria gliding motility requires cytoskeleton rotation powered by proton motive force, *Proc. Natl. Acad. Sci. USA.* **108** (2011) 2498–2503.
  102. H. G. Othmer and A. Stevens, Aggregation, blowup, and collapse: the ABCs of taxis in reinforced random walks, *SIAM J. Appl. Math.* **57** (1997) 1044–1081.
  103. P. Y. H. Pang, Y. Wang and J. Yin, Asymptotic profile of a two-dimensional chemotaxis-Navier-Stokes system with singular sensitivity and logistic source, *Math. Models Methods Appl. Sci.* **31** (2021) 577–618.
  104. I. Podlubny, *Fractional Differential Equations*, volume 198 of *Mathematics in Science and Engi-*

- neering (Academic Press, Inc., San Diego, CA, 1999).
105. C. Qiu, Q. Liu and J. Yan, Third order positivity-preserving direct discontinuous Galerkin method with interface correction for chemotaxis Keller-Segel equations, *J. Comput. Phys.* **433** (2021) 110191.
  106. C. Quan, T. Tang and J. Yang, How to define dissipation-preserving energy for time-fractional phase-field equations, *CSIAM Trans. Appl. Math.* **1** (2020) 478–490.
  107. M. Raissi, P. Perdikaris and G. E. Karniadakis, Physics-informed neural networks: a deep learning framework for solving forward and inverse problems involving nonlinear partial differential equations, *J. Comput. Phys.* **378** (2019) 686–707.
  108. H. H. Reichenbach and H. Kuczka, *Archangium violaceum (Myxobacteriales)—Schwammentwicklung und Bildung von Protocysten* (1968).
  109. H. Risken, *The Fokker-Planck equation*, volume 18 of *Springer Series in Synergetics* (Springer-Verlag, Berlin, 1989), second edition, methods of solution and applications.
  110. S. K. Saggiu, A. Nath and S. Kumar, Myxobacteria: Biology and bioactive secondary metabolites, *Res. Microbiol.* **174** (2023) 104079.
  111. N. Saito, Conservative upwind finite-element method for a simplified Keller-Segel system modelling chemotaxis, *IMA J. Numer. Anal.* **27** (2007) 332–365.
  112. M. M. Salek, F. Carrara, V. Fernandez, J. S. Guasto and R. Stocker, Bacterial chemotaxis in a microfluidic T-maze reveals strong phenotypic heterogeneity in chemotactic sensitivity, *Nat. Commun.* **10** (2019) 1877.
  113. D. Scheidweiler, A. D. Bordoloi, W. Jiao and et al., Spatial structure, chemotaxis and quorum sensing shape bacterial biomass accumulation in complex porous media, *Nat. Commun.* **15** (2024) 191.
  114. O. Sozinova, Y. Jiang, D. Kaiser and M. Alber, A three-dimensional model of myxobacterial aggregation by contact-mediated interactions, *Proc. Natl. Acad. Sci. U. S. A.* **102** (2005) 11308–11312.
  115. A. Stevens, The derivation of chemotaxis equations as limit dynamics of moderately interacting stochastic many-particle systems, *SIAM J. Appl. Math.* **61** (2000) 183–212.
  116. A. Stevens, A stochastic cellular automaton modeling gliding and aggregation of myxobacteria, *SIAM J. Appl. Math.* **61** (2000) 172–182.
  117. C. Stinner and M. Winkler, Global weak solutions in a chemotaxis system with large singular sensitivity, *Nonlinear Anal.-Real World Appl.* **12** (2011) 3727–3740.
  118. M. Sulman and T. Nguyen, A positivity preserving moving mesh finite element method for the Keller-Segel chemotaxis model, *J. Sci. Comput.* **80** (2019) 649–666.
  119. Z.-z. Sun and X. Wu, A fully discrete difference scheme for a diffusion-wave system, *Appl. Numer. Math.* **56** (2006) 193–209.
  120. K. Taira, *Analytic Semigroups And Semilinear Initial Boundary Value Problems*, volume 434 of *London Mathematical Society Lecture Note Series* (Cambridge University Press, Cambridge, 2016), second edition.
  121. Y. Tao and Z.-A. Wang, Competing effects of attraction vs. repulsion in chemotaxis, *Math. Models Methods Appl. Sci.* **23** (2013) 1–36.
  122. M. C. Uçar, Z. Alsberga, J. Alanko, M. Sixt and E. Hannezo, Self-generated chemotaxis of mixed cell populations, *Proc. Natl. Acad. Sci. USA.* **122** (2025) e2504064122.
  123. J. J. L. Velázquez, Point dynamics in a singular limit of the Keller-Segel model. I. Motion of the concentration regions, *SIAM J. Appl. Math.* **64** (2004) 1198–1223.
  124. J. J. L. Velázquez, Point dynamics in a singular limit of the Keller-Segel model. II. Formation of the concentration regions, *SIAM J. Appl. Math.* **64** (2004) 1224–1248.
  125. G. J. Velicer and Y.-t. N. Yu, Evolution of novel cooperative swarming in the bacterium *Myxococcus xanthus*, *Nature* **425** (2003) 75–78.
  126. K. Wang, E. Liu and X. Feng, Optimal error estimate of unconditionally positivity-preserving, mass-conserving and energy stable method for the Keller-Segel chemotaxis model, *Math. Comp.* **94** (2025) 2761–2793.
  127. R.-N. Wang, D.-H. Chen and T.-J. Xiao, Abstract fractional Cauchy problems with almost sectorial operators, *J. Differential Equations* **252** (2012) 202–235.
  128. S. Wang, S. Zhou, S. Shi and W. Chen, Fully decoupled and energy stable BDF schemes for a class

- of Keller-Segel equations, *J. Comput. Phys.* **449** (2022) 110799.
129. M. Winkler, Absence of collapse in a parabolic chemotaxis system with signal-dependent sensitivity, *Math. Nachr.* **283** (2010) 1664–1673.
  130. M. Winkler, Aggregation vs. global diffusive behavior in the higher-dimensional Keller-Segel model, *J. Differential Equations* **248** (2010) 2889–2905.
  131. M. Winkler, Global solutions in a fully parabolic chemotaxis system with singular sensitivity, *Math. Methods Appl. Sci.* **34** (2011) 176–190.
  132. M. Winkler, Global asymptotic stability of constant equilibria in a fully parabolic chemotaxis system with strong logistic dampening, *J. Differential Equations* **257** (2014) 1056–1077.
  133. M. Winkler, The two-dimensional Keller-Segel system with singular sensitivity and signal absorption: Global large-data solutions and their relaxation properties, *Math. Models Methods Appl. Sci.* **26** (2016) 987–1024.
  134. M. Winkler, Unlimited growth in logarithmic Keller-Segel systems, *J. Differential Equations* **309** (2022) 74–97.
  135. C. Wolgemuth, E. Hoiczyk, D. Kaiser and G. Oster, How myxobacteria glide, *Curr. Bio.* **12** (2002) 369–377.
  136. G. Zhou and N. Saito, Finite volume methods for a Keller-Segel system: Discrete energy, error estimates and numerical blow-up analysis, *Numer. Math.* **135** (2017) 265–311.